INTEGRATION OF REAL TIME AND SATELLITE WATER QUALITY MONITORING SYSTEMS: CASE STUDY LAKE MANZALAH, EGYPT

MOHAMED D. IBRAHIM

INTEGRATION OF REAL TIME AND SATELLITE WATER QUALITY MONITORING SYSTEMS: CASE STUDY LAKE MANZALAH, EGYPT.

by

Mohamed D. Ibrahim

A thesis submitted to the School of Graduate Studies

in partial fulfillment of the requirements for the degree of

Master of Engineering

Faculty of Engineering and Applied Science

Memorial University of Newfoundland

March, 2011

St. John's Newfoundland Canada

Abstract

Water quality monitoring is one of the corner stones of water resources management. Monitoring water quality using a Real Time Water Quality (RTWQ) monitoring approach provides high temporal resolution measurements, while monitoring through the use of satellite imagery produced high spatial resolution maps for the monitored water parameters. By combining approaches, RTWQ and satellite, high temporal and spatial resolution products can be obtained. The integration was done through developing statistical relationships between the extracted reflectances from the satellite imagery and measured real time water quality parameters in the field.

Lake Manzalah, the largest of the northern lakes in Egypt, was used as a case study for the proposed combined approach. The water quality parameters investigated were Turbidity (TUR), Chlorophyll-a (CHL), and Total Dissolved Solid (TDS). The results showed that there were statistically significant regression relationships between the satellite reflectance and the measured water quality parameters with $r^2 = 0.77$, n= 34; 0.65, n= 33; and 0.60, n= 56 for TUR, CHL, and TDS models, respectively. The corresponding Nash-Sutcliffe coefficients were 0.76, 0.64, and 0.61 for TUR, CHL, and TDS models, respectively. The results indicate the viability of using satellite reflectances to infer the state of the water quality in Lake Manzalah. The relationship between RTWQ measurements and satellite observations were subsequently used to generate other useful quantitative water quality products. This research has the potential for application to other large water bodies in Newfoundland and Labrador and internationally.

Acknowledgement

First of all, I would like to express my deepest sense of gratitude to my supervisor Dr. Leonard Lye and co-supervisors Dr. Amir Ali Khan and Mr Thomas Puestow for their patient guidance, encouragement and excellent advice throughout this study.

I would also like to express my gratitude to my scholarship sponsor the Institute for Biodiversity, Ecosystem Science & Sustainability (IBES), Government of Newfoundland and Labrador, and Memorial University for financing of my study.

I am also very thankful to Lori Hogan and Susan Carter of C-CORE for their generous assistance during my research.

I would like to take this opportunity to express my profound gratitude to my beloved parents, wife, brothers, sister, uncles, aunts, parents in law and rest of my family and friends for their moral support and patience during my study in Canada.

Finally, I would like to express my appreciations to the Egyptian people who launched the January 25th revolution especially the martyrs who gave their souls as a price for beginning a new era in the Egyptian history and gave me the motivation to work hard.

Table of Contents

List of Tables

List of Figures

1. Introduction

This chapter briefly introduces the background of the proposed research, the reasons why there is a need for new research, and the objectives of the thesis.

1.1. Background

Traditionally, water quality monitoring of lakes has two principal stages: field sampling and laboratory analysis. Field sampling consists of taking a representative portion of water from predefined locations of a water body and subsequently transporting the collected samples to the laboratory. In the laboratory, the water samples are analyzed using a wide variety of physical and chemical analytical techniques, to quantify the concentration of various constituents in the water sample.

One of the disadvantages of this traditional approach to monitor water quality has been the difficulty of collecting sufficient samples to capture the temporal variation of the water quality parameters in the water body being sampled. This has especially been an issue when the water body being sampled is situated far from the water quality analysis laboratory.

In recent years, digital sensors have been developed to monitor some of the water quality parameters. These sensors can address the challenge of capturing the temporal variation of measured water quality parameters as they can be deployed in the field for a sufficient long time. The pairing of these sensors with digital recording and control devices like data loggers allows for measurements to be taken at pre-programmed time intervals. The further pairing of the data loggers with remote communication devices such as phone modems and cell phone modems offers the option of transferring the stored data from the field to the office in real time. This combination of in situ monitoring coupled with real time reporting is usually referred to as real-time water quality (RTWQ) monitoring. RTWQ monitoring is used in conjunction with traditional water quality monitoring to provide a more extensive characterization of a water body.

In the specific case of sampling large lakes, another difficulty is the ability to sample the different areas of the lake simultaneously. This is especially so for lakes with islands and aquatic growth which results in different water quality zones within the same lake. Examples of such large lakes can be found all over the world such as the perialpine lakes of Europe, the Laurentian Lakes and Great Lakes in North America, and Lake Victoria in East Africa.

Table 1 summarizes the location and surface areas of some large lakes around the world. Herdendorf (1982) provides more details of the lakes listed. Studies carried out in these lakes are based on dedicated field trips for a limited period of time. Hence detecting seasonal or long term trends in water quality in these lakes are not possible.

Large lakes are a precious resource in every part of the world. Many civilizations have sprung up around large lakes. This is particularly true especially in Egypt along with the Nile River. They are a source of fresh water for agricultural, domestic, industrial, aqua-cultural, and recreational uses. One such large lake is Lake Manzalah. It is the largest of Egypt's northern lakes. Lake Manzalah covers an approximate area of 770 Km^2 and has approximately a 1000 small islands scattered in the lake, representing about 9% of the lake's total surface area.

Table 1: Examples of large lakes

Lake	Location	Surface Area (km^2)
Lake Superior	Canada,U.S., North America.	82,100 [*]
Lake Victoria	Kenya, Tanzania, Uganda, Africa.	62,940[*]
Lake Huron	Canada,U.S., North America.	59,500[*]
Lake Michigan	Canada,U.S., North America.	57,750[*]
Lake Erie	Canada,U.S., North America.	25,657[*]
Lake Ontario	Canada,U.S., North America.	19,000[*]
Lake Nasser	Egypt, Africa.	6000[♦]
Lake Okeechobee	U.S., North America.	1,730 *
Lake Constance	Germany-Switzerland-Austria, Europe.	540*
Lake Manzalah	Egypt, Africa.	1275•
Lake El-Burrullus	Egypt, Africa.	568•

*Herdendorf (1982) •Zalat and Vildary (2005) [♦] Ebaid and Ismail (2010)

The current water quality monitoring system in Lake Manzalah relies on the traditional water quality monitoring method described earlier located at drainage channels leading into the lake. Although this monitoring system can capture the changes in water quality of the catchments leading to the lake, this system does not provide a clear picture about the temporal and spatial variation of lake water quality. This in turn does not lead to effective decision making by authorities responsible for managing a wide variety of activities that make use of the lake.

The installation of RTWQ monitoring stations in different parts of the lakes can only partially address this spatial coverage problem as the in-situ readings are usually representative of only a small area around the sensor. The difficulty of spatial coverage can however be addressed using a satellite-based water quality monitoring approach.

Space based satellites have been used for the monitoring of some water quality parameters in oceans and open seas, since late 1960s and early 1970s. The water quality monitoring efforts were initially dedicated to mapping the chlorophyll and the ocean surface temperature (Doerffer *et al.*, 1999). In the last two decades, the effort has been extended to include monitoring coastal and inland waters quality as well. More recently this has been tested to monitor water quality in large lakes and to retrieve water quality parameters based on their optical properties. This was tested out for the Great Lakes in the U.S., and Canada (Gons *et al.*, 2008), Lakes Constance in Europe (Odermatt *et al.*, 2008; Guanter *et al.*, 2010; Matthew *et al.*, 2010), Lake Victoria in Africa (Swenson and Wahr, 2009; Cavalli *et al.*, 2009) and Lake Malawi in Malawi (Chavula *et al.*, 2009). This is done through developing statistical relationships between the extracted reflectances from the satellite images and in-situ measured parameters.

To produce quantitative estimates of water quality, the satellite imagery has to be calibrated with in-situ water quality readings from different parts of the lake. Coordinating the in-situ water quality monitoring in different parts of the lake to occur simultaneously that the satellite passes over the lake poses logistical challenges. However this can be addressed by using RTWQ monitoring at a few selected locations representing different parts of the lake. By combining the RTWQ monitoring and satellite water quality monitoring systems, there is a potential for developing a large lake water quality monitoring system with a high spatial and temporal resolution. With this approach, it is possible to develop a long term data collection program to keep track of the temporal spatial variation of water quality parameters.

1.2. Research Objectives

The main objective of the research is to evaluate the feasibility of developing a high spatial and temporal frequency lake water quality monitoring system for selected parameters through the integration of space satellite imagery with a real time water quality (RTWQ) monitoring system. The study area selected for this case study is Lake Manzalah, Egypt and the water quality parameters being investigated are Turbidity (TUR), Chlorophyll-a (CHL), and Total Dissolved Solids (TDS).

This research examines the feasibility of using statistical regression models to describe the relationship between the extracted reflectance from satellite imagery and specific water quality parameters measured at RTWQ monitoring stations in Lake Manzalah, Egypt.

This research has potential applications for the monitoring of other large lakes around the world, including large water bodies in Newfoundland and Labrador.

1.3 Outline of Thesis

This thesis contains six chapters and seven appendices. Chapter 1 briefly introduces the background of the research, the need for new research, and the objectives of the thesis. Chapter 2 is devoted to the review of previous literature on water quality monitoring and the historical background of the technologies used to monitor water quality. Chapter 3 describes the case study area which is Lake Manzalah, Egypt. Chapter 4 outlines the methodology that was followed in this research. Chapter 5 presents the results and also provides samples of final water quality products in terms of colored images of lake water quality. Chapter 6 contains the discussion about the results obtained, and the conclusions and recommendations for future work.

2. Literature Review

This chapter provides background information about the different methods of water quality monitoring and the effect of advanced applications of communication and sensor technologies in the last few decades on water quality monitoring methods; and the use of remote sensing based on satellite imagery for water quality monitoring.

2.1. Water Quality Monitoring

Fresh water is essential for human activities such as agriculture, industry, and drinking. Water quality is the key factor for deciding if the water is suitable for use in these activities. In particular, human health is directly related to the water quality conditions as evidenced by the number of people suffering from water-borne diseases (WHO, 1980, 1982).

While water quality influences human health, human activities, in forms of point or non-point pollution, human activities also impact water quality (Smith, 2002). It was estimated that the human activities resulted in the entrance of a total of 12,000 tonnes of Phosphorus and 304,000 tonnes of Nitrogen into Canadian fresh, ground, and coastal waters in 1996. Of these, municipal sewage represents 26 % and 47 %, respectively, of added Nitrogen and Phosphorus, and industrial waste water percentage of the total Nitrogen and Phosphorus were 4 % and 17%, respectively, (Chambers *et al.*, 2001).

The nutrient enrichment through the addition of Nitrites and Phosphorus into inland waters, such as a lake or a reservoir, results in eutrophication of the water. Eutrophication leads to a considerable increase in the algae load in the water system which causes serious water quality problems such as toxic algal blooms, loss of oxygen, fish kills, loss of biodiversity (including species important for commerce and recreation), loss of aquatic plant beds and coral reefs. Nutrient enrichment seriously degrades aquatic ecosystems and impairs the use of water for drinking, industry, agriculture, recreation, and other purposes (Carpenter *et al.*, 1998).

In order to define the quality water body for a given use, sufficient data about the main water constituents must be collected and studied. Collected water quality data must be reliable as they also are essential for decision makers in a number of areas, such as policy planning, program planning, and the general assessment of the water bodies as a valuable resource (Phillips *et al.*, 1974).

Water quality data collection is typically accomplished through a water quality monitoring program. Water quality monitoring program consists of collecting water samples that spatially and temporally represent the water body being monitored. These samples are analyzed for selected physical, chemical and biological parameters that are relevant to the intended use of the water or for understanding the state of the water body's quality.

Selected parameters are then compared to standards and guidelines to decide if the sampled water body is suitable for a particular use such as drinking, agriculture etc. The aim of monitoring may also extend to establishing trends for the measured parameters (Bartram *et al.*, 1996; Chapman, 1996; USGS, 2010).

Traditionally, the water sampled from the field is analyzed in the laboratory under controlled environments. Due to recent advances of sensor and computer technologies, some of the water quality parameters can now be sampled and analyzed automatically in situ in the field. The collected data can then be obtained either manually or it can be sent to the office remotely by wired or wireless network. More recently, satellite technology has been used to monitor some of the water quality parameters.

From a water quality monitoring point of view, one challenge of water sampling is to increase the frequency of the collected samples to capture the change of measured water constituents in small time interval. Another challenge is to cover the whole surface area of the water body to determine the distribution pattern of the measured water constituents. The spatial coverage is more challenging for large lakes and reservoirs as it requires a large number of stations to completely cover the surface area.

There are a lot of important water quality parameters monitored to assess the water quality. These parameters can be classified into three main categories physical, chemical, and biological parameters (Chapman, 1996, EPA, 2001, Environment Canada, 2011). Table 2 lists the common water quality monitored parameters.

Table 2 Important water quality monitoring parameters

Physical parameters	Water temperature
	pH
	Specific conductance
	Dissolved oxygen (DO)
	Turbidity
Chemical parameters	Nutrients (Nitrogen, phosphorus)
	Trace metals (ex. Nickel, cadmium, mercury)
	Major ions (ex. Calcium, Magnesium)
	Polychlorinated biphenyls (PCBs)
	Hydrocarbons
	Pesticides
Biological parameters	Chemical Oxygen demand (COD)
	Biological Oxygen demand (BOD)

EPA (2001), Environment Canada (2011).

Three important water parameters that are widely monitored in large lakes to assess the water quality status are: turbidity, total dissolved solids, and chlorophyll a. In the next few sections, background information as well as the standard methods of measuring of these parameters are presented.

Turbidity (TUR) is the presence of suspended matters in the water when it looks hazy and cloudy. The suspended matter that causes the turbidity could be clay, silt, sand, organic, inorganic particles, and other microscopic organisms (Dowing, 2005). Turbidity is measured optically by a turbidity meter in nephelometric turbidity unit [NTU]. Standard methods calculate the turbidity by measuring the amount of light that is scattered at 90 degrees by the sample (AWWA, 1995).

The angular distribution of scattered light depends on the fluid refractive indices and wavelength of the light as well as the particles' size. Small particles (the diameter of the particle is around 1/10 of the light wave length) scatter the light forward and backward at the same amount, while the intermediate size particles (the diameter of the particle is around 1/4 of the light wave length) scatter the light in the forward direction. The particles which have diameters bigger than the wavelength of the light nearly scatter the light forward in a cone shape (Dowing, 2005). As a result, the measurement of the turbidity is associated with variability. In another words, two samples of water with different suspended matters might have same turbidity measurement. On the other hand, the same sample of water might have different readings of turbidity by different turbidity meters (Purrington, 2010).

EPA 180.1 is a standard method for measuring low turbidity samples developed by U.S. Environmental Protection Agency (EPA). This method requires a turbidimeter with a tungsten-filament lamp (TFL) light source at temperature of operation between 220 and 3000 K, and detector plus bandpass filter with peak between 400 and 600 nm. TFL has peak intensity in the NIR near 860 nm. The detector must be at 90° to the light beam and accept the scattered light in a cone not wider than 60° (see Figure 1). In case that the sample turbidity is more than 40 NTU, sample dilution is required (Dowing, 2005).

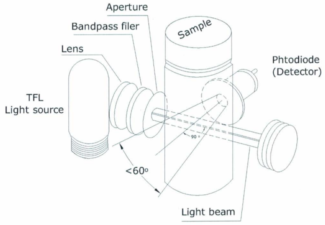

Figure 1: EPA Method 180.1 for measuring turbidity (Dowing, 2005).

The standard ISO 7027 method is developed by the International Standards Organization (ISO). ISO 7027 requires an 860 Nanometer Infrared laser diode as light source. The detector acceptance angle is 20-30° and must be oriented at 90 ± 2.5° (see Figure 2). In the case that the sample turbidity is more than 40 NTU, sample dilution is also required

(Dowing, 2005). Based on the previous review of both methods, the closer method to the standard methods is ISO 7027 (AWWA, 1995). Some turbidity meters that are commercially available along with their range and measurement method are listed in Table 3.

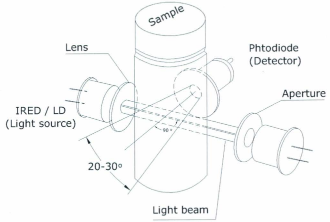

Figure 2: ISO 7027 design for measuring turbidity (Dowing, 2005)

Table 3: Commercially available turbidimeters, range, and method (Dowing, 2005)

Manufacturer	Model	Range [NTU]	Measurement Method
Hach Company	2100P	2000	EPA 180.1
HANNA Instruments	C102	50	EPA 180.1
HF Scientific Inc.	DRT-15CE	1000	EPA 180.1
Lamotte	2020	1100	EPA 180.1
HydroLab Inc.	DataSonde4	3000	ISO 7027
HANNA Instruments	HI93703	1000	ISO 7027
WTW Measurement sys. Inc.	Turb 350 IR	1100	ISO 7027
YSI Inc.	YSI 6136	1000	ISO 7027

Total dissolved solids (TDS) represent the total weight of the dissolved matter that is non-filterable in the water or wastewater. These dissolved matters could be ions, acids bases, salt, and certain gases such as carbon dioxide, hydrogen chloride and ammonia. (AWWA, 1995; Dowing, 2005) and are measured in mg/L (milligrams per one liter) or they can be expressed as ppm (part per million). The EPA limit for permissible TDS in drinking water is 500 mg/L (EPA, 2010). The concentration of TDS can be approximated by measuring the conductivity of the water sample. Conductivity measurements are then converted to TDS concentrations (Purrington, 2010). The standard method for measuring TDS is to filter the sample through a glass fiber filter, the filtrate is then evaporated until dryness in a weighted dish at 180° C. The increase in dish weight is the TDS concentration (AWWA, 1995).

Chlorophyll a (CHL) is an indicator of the presence of the algae and aquatic plants. Algae are the outcome of the water quality deterioration as it is results from the eutrophication process (Carpenter *et al.*, 1998). The standard method that is used to measure CHL in water and wastewater consists of filtrating the sampled water at low vacuum through a glass fiber filter; the pigments are then extracted from the phytoplankton and centrifuged. The centrifuged sample is transferred to a glass cuvette and fluorescence is measured before and after acidification, the CHL can then be calculated. The concentration is reported in μg/L, micrograms per one liter. (Arar and Collins, 1997).

In the next few sections, the methods of monitoring water bodies are reviewed. These methods include: laboratory-based, sensor-based, and satellite based methods.

2.1.1 Traditional water quality monitoring method (Laboratory-based)

Water quality monitoring programs started in the 1960s and 1970s. At that time, the water quality programs were developed to describe the general state of the water bodies' quality (Strobl and Robillard, 2006). The parameters under investigation were few and the frequency of sampling was 12-13 times a year. Later in the 1980s, collected water parameters increased dramatically to reach more than 100 (Wetering *et al.*, 1986).

Traditionally, water quality monitoring programs had been conducted using a costly, time-consuming, and labor-intensive in-situ sampling and data collection process with subsequent transport of the collected samples to laboratories for evaluation (Glasgow *et al.*, 2004). The typical sequence of steps for the traditional method of water quality monitoring begins with sampling the water from selected points throughout the water body. In case of large surface water body such as lakes, reservoirs and coastal zones, the selected points should represent the whole area under consideration in terms of spatial distribution to ensure adequate spatial coverage. Then the samples are transported directly to the laboratory. In case, the laboratory is far away from the site, the collected samples are preserved, using a variety of methods, to keep changes of the sample properties at a minimum. In the laboratory, the sample is analyzed using standardized methods to measure water parameters (AWWA, 1995). The analyzed data are then compared to standards based on the intended use of the water and reported to decision makers to take appropriate informed decisions.

Conventional water quality monitoring methods allows decision makers and scientists to observe a large number of parameters in the same monitoring program because there is no limitation on the number of observed parameters except the total cost of sampling and laboratory tests (Lettenmaier, 1978) and the laboratory capacity (Wetering *et al.*, 1986). In addition, the information that comes out from laboratory-based water quality monitoring programs is accurate and reliable (Kloiber *et al.*, 2002; Bierman *et al.*, 2011).

Although the traditional method of water quality monitoring can address a large number of parameters in the same sampling process, it has many disadvantages. Some of these disadvantages includes: the high cost of the water quality monitoring process, laboratory limitations in terms of the ability of analyzing a large number of samples at the same time, changing measuring standards over time and from country to country, poor temporal resolution in the best case scenario, and the dependency of the spatial coverage on the number and the distribution of sampling points. Details of these shortcomings as published in the literature will be elaborated in the next sections.

The cost of the monitoring process includes the capital cost of establishing permanent sampling points in the selected sampling locations in addition to the operational cost of collecting and analyzing the samples (Karamouz *et al.*, 2006). The operational cost consists of the cost of collecting and transporting the water samples, which requires a large group of dedicated workers, chemical analysis and reporting the results (Phillips *et al.*, 1974). The percentage of the chemical analysis cost is around 70% of the total water quality monitoring program cost (Wetering *et al.*, 1986). As a result, the cost of the monitoring program restricts the selection of sampling frequencies and sample station densities (Lettenmaier, 1978).

In case of long-term water quality monitoring programs, the observed parameters can be divided into two groups. One group of parameters is monitored continuously on a daily basis, while the second group is monitored in pre-defined intervals such as biweekly or monthly. The laboratory capacity plays an important role in deciding which parameters will be included in routine monitoring and which parameters will be included in periodic monitoring, as the optimal use of the available laboratory capacity is always a prerequisite (Wetering *et al.*, 1986).

The standard methods of analyzing the water samples differ from country to country and from time to time (Kwiatkowski, 1985; Greenberg *et al.*, 1995). As a result, the comparison and the establishment of trends using these data is invalid in case that the historical data was measured by a different method (Lettenmaier, 1978).

The laboratory-based monitoring method's shortcomings also include the time gap between taking the water samples and obtaining the results from the laboratory analysis due to the tests running time which may take up to a few days. This delay can lead to consequences that may affect the decision on human health. When human health is a concern, immediate information is critical (Vernon and Stack, 1972; Christensen *et al.*, 2001)

Because of the relationship between the water quality status and the human health, the rapid response is required especially in case of detecting any water quality contaminations or else human health will be put at risk (EPA, 2005). The effect of the mitigation process depends on the time between the occurrence of the contamination and the detection and identification of the contaminants which is called the response time. The response time depends mainly on the time between the sampling and the reporting of the results of the laboratory analysis. The time between occurrence of contamination and reporting in two hours or less is considered to be a rapid response time (EPA, 2005). This time may be influenced by the technologies used in sampling and the overall approach to identification of the contaminant. Due to the long time required to analyze and report the analyzed results which can take up to several days, the traditional method of water quality monitoring cannot be considered as a rapid response time method.

Traditional water quality monitoring has significant limitations from the perspective of temporal and spatial resolutions. In the best case scenario, the samples are taken on a daily basis which is not satisfactory in terms of understanding the behavior of water properties (Bourgeois *et al.*, 2001). This method can not detect changes and trends of critical water parameters in a period of time less than 24 hours. As an example, pH may change significantly in a matter of minutes through losing or gaining of dissolved gases (Phillips *et al.*, 1974).

In addition to the temporal limitations, the results of the laboratory-based water quality monitoring method are limited in describing the sampled water body in terms of spatial coverage as it is based on point-samples (Bierman *et al.*, 2011). This spatial limitation becomes a serious problem in cases of monitoring water bodies that have a huge surface area such a large lake or reservoir.

The limitation in temporal and spatial scales and reporting in real time, especially for a large lake or reservoir case, make it hard to address certain serious problems such as harmful algal blooms, oxygen depletion, fish-kills, and contamination of shellfish beds by enteric bacteria (Glasgow *et al.*, 2004).

Since the late 1960s a monitoring program has been implemented mainly using the laboratory-based method monitoring program to monitor the water quality status and trends in Lake Ontario. Kwiatkowski (1985) concluded that the main reasons for limited water quality information from the monitoring program are:

- Water records are often short in time and the measurements were not taken simultaneously in all sampling locations.
- The sampling frequency was only 13-15 times per year.
- The techniques and limitations of analytical methods that have been used in monitoring in the program have changed over the years.
- Sampling locations and the frequency have changed between the years due to the site conditions.
- The natural background variability often hides the true water quality trend.

Therefore, for cases of large lakes such as Lake Manzalah and Lake Ontario, the expense, time, and sampling frequency make the traditional way of water quality monitoring impractical to be applied to such large areas (Kloiber *et al.*, 2002).

From the above review, the need for rapid, frequent analysis of water quality is quite clear. The next sections discuss new technologies that have been developed in the water quality monitoring area to improve upon the traditional water quality monitoring method.

2.1.2 Sensor-based water quality monitoring

Recent advances in sensor technology along with the rapid advances in computer processing capabilities have made digital sensors capable of measuring a large number of water quality constituents simultaneously (Brignell, 1996; Glasgow *et al.*,2004). This section presents overview of sensor-based water quality monitoring method in the published literature.

A sensor is a device that contains a primary sensing element, filtering system, and signal amplification, in addition to software for data processing and compensation. The sensor element transfers the physical or chemical or biological property into an electrical signal. The signal is processed into engineering values such as mgL-1 or NTU (Tanner and White, 1996; Charef *et al.*, 2000; Jer´onimo *et al.*, 2007). There are three types of sensors that can be used in water quality monitoring process: optical sensors, biosensors, and sensor arrays (Bourgeois *et al.*, 2001).

An optical sensor is a sensor in which electromagnetic radiation is used in sensing the chemical and physical properties of the surrounding environment such as water, air etc. The principles that can be used in sensing and quantifying the measurements are: absorbance, reflectance, luminescence, and fluorescence. The spectral range used in different optical sensors covers UV, visible, IR, and NIR spectra (Jer´onimo *et al.*, 2007). The optical sensor can be a direct sensor (i.e. the sensor's components are located at the sensing point) or attached with an optical fiber to transmit the electromagnetic radiations to/from the sensed point (Kersey, 1996; Gauglitz, 2005). Figure 3 shows a layout of a direct optical sensor, while Figure 4 depicts a layout of a fiber optical sensor.

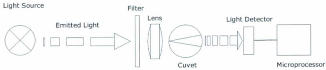

Figure 3: Direct optical sensor layout (Hanna, 2010).

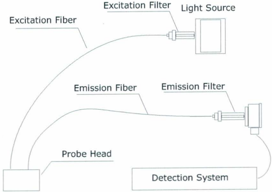

Figure 4: Fiber optical sensor layout (MacCraith et al, 1994; and Grattan, 1997)

Some of the parameters that can be measured using the optical sensors are: turbidity, pH, ionic species such as Al, Bi, Cu, and Cd, gases, Oxygen, Carbon oxide and Hydrogen (Kersey, 1996 Jer´onimo *et al.*, 2007; Liu, 2009; Purrington, 2010). The applications of optical sensors include water quality monitoring, and monitoring in the chemical and food industries.

The bio-sensor is a sensor that has a biological sensing element such as enzymes, antibodies, and microbial cells (bacteria or yeast that are genetically modified). Examples of the contaminants that can be monitored using bio-sensors are: pesticides, herbicides, penicillin, phenol, mycotoxins, antibiotics and other chemical contaminants. It is also used to measure some water quality parameters such as BOD, COD, and DO (Patel, 2002). The applications of bio-sensors can be used in many areas such as pharmaceutical, food quality and food security industries, as well as water and wastewater quality monitoring and environmental agencies. The limits of the bio-sensor need to be improved in order to compete with other methods of water quality monitoring. Improvement is required in areas such as:

- Improving the sensor's sensitivity
- Reducing the sensor's response time
- The specificity of the bio-sensor which is dependent on the sensing element

(Bourgeois *et al.*, 2001; Patel, 2002; Wilson, 2005).

The third type of sensors that can be used in water quality monitoring is the sensor array. The sensor array is a group of bio- or optical-sensors which analyzes the response pattern by a pattern recognition routine or chemometrical method (Krantz-Rülcker, 2001). Examples of the sensor arrays that can be used in detecting contaminants in the water are the electronic noses and electronic tongues. The electronic nose is used to monitor the pollutants in the gaseous state. (i.e. the electronic nose is more applicable for volatile and odorous compounds) while the electronic tongue is used to monitor the pollutants in the liquid state (Dewettinck, 2001). The main difference between the sensor array and other sensors is the measuring concept. The concept of electronic nose and tongue often predict a quality of a sample rather than measuring exact values of the individual parameters. Only in special cases the concentrations of individual parameter are measured in the sample (Krantz-Rülcker, 2001).

The electronic tongue and noses are used in the food and beverage industries in addition to quality control and classifications of water, food and air. It is also reported that the electrical nose and tongue are used to monitor wastewaters quality as well as the detection and identification of micro-organisms (Gardner and Bartlett, 1992; Hobbs *et al.*, 1995; Gibson *et al.*, 1997; Misselbrook *et al.*, 1997; Gardner *et al.*, 1998; Holmberg *et al.*, 1998; Dewettinck, 2001). Sensor arrays have been successfully employed for detecting cyanobacteria in water as well as heavy metals and pesticides (Canhoto and Megan, 2005; Bastos and Magan, 2006).

Based on the previous overview, the recent advances in sensor technology have resulted in robust, versatile, speed-response devices that can measure a wide range of environmental parameters at different sites in a locality (Mimendia, 2010). There are many rewards that can be gained from using the sensor-based method for monitoring water quality. Some of these rewards are: the automation of operation, the high temporal resolution of the measurements, the minimum exposure to wet chemicals, a short response time, and the possibility to be paired with communication tools to report the measurements in real-time. The advantages of the sensor based monitoring method are discussed below with more details.

Sensor-based water quality monitoring programs are designed to be automatically operated and to take readings continuously at user-defined intervals such as 10, 15, 30 minutes or more. As a result, a stream of data flows describing the changes of water properties in high temporal resolution can be achieved (Phillips *et al.*, 1974).

Usage of the sensor-based monitoring method avoids workers' direct exposure to wet chemicals in the monitoring process. Sensor-based water quality monitoring methods are measuring water quality constituents based on the optical, chemical, and physical properties of the water to estimate the water parameters. The usage of wet chemicals is confined only to the calibration process of the sensors (Phillips *et al.*, 1974; Charef *et al.*, 2000).

Unlike the traditional way of water quality monitoring, which requires collecting samples manually from the site, the sensors are sited in-situ and samples are taken automatically at short time intervals. These short intervals allow the trends and changes in critical water parameters to be detected early. As a result, appropriate action can be taken quickly to prevent undesirable consequences which can happen if the decision is taken too late (Glasgow *et al.*, 2004).

It is also possible to monitor more than one parameter at the same time using a multi-parameter sensor probe. EPA (2005) reported that there are sensor-based water quality monitoring systems that can monitor up to eight parameters at the same time. In addition, the process of sampling and measuring are conducted automatically regardless of the time gap between sampling and analyzing the samples.

Pairing the sensor-based water quality equipments with data loggers saves time and effort that is usually wasted in collecting the recorded data from the field. Further pairing the monitoring system with remote data transferring capability such as a telephone network, wireless network, or satellite retrieving data system can enhance the whole monitoring system performance and increase the reliability of transferring the data from the field to the office in real time (Glasgow *et al.*, 2004).

As described, recent advances in communication technology have catalyzed progress in water quality monitoring methods to become automated remote monitoring systems. Therefore, the ability of monitoring water quality properties at adequate temporal resolution has greatly improved. Moreover, the real time monitoring programs open a new window for setting up an early warning system (EWS). The early warning system can help decision makers take informed decisions in a shorter time frame to avoid the consequences which might take place in case of late decisions (Phillips *et al.*, 1974; Glasgow *et al.*, 2004; EPA, 2005).

Although the sensor-based water quality monitoring system have improved and enhanced traditional water quality monitoring, it cannot entirely replace the traditional way of monitoring. The main reason is the limitations of the existing sensor technology. The sensor-based water quality method can only measure some of the water quality parameters that can be measured using the laboratory-based method (Horsburgh *et al.*, 2010).

In addition, the sensors need to be calibrated frequently to ensure sensor accuracy. Moreover, there are uncertainties associated with sensor measurements as they vary from sensor to sensor and from manufacturer to manufacturer. For example, DO sensors generally have 15-20% uncertainty in the results (Bourgeois *et al.*, 2001).

Despite the high temporal resolution and in-situ deployment, a sensor-based water quality monitoring method is still a point measurement method which means that it is poor in terms of spatial representation of a large water body. Lakes or coastal areas require a large number of sensor-based stations in order to completely cover the study area spatially.

Based on the previous discussion, it is obvious that there is a need for a system that can gather the high temporal measurements along with a high spatial coverage. Satellite-based water quality monitoring method can provide the spatial dimension for the monitoring system. An overview of the satellite based water quality monitoring system is thus presented in the next section.

2.1.3 Satellite-based water quality monitoring

The need for a method that provides high spatial resolution measurements to monitor a water quality is concluded from the literature review in the previous sections. Satellites can be used to close the gap of spatial coverage in monitoring methods. The overview herein consists of a brief review of remote sensing followed by a discussion of the role of satellite sensors in monitoring water quality as well as the different methods of extracting water quality information from the satellite data.

Remote sensing is the science which deals with acquiring information about the Earth's surface remotely without a direct contact (Colwell, 1983). The concept of this science is built on collecting images of the Earth's surface using sensors. The remote sensor can be carried by two different platforms: airplanes and satellites. In this thesis the focus will be on satellite-based remote sensing. The collected imagery is then analyzed using a wide range of techniques to extract the useful information. Around 71 % of the Earth's surface is covered by water which can be found in oceans, seas, lakes, rivers, snow, and glaciers (Chen and Yu, 2009). Since the late 1970s, attention has been drawn to monitoring waters in oceans and open seas using a dedicated satellite sensor. The Coastal Zone Color Scanner (CZCS) was designed for water-monitoring purposes and was launched mainly to measure the water leaving reflectance to detect chlorophyll-a concentrations in open waters (Antoine *et al.*, 1995; Longhurst *et al.*, 1995; Behrenfeld and Falkowski, 1997; Gones, 2002).

2.1.3.1. Water quality monitoring satellite sensors

CZCS was launched aboard the Nimbus-7 satellite (1978–1986) (Doerffer *et al.*, 1999). CZCS greatly enlarged the information about the distribution of chlorophyll (Chl) a in the oceans and open waters (Barale and Schlittenhardt, 1993; Hooker and McClain, 2000). CZCS provided lessons regarding the requirements for calibration, validation, and atmospheric correction of the data (Hooker and McClain, 2000). The success of the CZCS mission to retrieve the phytoplankton concentrations in oceans and open seas was significant. However, despite the name of the sensor, the algorithm used to retrieve the water properties in case of ocean waters was not applicable to the case of coastal zone areas. The algorithm was also not applicable for inland waters such as large lakes and reservoirs. The restrictions which limit the CZCS applications to open waters were related to the difference in optical properties between the open and coastal waters zones as well as the limitations in the spectral and radiometric resolutions of the CZCS (Doerffer *et al.*, 1999). The spectral and radiometric limitations are mainly attributed to the lack of infrared bands which reflected in poor atmospheric correction procedures. As a result, the accuracy of estimating inorganic or biogenic particulate material on the water was low (Doerffer *et al.*, 1999).

There are other sensors, such as the Advanced Very High Resolution Radiometer (AVHRR) on the National Oceanic and Atmosphere Administration (NOAA) weather satellites and the Thematic Mapper (TM) sensor on Landsat, that have been used for some ocean color applications and estimating some water parameters like CHL *a,* but are not optimized for water monitoring and have more limitations than CZCS. The reason was that their spectral bands, spatial resolution and dynamic range were optimized for land or meteorological use and had limited sensitivity in this area (Doerffer *et al.*, 1999; Tyler *et al.*, 2006).

CZCS inspired a new generation of satellite sensors dedicated for environmental monitoring such as SEAWiFS and MODIS. Under NASA's Earth Science Enterprise, Sea-viewing Wide Field-of-view Sensor (SeaWiFS) was launched on August 1, 1997. The Earth Science Enterprise is designed to monitor earth's system and behavior through satellite imaging. SeaWiFS is one of the first dedicated instruments for environmental studies especially for water quality applications (Fu *et al.*, 1996; Hooker and McClain, 2000).

The experience gained from the SeaWiFS mission and the conclusion drawn based on the data extracted from its imaging have encourage NASA's technicians and scientists to design and lunch EOS's MODerate resolution Imaging Spectroradiometer (MODIS) instrument, as well as the National Polar-Orbiting Environmental satellite System (NPOES), and the Visible/Infrared Imager/Radiometer Suite (VIIRS) (Hooker and McClain, 2000).

In 1998, NASA launched the first EOS (Earth Observing System) satellite (EOS AM-1) with five sensors: MODIS (Moderate-resolution Imaging Spectroradiometer), ASTER (Advanced Space-borne Thermal Emission and Reflection Radiometer), CERES (Clouds and the Earth's Radiant Energy System), MOPITT (Measurements of Pollution in the Troposphere), and MISR (Multi-angle Imaging Spectro-Radiometer).

MODIS is a passive, imaging Spectroradiometer. It has 36 bands that cover visible and infrared spectrum. Its swath is 2330 km cross track by 10 km along track at nadir. Its spatial resolution varies from band to band. For example, 250 m (bands 1-2), 500 m (bands 3-7) and 1000 m (bands 8-36). For temporal resolution, it covers the whole earth in 1-2 days. So it has a high spatial and temporal resolution (Morel, 1998). MODIS has been dedicated to provide high quality observations of land surfaces, atmosphere and oceans (Yamaguchi *et al.*, 1998; Jacob *et al.*, 2004).

In March 2002, the European Space Agency (ESA) launched ENVISAT, an advanced polar-orbiting Earth observation satellite which provides measurements of the atmosphere, ocean, land, and ice. MERIS (MEdium Resolution Imaging Spectrometer) was one of the instruments which was on the ENVISAT spacecraft (Gaunter *et al.*, 2010). MERIS spectral range is 390- 1040 nm and has been designed to acquire 15 bands (see

Table 4).

The MERIS spectral range is restricted to the visible and near –infrared part of the spectrum. Table 5 shows a summary of the ocean color sensors.

One of the main reasons for selecting the bands centers is its sensitivity to the most important optically-active water constituents. For example, wavelength 412.5 is sensitive to colored dissolved organic matter and detritus which means it can be used to retrieve data with yellow substances, 442.5, 490, and 665 nm are sensitive to chlorophyll, 510 and 620 nm are sensitive to turbidity, 510 nm is sensitive to red tides, and 665, 681, and 709 nm are sensitive to chlorophyll fluorescence (Doerffer *et al.*, 1999; Gaunter *et al*, 2010).

Table 4: The MERIS specteral bands center and width (Schroeder *et al.*, 2006)

Band	Band Center (nm)	Band Width (nm)
1	412.5	10
2	442.5	10
3	490	10
4	510	10
5	560	10
6	620	10
7	665	10
8	681.25	7.5
9	709	10
10	753.75	7.5
11	761	2.5
12	779	15
13	865	20
14	890	10
15	900	10

Table 5: Summary of ocean color sensors

Sensor	CZCS	SeaWiFS	MODIS	MERIS
Platform (Satellite)	Nimbs-7	OrbView-2	EOS-AM1	Envisat
Agency	NASA	NASA	NASA	ESA
Launched	October-78	August-97	1998	Mar-02
Ground resolution	825 m	1.13 km	1.0km/250m	1.2km/300m
Global coverage	-	2 days	1-2 days	3 days

2.1.3.2. Case 1 and Case 2 waters

Waters which are remotely sensed by satellites have been classified into two types: Case 1 and Case 2 waters (Morel and Prieur, 1977). By definition, Case 1 waters are those waters whose optical properties depend mainly on the phytoplankton and related particles. Case 1 waters are represented in the ocean and open sea waters. The optical properties of Case 2 waters are more complicated as they are not only dependent on the phytoplankton, but also depend on factors such as inorganic matters, suspended solids, and yellow substances. Case 2 waters are represented in the coastal zones and inland waters, lakes and reservoirs (Morel and Prieur 1977, Gordon and Morel 1983; Doerffer *et al.*, 1999; IOCCG, 2000; Schroeder *et al.*, 2007).

In addition to phytoplankton, the optical properties of Case 1 waters also depend on other factors such as the biological debris generated by grazing, the natural decay of phytoplankton organisms, and dissolved organic matter (yellow substances) which results from biological particles. However, the contribution of these factors to the optical properties of Case 1 waters is relatively small and can be considered as a function of phytoplankton concentration (Sathyendranath and Morel, 1983; IOCCG, 2000). On the other hand, the contribution of factors such as yellow substance and suspended matters in Case 2 waters is significant and it is not related to the phytoplankton concentration. Because of this, these factors have to be treated independently.

Figure 5 shows a triangular diagram to differentiate between Case 1 and Case 2 waters based on the concentration of the phytoplankton (P), the yellow substance (Y), and suspended matters (S). The diagram was first presented by Prieur and Sathyendranath (1981), and is now adopted by IOCCG (2000).

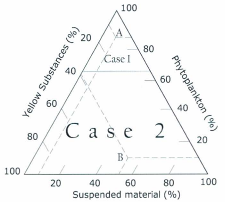

Figure 5: A triangle diagram to classify the water into Case1 and Case2 (IOCCG, 2000)

The procedure to classify a water body is by determining the concentrations of P, Y, and S. For example, given the concentrations of P, S, and Y in a particular point in a water body are 90%, 10 %, and 10%, respectively, from Figure 5, point A, this part of the water body is classified as a Case 1 water. In another case (see Figure 5, point B), the concentrations of P, S, and Y were 10%, 55%, and 42% respectively; the classification for this point is a Case 2 water.

As shown in Figure 5, the optical properties of Case 1 waters are dominated by the presence of phytoplankton, but there is room for the presence of other constituents. On the other hand, the optical properties of Case 2 waters are affected by all three parameters. Case 2 waters are also known as optically-complex waters due to the challenge in differentiating between all the water constituents that affect the optical properties of the water at the same time.

The algorithm used to extract the water constituents concentrations in Case 1 waters is based on the general principle that the signal received by the satellite sensor consists of two main parts. The first part is the water-leaving reflectance and the other part is the atmospheric contribution to the signal. The procedure of removing the atmospheric effect relies on the signal from the Near Infra Red (NIR) bands. This procedure is based on the assumption that the water-leaving reflectance can almost be neglected. This allows the determination of the atmospheric contributions to the recorded signal. The visible portion of the spectrum is then corrected for the atmospheric effect. The water leaving reflectances are then calculated and used to extract the phytoplankton concentrations of the sensed waters (IOCCG, 2000; Chen and Yu, 2009).

The algorithms that have been used to extract the water's constituents in Case 1 waters assume that the contribution of substances other than phytoplankton is negligible. This is one of the two main reasons why there is a need to develop algorithms that take into consideration the presence of all substances that affect the optical properties of Case 2 waters (IOCCG, 2000; Chen and Yu, 2009).

The other main reason for developing algorithms for Case 2 waters is that the assumption of almost negligible water-leaving reflectance in the NIR portion of the spectrum is inaccurate. This assumption may work for Case 1 waters but it is not true for Case 2 waters. Figure 6 shows the spectral signature of Case1 and Case 2 waters. As an example, the presence of yellow substances as well as suspended matters can significantly affect the reflectance of the NIR. This is beside the fact that Case 2 waters are mostly shallow, which means there is a contribution in the reflectance of NIR from the bed of the water body (Schroeder *et al.*, 2007; Chen and Yu, 2009).

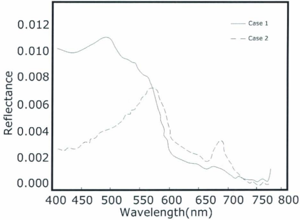

Figure 6: Spectral Signature of Case 1 and Case2 waters (Doerffer *et al.*, 1999)

In order to determine the optical properties of the remote sensed water and the concentrations of its constituents, an atmospheric correction procedure has to be implemented to correct the atmospheric influence on the measured reflectances. The optical-active water constituents then can be retrieved from the satellite imagery (Doerffer and Schiller, 2008). The atmospheric correction procedure removes the effects that result from the interactions between the recorded signals and the atmosphere. These interactions can be in forms like scattering and absorption. The atmospheric procedure also removes the effects of reflection at the water surface from the measured top-of-atmosphere (TOA) radiances. As a result, accurate estimations of the optical-active water parameters can be obtained from the remotely sensed images (Schroeder *et al.*, 2007).

The main idea behind the atmospheric correction is based on the assumption that the ocean color in the near-infrared (NIR) is black (i.e. the amount of reflected radiations from the ocean surface is zero at NIR). As a result, the algorithm of atmospheric correction is to subtract the assumed, atmospheric signals from the total measured reflectance at the TOA (Schroeder *et al.*, 2007; Gaunter *et al.*, 2010). However, it has been proven that this method leads to errors if there are any absorbing aerosols in the atmosphere (Gordon, 1997; Biailey and Werdell, 2006; Gaunter *et al.*, 2010) or over Case 2 waters, where suspended and yellow matter and high concentrations of phytoplankton exist. Yellow substance and suspended matters may generate a considerable reflectance at NIR region of the spectrum (Dekker *et al.*, 1997; Lavender *et al.*, 2005; Morel and Bélanger, 2006; Gaunter *et al.*, 2010).

For Case 2 waters, inland and coastal waters, there are different techniques to remove the atmospheric effects taking into consideration the presence of yellow and suspended matters along with the phytoplankton in the water such as the approach presented by Gao *et al.* (2007). This approach uses wavelengths larger than 860 nm to implement the atmospheric correction, where the contribution of suspended matters is supposed to be a minimum. Other approaches use complete visible and near-infrared (VNIR) range and coupled atmospheric and bio-optical irradiative transfer models to retrieve the atmospheric and water components by a multi-parameter inversion model (Moore *et al.*, 1999; Gaunter *et al.*, 2010). This inversion model can be carried out using either non-linear optimization (Kuchinke *et al.*, 2009) or neural networks (NN) techniques (Schroeder *et al.*, 2007).

These methods are adequate to handle the coupled water-atmospheric radiative transfer problems. However these models may be typically site-specific, i.e. these methods are adequate only for the site where it is developed for. As the outputs of these models are dependent on input values that applied to constrain the bio-optical model (Kuchinke *et al.*, 2009; Gaunter *et al.*, 2010).

Examples of the inversion-based models using NN techniques in atmospheric correction are presented in Doerffer and Schiller (2008). C2R is a processor that has been developed to retrieve case-2 waters' parameters using radiative transfer simulations to train a neural network. The developed neural network is then used for the parameterization of the relationship between the TOA radiance reflectances. The training data collected from the North Sea, Baltic Sea, Mediterranean Sea and North Atlantic (Schroeder *et al.*, 2007) while Boreal and Eutrophic processors have been trained with data collected from Finnish and Spanish lakes, respectively. For WeW/FUB processor, it was especially designed for European coastal waters and uses neural network procedure to correct the atmospheric effects and calculate TOA of MERIS Level1b imagery. The TOA reflectances are then used to retrieve water quality parameters from the C2R, Boreal, Eutrophic, and WeW/FUB processors which are developed as plug-ins in Basic (E) ERS & ENVISAT (A)ATSR and MERIS Toolbox (BEAM). BEAM is a toolbox for processing MERIS and ATSR data (Schroeder *et al.*, 2007; Fomferra and Brockmann, 2005; Doerffer and Schiller, 2008).

Atmospheric correction is another step in retrieving the water constituents process from the satellite data. The retrieving process consists in addition to the atmospheric correction a model that is established to extract the water parameters. Due to the difference in optical properties between Case 1 and Case 2 waters, several new methods have been developed to retrieve the water quality parameters of Case 2 waters from the satellite images. These methods take into consideration the presence of phytoplankton and substances such as yellow and suspended matters. The new algorithms are classified by Giardino *et al.* (2007) into three main methodologies: empirical, semi-empirical, and analytical. The first two methodologies are almost the same but the semi-empirical is used when the spectral properties of the monitored parameters are previously known. Both the empirical and semi-empirical methods use the same technique of extracting the water constituents from the satellite images. The analytical method is discussed in details under model-based approaches in the next few sections. A more comprehensive classification is presented by IOCCG (2000).

The algorithms of Case 2 waters are divided by IOCCG (2000) into mainly two groups: empirical approaches and model-based approaches. The empirical approach is based on establishing statistical relationships between extracted reflectances from the satellite images and coincident measurements of water quality parameters of in-situ concentrations. The relationship can be described by

$$\hat{p} = \alpha \left(\frac{R_1}{R_2}\right)^{\beta} + \gamma \qquad [1]$$

Where $\hat{\mathbf{p}}$ is the physical quantity to be estimated such as chlorophyll concentration and R_i is the reflectance of the spectral channel i. The coefficients α, β, and γ are derived from the regression analysis between the radiance combinations and water quality parameters under investigation. The ratio in the equation is a demonstration of how spectral bands can be combined. There can also be a single band, or other combinations such as addition, multiplication or more complicated combinations of these operations. In case the water parameter is not explained properly by one combination of bands, it is recommended to add more correlated bands or combinations of bands to explain the variability of the measured parameters (Hoge and Swift, 1986; Cippolini *et al.*, 1999).

Further improvement in describing the optical characteristics of the water parameters will be gained if the spectral bands are employed correctly. For example, it is reported that the description of the pigments in chlorophyll case-2 waters can be improved by using wave bands longer than the typical blue and green bands used in Case 1 waters. This decreases the influence of the yellow substances on the algorithm which gives an opportunity to explain the chlorophyll variability in the water (Dekker *et al.*, 1991; Gitelson, 1992; Sathyendranath *et al.*, 1997a; Schalles *et al.*, 1998).

Empirical approaches are simple, easy to derive (even in cases where the in-situ measurements are limited), and easy to implement. This is in addition to the minimal time requirement needed to develop a relationship between the extracted reflectances and in-situ measurements. The empirical relationships can also relate between the water extracted reflectances and the water parameters which are not optically active. This can be done through surrogates that are optically active and have high correlation with the non-active water properties. The results of the empirical approach are stable but there are several limitations that affect the empirical approach. One of the limitations is that the data is only valid for the range and location of the in-situ measurements it was developed for. It is also sensitive to seasonal trends so it has to cover the seasons that may occur in the training area. A further problem in the empirical approach is that it can easily violate the acceptable statistical limits and assumptions that govern the developed relationship between the reflectances and the concentration of water quality parameters.

Many studies have used the empirical approach to develop relationships between the satellite data and in-situ measurements to monitor water quality parameters such as chlorophyll, Dissolved Oxygen (DO), and Chemical Oxygen Demand (COD). These studies used a wide selection of satellite sensors including Landsat TM, MODIS, and MERIS. Gons *et al.* (2002) used the empirical approach to estimate Chl-a concentrations from MERIS data over inland waters and coastal zones. The developed model was calibrated and validated using data collected from IJssel Lagoon in the Netherlands. Two empirical models were developed by Gons *et al*. (2008) for Lake Michigan and Lake Superior to estimate the Chl-a concentrations. The great lakes empirical models revealed a strong linear relationship between MERIS bands 7, 8, and 9 and the in-situ measurements.

Qui *et al.* (2006) used the Landsat TM sensor data to estimate DO and COD concentrations of Dianshan Lake, Shanghai, China. The developed empirical relationships were linear and non-linear relationships between ratios of extracted reflectances from the Landsat TM data and field measurements. Although DO and COD parameters are not optically active, a relationship has been found between them and the extracted water reflectances. This relationship can be explained if it is known that the DO and COD are related to optically-active parameters which are used as surrogates. MODIS data used by Chavula *et al.* (2009a) to estimate the Chl-a concentrations of Malawi Lake in the southern part of Africa through an empirical linear relationship. The relationship was developed between the in-situ measured data by 3 stations and MODIS extracted reflectances.

The second approach to extract the water quality parameters is the model-based method. This approach uses the bio-optical models to explain the relationship between the water-leaving reflectances and the water quality parameters. It also uses the radiative transfer models to imitate the transmission of the electromagnetic waves in the atmosphere and the water. These models simulate the spectra above the water surface or at the TOA for some of the water constituents in different states of the atmosphere. This simulated information is then used to establish an algorithm to inverse map the water constituents from the measured radiances or reflectance spectra. The model-based approach can be implemented using different approaches including: algebraic, non-linear optimization, principal components, and neural network (NN) approaches (IOCCG, 2000; Kuchinke *et al.*, 2009).

The Algebraic approach is the simplest among the model-based methods to retrieve the water quality parameters from the satellite data based on their optical properties. This method uses algebraic expressions to relate semi-analytical models of ocean color to the geophysical product; consequently the water parameters can then be retrieved (Carder *et al.* 1999; Lee *et al.* 1996; Lee *et al.*1999). The disadvantage of this method is that it only can handle limited parameters and variables. In case more variables need to be considered, the other model-based approaches can be used.

The non-linear optimization method inverts a forward model directly by minimizing the differences between the calculated values and measured radiances. The forward model describes the relationship between the radiances recorded by the satellite sensor and the optical properties of the water quality parameters.

The inverted model can be at the water surface level or at the TOA level (Bukata *et al.*, 1981a; Bukata *et al.*,1981b; Bukata *et al.*, 1991). The minimization can be done using many techniques such as the Levenberg-Marquardt and simplex algorithm (Nelder and Mead, 1965). Equation 2 explains the basic technique of the non-linear optimization concept.

$$x^2 = \sum_{\lambda}(L_{sat} - L_{mod})^2 \qquad [2]$$

Where L_{sat} is the radiance measured by the satellite sensor, L_{mod} is the modeled radiance, and the summation is taken over all the wavelengths (λ). The goal of this method is to minimize the difference (x) between the modeled and the measured radiances by varying the concentrations of the model input variables. This method does not depend on a predefined data set while the other analytical techniques such as neural network and principal components, as described in the next two sections, depend on a pre-defined simulated data set. The predefined data sets need a wide range of concentrations of the water parameters where is it difficult to select the range and frequency that represent the natural variability in such approaches. An example of a study that uses non-linear optimization in extracting the water quality constituents is presented in Bukata *et al.*, (1981a, 1981b, 1991). The authors implemented a study in Lake Ontario using information of the inherent optical properties that is tailored for Lake Ontario and the CZCS data. Bukata found that the modeled and measured values of Chlorophyll, suspended matter, and dissolved organic carbon match well.

Doerffer and Fischer (1994) used a TOA model and the simplex method to extract Chlorophyll, suspended solids, colored organic matter concentrations over the North Sea surafce using the CZCS data. It was reported that there is a good agreement between the retrieved data from the satellite imagery and the in-situ measured data which were collected at the same time. One of the advantages of the non-linear optimization method is that the model changes can be modified easily. The major concern of this approach is the long computation time required (Roesler and Perry, 1995; Lee *et al.*, 1999).

In the principal components approach, the optical properties of the atmosphere are considered as a variable in an inversion model. This concept is dissimilar to the empirical approach which implements an atmospheric correction to calculate the water-leaving radiances. The input data of this approach are the TOA reflectances obtained from an ocean-color sensor and the outputs are the optical properties of the atmosphere and the three main constituents of the water (*i.e.* concentration of chlorophyll-a, yellow substances, and inorganic suspended particles). The principal component analysis (PCA) is used to deal with the high correlation between the signals from different wavebands (Mueller, 1973, 1976; Fischer, 1985; Sathyendranath *et al.*, 1989; Sathyendranath *et al.*, 1994).

The principal component approach's algorithm uses a radiative transfer model to generate a data set of radiances at the TOA for water constituents and atmosphere properties as well as the spectral characteristics of the sensor under consideration. Then, PCA is used to analyze the spectral data taking into consideration the high correlation between the bands (Krawczyk *et al.*, 1993; Krawczyk *et al.*, 1999; Neumann *et al.*, 2000).

The main advantage of the principal component approach is the linearity of the algorithm. This advantage gives simple results, and a stable algorithm which leads to the short computational time. This, in turn, gives the algorithm the ability to be implemented on any computer system. As an example, it only requires a few seconds to compute the water constituents and the atmosphere properties of a full inversion of the MOS-IRS satellite sensor scene. The main limitation facing this approach is the non-linearity of the relationship between the water and atmospheric properties from one side and the radiances from the other side. To overcome this limitation, the linear relationships can be implemented on certain sub-ranges which result in the segmentation of the parameters (Neumann *et al.*, 2000).

The last approach that lies under the model-based algorithms is the neural network (NN) approach. The NN consists of a large number of nodes arranged in input and output layers with a number of hidden layers. Each node of a layer is connected to the output of all nodes in the previous layer. All inputs of a node are weighted independently and fed into a logistic or other nonlinear function. In case of remote sensing, the logistic function is appropriate. In the development phase, the input is the reflectances of the satellite imagery and the output is the concentrations of the water constituents (Doerffer and Schiller, 2008).

An example of this approach is the developed procedure for MERIS and MOS data which based on radiance simulation using a Monte Carlo photon-tracing model. This model combines the advantage of realistic radiative transfer model with high speed of a neural network for processing. This algorithm consists of two phases neural network, first is for atmospheric correction and the second is for retrieval of the water constituents (Doerffer and Schiller, 1999; Neumann *et al.*, 2000).

The neural network is a powerful approach for the retrieval of water constituents as well as for atmospheric correction over Case 2 waters. It can gather between the most complicated radiative transfer models with a short time for processing which is useful in real-time processing. One of the disadvantages of this algorithm is that it is valid only for a particular region and season that is trained for. This means that in the case of using this algorithm in two different regions, or two different seasons, it has to be trained twice. In addition to it is relatively expensive to prepare, especially when the model used is complicated and consider a large number of variables that need data collection work (Neumann *et al.*, 2000).

Monitoring water quality using satellite sensors offers many significant advantages. First is the extensive spatial coverage which cannot be offered by any other way of monitoring. This advantage makes it possible to monitor large water bodies by integration with traditional and sensor-based water quality monitoring approaches.

The global coverage is the second advantage offered by satellite water quality monitoring which allows the estimation of water quality in remote and inaccessible areas. Moreover, satellite water quality monitoring is comparable and it has relatively long record of archived imagery. For example, Landsat has an archive since the early 1970s (Hellweger *et al.*, 2004).

Although satellite water quality monitoring has significant advantages, it also has some disadvantages such as the ability to distinguish between different water parameters is limited. In addition, the values extracted from satellite images are considered as relative values and not exact values. Besides, the depth of monitored water is limited to the surface and depends on water clarity. Furthermore, the spatial and temporal resolutions are not always controllable (Hellweger *et al.*, 2004).

Moreover, cloud cover limitation also makes satellite water quality monitoring problematic for areas which has a significant cloud cover. Also, the effect of the atmosphere is significant e.g. if the surrounding atmosphere is turbid it is not possible to extract reliable observations (Hellweger *et al.*, 2004).

The most effective way of water quality monitoring is the integration of traditional, sensor-based, and satellite water quality monitoring approaches. For example, satellite imagery can be used to interpolate and extrapolate the sensor-based observation for large water bodies. This integration decrease the number of in-situ samples and increase the spatial and temporal resolution of the combined method of monitoring (Hellweger *et al.*, 2004).

2.2. Water Quality Monitoring in Lake Manzalah

The monitoring program currently operated by the Egyptian water authorities represented by the Egyptian Drainage Research Institute (DRI), relies on monthly measurements of water quality sampled at drainage channels leading into Lake Manzalah. The measured parameters including a wide selection of the water physical, chemical, and biological parameters such as temperature, color, pH, odour, salinity, turbidity, total dissolved solids, dissolved oxygen, calcium, magnesium, potassium, in addition to, biological oxygen demand, and chemical oxygen demand. Some of these parameters are measured in the field while the other parameters are measured in the laboratory.

However, this program provides insufficient information on the spatial and temporal variation of the parameters of Lake's water quality since there are no measurements taken inside the lake itself. Therefore, there is a need for a water quality monitoring program that provides information about the spatial distribution and temporal variation of water quality parameters. This program provides information used to determine the source of pollution and the current as well as the future status of the polluted areas. Once the problems have been identified, the appropriate decisions could be made to mitigate the affected areas. Moreover, the water quality monitoring program will also provide information about how much the improvement has occurred, if any, in the mitigated polluted areas. .

In 2007, a field investigation campaign took place to investigate the feasibility of monitoring Lake Manzalah's water quality using satellites. The data collected in this field investigation consists of two main parts. First is the in-situ measured data which continue for 4 days, while the second part is the coincident satellite data from MERIS and MODIS sensors. The preliminary results of the investigation show the high correlation between the turbidity (TUR) and band 1 of MODIS and band 7 of MERIS. Besides, the high correlation between total dissolved solids (TDS) and band 1 of MODIS and band 7 of MERIS. It is found that the ratio between band 7 and band 9 of MERIS explains the chlorophyll-a (CHL) concentrations variability in the lake. it was also concluded that the Lake Manzalah has 5 different water quality zones, and in order to establish a quantitative water quality monitoring system based on the satellites, it is recommended to establish real-time water quality monitoring (RTWQM) stations to represent the different regimes of water quality in the lake, which provides a high temporal measurements, to calibrate and validate the models of the water quality parameters. The proposed system will produce and outputs in near-real-time (NRT) to support the decision makers in taking the right decision based on reliable information (Ibrahim *et al.*, 2010).

3. Study Area and Data Collection

This chapter provides a general description of Lake Manzalah, Egypt, followed by a historical overview and the current state of the lake's water quality based on observations from published literature. A description of the current water quality monitoring program in the Lake Manzalah watershed is also presented. In-situ and satellite data collection works are described.

3.1. Study Area

Lake Manzalah is located in the northeastern part of the Nile River delta, Egypt (

Figure 7). Lake Manzalah is the largest of the five northern lakes and bordered by the Mediterranean Sea in the north and the Damietta branch of the Nile in the west. The Suez Canal is located east of Lake Manzalah. Lake Manzalah is located in five administrative Governorates including Damietta, Daqahliya, Ismailiya, Port Said and Sharqiya.

Figure 7 shows the location and borders of Lake Manzalah.

Lake Manzalah (31° 45'- 32° 15' E and 31° 00' – 31° 30') is rectangular in shape. The dimensions of the lake are about 60 km in length and 40 km in width. The lake has an average depth of 1.3 m allowing it to be classified as a shallow lake (Dewidar and Khadr, 2001).

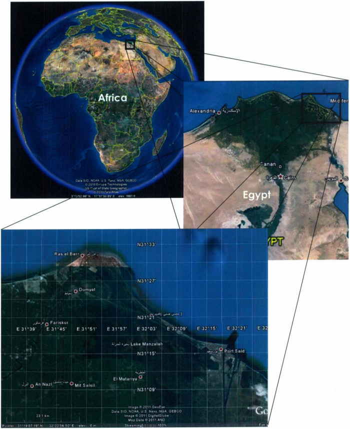

Figure 7: The location and borders of Lake Manzalah (Google Earth, 2010)

There are approximately 1000 small islands scattered in the lake, representing about 9% of the lake's total surface area (Zahran *et al.*, 1989; Khedr, 1997). There are agricultural and aquacultural activities in the area of the lake. The western and southern parts of the Lake are dominated by agricultural activities whereas the northern and eastern parts include the aquacultural activities such as fish farming. The Lake Manzalah production of fish represents around 50 % of the Egyptian fish production (Khalil, 1990; Dewidar and Khadr, 2001).

At the beginning of the twentieth century, the total area of Lake Manzalah was 1700 Km^2. Lake Manzalah area decreased to 1400 km2 in 1937 (Montasir, 1937; Zahran *et al.*, 1989). By 1970, the area was reduced to 1300 Km^2 due to land reclamation (Wakeel and Wahby, 1970). In 1981, the area of Lake Manzalah was 900 Km^2 but by 1988, according to UNDP (1997), the area was cited to be 770 Km^2. In 2000, the Lakes area was around 500 km^2 (C-Core, 2007) Figure 8 shows graphically the reduction in Lake Manzalah's area during the last 100 years.

The reduction in Lake Manzalah's area was attributed to the human activities in the lake area such as land reclamation including: agriculture, building roads and marine aquaculture (Frihy *et al.*, 1998; Dewidar and Khadr, 2001). The rate of reduction in the area of Lake Manzalah in the time between 1922 and 1995 was estimated at 5.22 km^2/year. The most affected parts of the lake by the area decrease were the western and southern regions of the lake besides the growing in the size of the islands inside the lake. Moreover, it was detected that siltation was occurring along the southern and western parts of the lake which was due to the increase of drain water discharge (Dewidar and Khadr, 2001). Various agencies have stated that if land reclamation proceeds at the same rate, the total area will be reduced to 469 Km^2 in a few years (BirdLife International,2009).

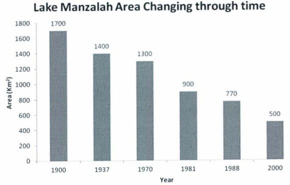

Figure 8: Reduction of Lake Manzalah surface area over the last 100 years

3.1.1 Historical Overview

Historically, Lake Manzalah was known as "Lake Tanis" during the seventeenth century. Lake Manzalah was formed as a result of water accumulation at the spilling points into the Mediterranean Sea. Wakeel and Wahby (1970) note that although the main feeders have dried up, the lake still exists. It was traversed by three (Pelusica, Tanitic and Mendesian) of the seven historical ending branches of the Nile Delta (ECRI, 2003). Figure 9 shows the seven historical branches of the Nile Delta.

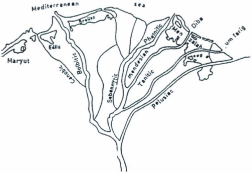

Figure 9: Nile Delta before the seventeenth century (ECRI, 2003).

3.1.2 Lake Manzalah Water Quality Status

Lake Manzalah water system begins from the collection networks of agricultural wastewater in the eastern Nile delta and eastern great Cairo area. The minor drains discharge their collected wastewater into major drains. The major drains, in turn, dispose the collected wastewater into Lake Manzalah. The main drains which flow into Lake Manzalah are the Bahr El-Baqar, Hadous, Farskour, and Lower Serw, see Figure 10.

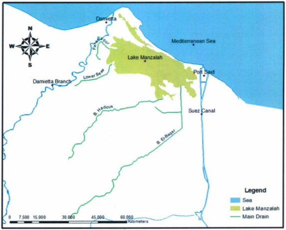

Figure 10: Main drains discharging into Lake Manzalah (DRI, 2010)

The major drains that discharge wastewater into Lake Manzalah are Bahr El-Baqar, Hadous, Lower Serw, and Farskour. The Hadous drain discharges 49 % of the total water discharging into Lake Manzalah, followed by Bahr El-Baqar at 25 %, Lower Serw drain at 13 %, and Farskour drain at 4 % of the total discharge. The remainder of the total discharged water into Lake Manzalah is divided among the Inaniya canal, Port Said canal (fresh water), Ramsis, and Matariya drains. These contribute only 1 to 4 % to the total discharge (ECRI, 2003).

Drains are the main source of pollutants which are transported to the lake. The most polluted drain is the Bahr El-Baqar drain which carries a mixture of treated and untreated waste water from eastern Cairo over a distance of 170 Km. The drain is anoxic over its entire length (UNDP, 1997; El-Baz *et al.*, 2005). It accounts for approximately 25% of the fresh water input and carries 60% of the nutrient loading into Lake Manzalah. The Hadous and Faraskour drains carry predominately agricultural discharges but contribute only half the nutrient loading of the Bahr El Baqar drain to the lake (El-Baz *et al.*, 2005). Although the stated main drains are considered as agricultural drains, they also receive treated and untreated wastewater from municipal and industrial zones that are located in the drains basin (El-Baz *et al.*, 2005).

Lake Manzalah is connected to the Mediterranean Sea through three main connection points. The primary connection is at Bughaz El-Gamil (UNDP, 1997). Other connections occur from time to time at weak points along the narrow sand ridge that separates the lake from the sea (Wakeel and Wahby, 1970). The lake is also connected to the Suez Canal at El-Qabouti (Wakeel and Wahby, 1970; Dewidar and Khadr, 2001).

These open connections allow an exchange of water between the lake and the Sea. As a result, the salinity in the lake varies greatly. While the salinity is low near drain and canal outflows in the south and west, it is high in the extreme north-west. Brackish conditions predominate over much of the remainder of the lake (BirdLife International, 2009). Figure 10 shows the main drains that discharge into Lake Manzalah.

Based on records of daily air temperature at the El-Gamil Metrological Station, the maximum air temperature occurs in August (around 44.0^{o} C) and the minimum occurs in February (around 8.6^{o} C). For rainfalls, they occur only in the winter averaging 112.2 mm per year (Wakeel and Wahby, 1970; Ramdani *et al.*, 2001). Maximum sunshine observations are recorded in June-August. The prevailing wind blows from the south-western direction in January and February, from the north and north west from April to September. The winds predominately blow from the north east in October and November; and south westerly in December.

Published water quality data for Lake Manzalah is fairly limited. Currently, a water quality program which is operated by the Drainage Research Institute (DRI), Government of Egypt, is monitoring the main drains and canals that discharge into the Lake. The monitoring is once per month and there is no regular monitoring of the lake water itself. Some results and conclusions of previous researchers on Lake Manzalah water quality are summarized in the next section.

Lake Manzalah was divided into three main zones from a water quality perspective by Wakeel and Wahby (1970) as follows:

1) The South Eastern region which receives mainly drainage water.

2) The North Eastern region that is affected by both sea water and drainage water.

3) The Western region that is affected by drainage water, sea water and freshwater during floods only.

In terms of water quality parameters,

Table 6 shows some observations as well as the references.

Table 6: Water Quality from various researchers

Parameter	Max.	Min.	Reference
Temperature (C °)	44.0	8.6	(Ramdani *et al.*, 2001)
pH (pH units)	7.86	8.48	(Wakeel and Wahby, 1970)
	8.1	9	(Fishar, 1999)
Chlorophyll (mg/m^3)	Average from 12.66 to 32.38		(Hamza, 1983)

The south-eastern and western parts of the lake are supplied by drains water. The water of these drains carries a considerable load of nutrients including phosphates, nitrates and silicates, in addition to the untreated municipal and industrial sewage water (El Raey *et al.*, 1999; Dewidar and Khadr, 2001). El Raey *et al.*(1999) defined the connections of the south-eastern part of the lake and the drains as a "black spot" due to the heavy load of the contamination that gets into the lake from these connections. This is supported by Siegel *et al.* (1995) who detected high values of Hg (822 ppm), Pb (110 ppm), and Zn (635 ppm) in the bottom sediments of the south-eastern part of the lake.

3.2. Data Collection

Based on the earlier field investigation in 2007, see the literature review, three locations were chosen to setup the water quality monitoring stations. In August 2009, three identical stations were installed in Lake Manzalah. Initially, the locations for the stations 1, 2, and 3 were chosen as shown in Figure 11. However due to several failures station 2 was moved to 2a on September 23, 2009. Figure 12 shows a typical station after installation (C-Core, 2009).

Figure 11: RTWQ station locations in Lake Manzalah (The background is Landsat TM+)

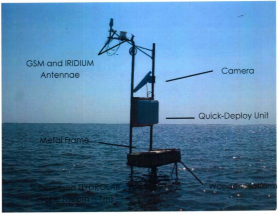

Figure 12: Typical water quality monitoring station (C-Core, 2009)

The water quality instrument used in collecting water quality parameters in Lake Manzalah is the Hydrolab Data Sonde 5X multi probe (DS 5X). (See Figure 13) The Data Sonde is equipped with sensors that can read specific conductance, pH, turbidity, luminescent dissolved oxygen (LDO), chlorophyll, total dissolved solids, temperature, and water level.

The probe can measure conductivity with a range of 0 to 100 mS/cm and accuracy of ± 0.001 mS/cm at a resolution of 0.0001 mS/cm. For pH, the probe can read with a range of 0 to 14 pH units with accuracy of ± 0.2 units at a resolution of 0.01 units. The turbidity measuring range is from 0 to 3000 NTU with an accuracy of ±1% for a range of 0 to 100

NTU, ±3% for a range of 100 to 400 NTU, and ±5 % for a range of 400 to 3000 NTU. The resolution is 0.1 NTU for a range of 0 to 400 NTU and 1 NTU for a range of 400 to 3000 NTU. LDO can be measured with a range of 0 to 60 mg/L and accuracy ± 0.1 mg/L for a range of 0 to 8 mg/L and ± 0.2 for a range of 8 to 60 mg/L. The resolution is 0.01 mg/L.

Chlorophyll can be measured by the probe with a range of 0 to 500 µg/L and an accuracy of ± 3% with a resolution of 0.01 µg/L. The temperature measuring range is from -5 to 50° C with an accuracy of ± 5% and a resolution of 0.01° C. For water depth, it can be measured with a range of 0 to 10 meters with an accuracy of ±0.003 meters and resolution of 0.001 meter. The probe measuring ranges, accuracy, and resolution of all sensors are summarized in

Table 7.

The water quality probe is connected to the data logger using a cable rather than a wireless link. This is due to the need to transfer camera images. The data logger is connected to satellite and GSM modems to transfer the measured data to the office through the Iridium satellite system and the cell phone network.

Figure 13: Hydrolab Data Sonde DS 5X

Table 7: Ranges, accuracy, and resolution of water quality sensors (Hydrolab, 2006)

Sensor	Range	Accuracy		Resolution	
Specific Conductivity (mS/cm)	0 to 100	± 0.001		0.0001	
pH (pH Units)	0 to 14	± 0.2		0.01	
Turbidity (NTU)	0 to 3000	±1%	0-100	0.1	0-400
		±3%	100-400		
		±5%	400-3000	1	>400
Dissolved Oxygen (mg/L)	0 to 60	± 0.1	0-8	0.01	
		± 0.2	8-60		
Chlorophyll (µg/L)	0 to 500	± 3%		0.01	
Temperature (C °)	-5 to 50° C	± 5%		0.01° C	
Water Level (m)	0 to 10	±0.003		0.001	

3.2.1 In-Situ Data

Data was collected from the RTWQ stations from the first day of installation, July 29, up to the end of October, 2009, around 3 months. Collected data points were measured once per hour. For each parameter, the number of points was around 2250 points. In total the collected in-situ points were 42250. The collected data included turbidity (TUR) [NTU], total dissolved solids (TDS) [g/l], pH, Chlorophyll-a (CHL) [µg/l], dissolved oxygen concentration (DO) [mg/l], dissolved oxygen saturation [%], specific conductance (COND) [µS/cm], and temperature (TEMP) [°C].

3.2.2 EO (Satellite) Data

MERIS imagery was the primary satellite data source for this research. Images were collected on July 29, August 1, 7, 10, 13, 16, 19, 20, 23, 26, 29, September 1, 4, 5, 8, 11, 14, 17, 20, October 6, 9, 10, 13, 22, and 25. See Table 8. The collected imageries were in form of N1, MERIS standard format. In total, 25 MERIS scenes were collected.

Table 8: Dates of acquired MERIS images

Jul., 2009	1	8	15	22	**29**	Sep., 2009	**1**	**8**	15	22	29
	2	9	16	23	30		2	9	16	23	30
	3	10	17	24	31		3	10	**17**	24	
	4	11	18	25			**4**	**11**	18	25	
	5	12	19	26			**5**	12	19	26	
	6	13	20	27			6	13	**20**	27	
	7	14	21	28			7	**14**	21	28	
Aug., 2009	**1**	8	15	22	**29**	Oct., 2009	1	8	15	**22**	29
	2	9	**16**	**23**	30		2	**9**	16	23	30
	3	**10**	17	24	31		3	**10**	17	24	31
	4	11	18	25			4	11	18	**25**	
	5	12	**19**	**26**			5	12	19	26	
	6	**13**	**20**	27			**6**	**13**	20	27	
	7	14	21	28			7	14	21	28	

Date when MERIS images acquired

In the next chapter, how the collected RTWQ and satellite data are processed and finally used to develop statistical models will be described in detail.

4. Methodology

This chapter outlines the methodology used to screen the collected in-situ data and the steps taken to extract the reflectances from the satellite data. The statistical methods used to analyze the processed data are also briefly described.

The process of extracting the water quality parameters consists of collecting satellite and in-situ data in concurrently followed by processing both data sets. The concurrent data sets then will be generated. The concurrent data set will be statistically analyzed and models will be then developed. After developing the models, the final water quality parameters maps will be generated. The processing steps are depicted in Figure 14

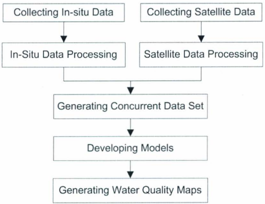

Figure 14: Processing Steps

4.1. In-Situ Data Processing

The in-situ data used to develop the statistical models were collected from July 29 to October 25, 2009. Collected data has been screened since the regular calibration information was not available. The screening process, which was implemented by C-Core staff, excludes the unusual measurements from the data set based on a close examination of the data series acquired at each RTWQ station. Figure 15 shows an example of screened data, appendices A, B, and C show plots for each measured water parameter and the screened measurements. After screening, a total of 56, 34, and 33 points of TDS, TUR, and CHL are paired with the satellite extracted reflectance, respectively. Valid data date ranges after screening are summarized in table 2. The plots in the appendices show the collected data until November 17, 2009. Due to time constraints, the data considered for analysis are only those between July 29 and October 25, 2009 (C-Core, 2009b).

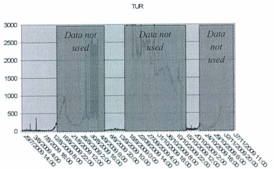

Figure 15: In-situ TUR of station 3 time series shows screened data (C-Core, 2009a)

Table 9: Valid Date Ranges for In-Situ Data (C-Core, 2009a)

Water Quality Parameter	Station 1	Station 2	Station 2a	Station 3
Temperature [°C]	Jul. 28 – Nov. 17	Jul. 29 – Sep. 2 (not Aug. 14)	Sep. 23 – Nov. 17	Jul. 29 – Nov. 2
Total dissolved solids (TDS) [g/l]	Jul. 28 – Nov. 17	Jul. 29 – Sep. 2	Oct.5 – Nov. 17	Jul. 29 – Oct. 14
Turbidity (TUR) [NTU]	Jul. 29 – Aug. 29 Oct.16 – Nov. 1	Jul. 29 – Sep. 2	Sep. 23 – Nov. 17	Jul. 29 – Aug. 13 Sep. 5 – Sep. 18 Oct. 15 – Oct. 21
Chlorophyll-a (CHL) [μg/l]	Jul. 29 – Sep. 9	Jul. 29 – Aug. 19	Oct. 10 – Nov. 17	Jul. 29 – Oct. 14
pH	July 29 – Oct. 13	Jul. 29 – Sep. 2 (not Aug. 14)	Sep. 23 – Nov. 17	Jul. 29 – Oct. 14
Specific conductance [μS/cm]	Jul. 28 – Nov. 17	Jul. 29 – Sep. 2	Oct.5 – Nov. 17	Jul. 29 – Oct. 14
Dissolved oxygen saturation [%]	Jul. 28 – Nov. 17 (not Oct. 13)	Jul. 29 – Sep. 2	Oct.5 – Nov. 17	Jul. 29 – Oct. 14
Dissolved oxygen concentration [mg/l]	Jul. 28 – Nov. 17 (not Oct. 13)	Jul. 29 – Sep. 2	Oct.5 – Nov. 17	Jul. 29 – Oct. 14

4.2. Satellite Imagery Processing

To extract TOA reflectances from the MERIS imageries, the procedure shown in Figure 16 was followed using BEAM 4.6.1 (Fomferra and Brockmann, 2005). The procedure includes collecting and screening the imageries visually to filter the imageries that are partially or fully covered by the clouds, then, subsetting the filtered images to the area of interest.

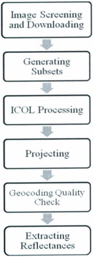

Figure 16: Satellite imagery Processing steps (C-Core, 2009a)

ICOL (The Improved Contrast between Ocean and Land) processor aims to remove the adjacency effect which results from the high reflected electromagnetic waves from the land surrounding the water body. Infrared is the most affected part of the spectrum. The adjacency effect causes overestimation of the atmospheric radiance and a subsequent underestimation of the water leaving radiance. The subsets are then projected to the Egyptian national grid (red zone). The procedure also includes calculating of TOA reflectances. The Radiance-To-Reflectance Conversion Processor converts TOA radiances L_{TOA} into reflectances explained in Equation 3 (Brockmann, 2011).

$$R_{TOA}(\lambda) = \frac{\pi L_{TOA}(\lambda)}{E_o(\lambda)\cos(\theta)} \qquad [3]$$

Where $E0$ and θ are the solar spectral irradiance and the sun zenith angle, respectively. And L_{TOA} is the radiances. The TOA reflectances calculations were implemented using BEAM software's water quality processors. The process also includes geocoding and extracting of the image values from pixels that match each in-situ stations.

The water quality processors generate masks for land and clouds. If the in-situ station falls into a pixel that included in any of these masks, the closest pixel that is valid to represent the station was chosen. The closest pixel, that is not included in the land or cloud masks, is considered as a valid pixel. In addition, a geocoded LANDSAT image acquired March, 2009 was used to verify visually that the chosen location is within the water.

For the atmospheric correction, C-Core staff applied different atmospheric correction procedures on MERIS data including dark object subtraction as well as NN based atmospheric correction procedures associated with Case 2 waters processors in BEAM. The conclusion was there is no significant change in the relationship between the water parameters and the extracted TOA reflectances before and after applying the atmospheric correction (C-Core, 2009a). This is supported by a study done using Landsat TM data by Song et al. (2001) who concluded that the atmospheric correction led to some improvement on the extracted data. But the achieved improvement didn't affect the final results in both cases with and without atmospheric correction. In addition, the improvement which can be achieved after the atmospheric correction is not guaranteed (Dell'Acqua, 2005). As a result, applying wrong atmospheric correction can led to errors that affect the extracted reflectances which, in turn, affect the final results (Chafez, 1988; Gaunter *et al.*, 2010). Based on previous arguments, there is no atmospheric correction applied in this study.

4.3. Statistical Analysis

4.3.1 Preliminary Statistical Analysis for In-situ and Extracted Reflectances

Parametric and non-parametric statistical procedures will be used to investigate the relationship between the primary water quality parameters and the measured TOA reflectances that were extracted from MERIS imagery. Statistical analysis would start with extensive use of graphical procedures such as boxplots, X-Y plots, and normality plots. Logarithmic transformations will be applied when necessary to meet with all necessary assumptions of ANOVA or regression. If assumptions are still not met, nonparametric methods such as Kruskal-Wallis test will be used to compare among the samples and nonparametric correlation analysis such as Kendall's tau and Spearman's rho will be used to assess the association between the in-situ measured parameters and satellite extracted data. For the extracted reflectances, correlation matrix plots will be used to evaluate the correlation between the bands. Correlation analysis will also be used to examine the relationships between individual bands and their combinations and the water quality parameters. The chosen water parameters analyzed were TUR, CHL, and TDS. TUR and CHL were chosen because they are optically active while TDS shows high correlation in previous statistical analysis with the ratios of the extracted reflectances from MERIS imagery.

4.3.2 Models Development

Linear regression analysis will then be used to develop relationships between the water quality parameters and ratios of the MERIS extracted TOA reflectances. Simple and multiple regression models will be investigated. The validation of the relationship will be assessed primarily based on the coefficient of determination (R^2) and the Nash-Sutcliffe coefficient, see $NSE = 1 - \frac{\Sigma(Obs - Pre)^2}{\Sigma(Obs - \overline{Obs})^2}$.

$$NSE = 1 - \frac{\Sigma(Obs - Pre)^2}{\Sigma(Obs - \overline{Obs})^2} \quad [4]$$

Where *Obs* is the in-situ observed measurements, *Pre* is the estimated values using the developed models, and $\overline{Obs}$ is the mean of the in-situ observed values. The Nash-Sutcliffe coefficient evaluates the agreement between a simulated and a reference data. A Nash-Sutcliffe of 1 indicates a perfect agreement between simulated and reference data. So when the simulated and reference data plotted as a scatter plot they should fall on the perfect line i.e. 45 degree line (Nash and Sutcliffe, 1970).

4.3.3 Models selection

The best models should have high R^2 and high NSE in addition to fulfilling all the required assumptions of regression analysis such as normality of residuals, homogeneity of variance, and independence of the residuals.

5. Results

This chapter discusses the results of the statistical analysis of the in-situ data and the regression models developed to predict water quality from satellite imagery data. The models were subsequently used to generate maps showing the distribution of water quality parameters in Lake Manzalah.

5.1. In-situ Water Quality Parameters

For the in-situ measured water quality parameters, Figure 17 shows a plot for the water quality parameters (TDS, TUR, and SPCON) with LOWESS (LOcally Weighted Scatter-plot Smoothing) line. Table 10 and Table 11 display the correlation matrices while Table 12 displays the p-values for calculated Spearman's rho. Due to non-normality distribution of the water quality parameters, Spearman's Rho and Kendall's Tau were used to investigate the correlation between the measured water quality parameters.

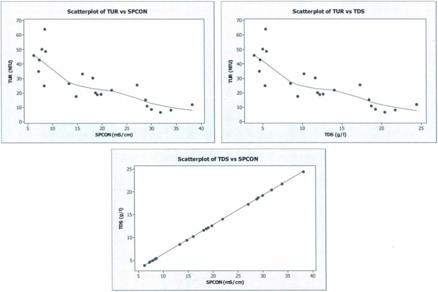

Figure 17: Scatter plots of in-situ water quality parameters (TUR, TDS, and SPCON) (with LOWESS line)

Table 10: Correlation Matrix for In-situ Water Quality Parameters (Spearman's Rho)

	TEMP	PH	SPCON	TDS	DOS	DOC	TUR	CHL
TEMP	1.00	-0.11	-0.20	-0.20	0.45	0.45	0.25	-0.27
PH	-0.11	1.00	0.31	0.31	0.39	0.34	-0.35	-0.27
SPCON	-0.20	0.31	1.00	1.00	-0.01	-0.11	-0.86	-0.43
TDS	-0.20	0.31	1.00	1.00	-0.01	-0.11	-0.86	-0.43
DOS	0.45	0.39	-0.01	-0.01	1.00	0.98	0.03	-0.20
DOC	0.45	0.34	-0.11	-0.11	0.98	1.00	0.13	-0.12
TUR	0.25	-0.35	-0.86	-0.86	0.03	0.13	1.00	0.47
CHL	-0.27	-0.27	-0.43	-0.43	-0.20	-0.12	0.47	1.00

> 0.5 & <-0.5

Table 11: Correlation Matrix for In-situ Water Quality Parameters (Kendall's Tau)

	TEMP	PH	SPCON	TDS	DOS	DOC	TUR	CHL
TEMP	1.00	-0.05	-0.12	-0.12	0.29	0.29	0.16	-0.16
PH	-0.05	1.00	0.21	0.21	0.28	0.25	-0.18	-0.15
SPCON	-0.12	0.21	1.00	1.00	0.02	-0.06	-0.66	-0.34
TDS	-0.12	0.21	1.00	1.00	0.02	-0.06	-0.66	-0.34
DOS	0.29	0.28	0.02	0.02	1.00	0.92	0.04	-0.13
DOC	0.29	0.25	-0.06	-0.06	0.92	1.00	0.12	-0.06
TUR	0.16	-0.18	-0.66	-0.66	0.04	0.12	1.00	0.37
CHL	-0.16	-0.15	-0.34	-0.34	-0.13	-0.06	0.37	1.00

> 0.5 & <-0.5

Table 12: P-value matrix of correlation matrix (Spearman's Rho)

	TEMP	PH	SPCON	TDS	DOS	DOC	TUR
PH	0.629						
SPCON	0.360	0.167					
TDS	0.360	0.167					
DOS	0.036	0.076	0.954	0.954			
DOC	0.034	0.119	0.631	0.631	0.000		
TUR	0.264	0.112	0.000	0.000	0.907	0.564	
CHL	0.223	0.225	0.047	0.047	0.382	0.597	0.027

Table 10 and Table 11 show that there is no correlation between most of the in-situ parameters, however it shows a high correlation between Specific conductivity and TDS, see Figure 17. In fact the correlation is practically perfect. It is also noticed that the there is a high negative correlation between TUR and TDS. Spearman's Rho equals -0.86 and Kendall's Tau equals -0.66, the correlation is statistically significant at $\alpha = 0.05$. For the 34 TUR points concurrent with satellite reflectances, values ranged from 4.8 to 96.4, Figure 18 and 19 show the boxplots of the TUR and Log TUR values by sampling location. The overall median and IQR (InterQuartile Range) are 23.05 and 25.95 NTU, respectively. The summary statistics at each station are shown in Table 13. For the 33 CHL points, the values ranged from 11.64 to 86.53 g/l, with an overall median of 3.15 g/l and IQR of 25.23 g/l. The summary statistics by station is shown in Table 14 and displayed in Figures 17 and 18. For 56 TDS data points, they ranged from 3.93 to 24.4 μg/l with an overall median of 15.35 μg/l and IQR of 8.8 μg/l. The summary statistics at each station is shown in Table 15 and displayed in Figure 22 and 23. As can be seen from the boxplots and summary statistics, the distribution of the data are positive skewed with the possibility of some outliers.

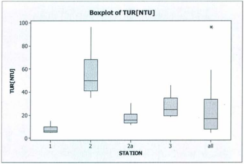

Figure 18: Distribution of TUR at all sampling stations

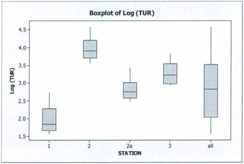

Figure 19: Distribution of Log (TUR) at all sampling stations

Table 13: Descriptive statistics of TUR [NTU]

STATION	N	Mean	StDev	Minimum	Q1	Median	Q3	Maximum
1	13	7.654	3.197	4.800	5.300	6.300	9.800	15.200
2	6	55.45	21.58	35.10	40.95	49.70	68.28	96.40
2a	6	17.48	6.68	11.90	13.10	15.70	20.83	30.50
3	9	27.40	9.26	18.80	19.60	25.10	34.65	45.90
all	34	23.05	19.92	4.80	7.65	16.85	33.60	96.40

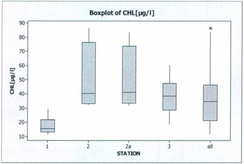

Figure 20: Distribution of CHL at all sampling stations

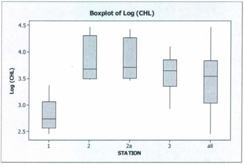

Figure 21: Distribution of Log (CHL) at all sampling stations

Table 14: Descriptive statistics of CHL

STATION	N	Mean	StDev	Minimum	Q1	Median	Q3	Maximum
1	9	17.50	6.04	11.64	13.05	15.45	21.70	29.20
2	4	49.8	25.2	32.4	32.9	40.1	76.3	86.5
2a	4	49.4	23.3	31.9	33.5	41.1	73.6	83.5
3	16	39.00	11.50	18.81	28.69	38.43	47.27	60.23
all	33	35.71	18.12	11.64	21.01	34.57	46.23	86.53

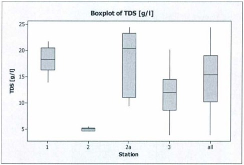

Figure 22: Distribution of TDS at all sampling stations

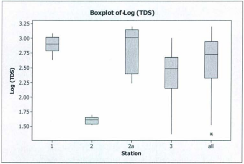

Figure 23: Distribution of TDS at all sampling stations

Table 15: Descriptive statistics of TDS

Station	N	Mean	StDev	Minimum	Q1	Median	Q3	Maximum
1	24	18.229	2.220	13.900	16.225	18.250	20.475	21.700
2	6	4.985	0.315	4.600	4.668	5.005	5.222	5.470
2a	6	18.18	6.31	9.40	11.05	20.40	23.28	24.40
3	20	11.259	4.130	3.930	8.582	12.000	14.525	20.100
all	56	14.316	5.727	3.930	10.200	15.350	19.000	24.400

For TUR, TDS and CHL, Kruskal-Wallis tests were carried out to compare measurements observed at the stations 1, 2, 2a, and 3 respectively. It was found that the median measurements at different sampling locations are significantly different from one another. The test is statistically significant at $\alpha = 0.05$. Table 16 shows the output of the Kruskal-Wallis tests

Table 16: Kruskal-Wallis tests outputs

	H-Value	P-Value
TUR [NTU]	28.52	0.000
CHL [μg/l]	17.29	0.001
TDS [g/l]	33.97	0.000

The distribution of water quality parameters varies from one station to another, as shown in Figure 18-23. This indicates variations in water quality parameters concentrations across the Lake. For TUR, Figure 18, and Figure 19 show that Station 2 records the highest values while Station 1 records the lowest values. Figure 20, and Figure 21 show that the distribution of CHL is similar across Stations 2, 2a, and 3. While the lowest values recorded at Station 1. TDS measurements in Figure 22 and Figure 23 have similar ranges at 1, 2a, and 3. While the lowest median and range recorded at Station 2.

5.2. Satellite-extracted data

The extracted reflectances were combined to get the concurrent data set with the water quality parameters. The result of combination is 34, 33, and 56 points For the TUR, CHL and TDS respectively.

Figure 24-29 show boxplot of the concurrent reflectances before and after Log transformation. The distributions of the reflectances after log-transformation show a higher normality than the distribution without transformation. the reflectances ranged from a minimum of 0.00371 to a maximum of 0.0917. It is noted that most of the bands are positive skewed. All of the individual bands are not normally distributed.

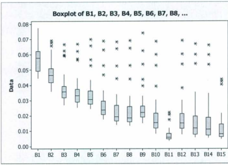

Figure 24: TUR-concurrent reflectances box plot

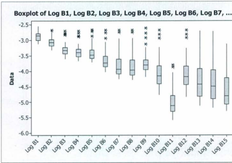

Figure 25: Log transformed TUR-concurrent reflectances box plot

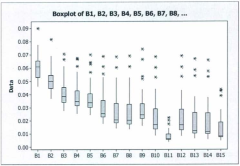

Figure 26: CHL-concurrent reflectances box plot

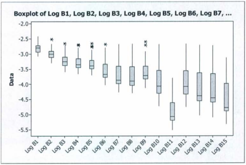

Figure 27: Log transformed CHL-concurrent reflectances box plot

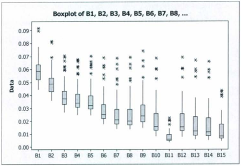

Figure 28: TDS-concurrent reflectances box plot

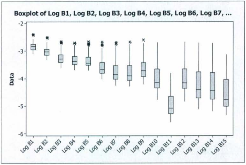

Figure 29: Log transformed TDS-concurrent reflectances box plot

Figures 24 to 29 show that the reflectances are not normally distributed. As a result, non-parametric correlation methods used to investigate the correlation between the individual bands. Figure 30 shows the matrix plot between the MERIS 15 individual bands. Table

17 and 17 present the correlation matrices between the TUR-concurrent reflectances and corresponding p-values matrices. See appendix D for the rest of the figures and tables of concurrent reflectances of CHL and TDS.

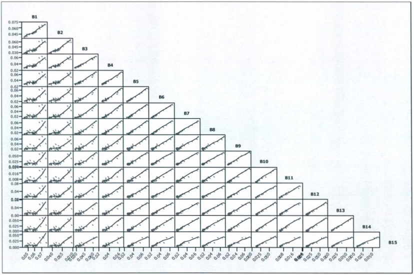

Figure 30: Matrix plot of TUR-concurrent reflectances

Table 17: Correlation Matrix for TUR-concurrent (Spearman Rho)

	B1	B2	B3	B4	B5	B6	B7	B8	B9	B10	B11	B12	B13	B14	B15
B1	1.000	0.983	0.891	0.859	0.745	0.711	0.669	0.677	0.497	0.486	0.473	0.472	0.488	0.470	0.497
B2	0.983	1.000	0.950	0.923	0.825	0.792	0.752	0.759	0.572	0.579	0.559	0.564	0.593	0.578	0.593
B3	0.891	0.950	1.000	0.990	0.938	0.919	0.893	0.901	0.701	0.739	0.724	0.726	0.765	0.754	0.760
B4	0.859	0.923	0.990	1.000	0.965	0.952	0.928	0.936	0.747	0.778	0.763	0.767	0.805	0.793	0.789
B5	0.745	0.825	0.938	0.965	1.000	0.991	0.977	0.980	0.761	0.806	0.808	0.800	0.858	0.852	0.843
B6	0.711	0.792	0.919	0.952	0.991	1.000	0.984	0.991	0.781	0.837	0.840	0.832	0.889	0.886	0.867
B7	0.669	0.752	0.893	0.928	0.977	0.984	1.000	0.994	0.731	0.814	0.835	0.809	0.881	0.881	0.864
B8	0.677	0.759	0.901	0.936	0.980	0.991	0.994	1.000	0.782	0.854	0.872	0.850	0.909	0.907	0.893
B9	0.497	0.572	0.701	0.747	0.761	0.781	0.731	0.782	1.000	0.964	0.913	0.967	0.895	0.877	0.880
B10	0.486	0.579	0.739	0.778	0.806	0.837	0.814	0.854	0.964	1.000	0.967	0.998	0.960	0.951	0.951
B11	0.473	0.559	0.724	0.763	0.808	0.840	0.835	0.872	0.913	0.967	1.000	0.966	0.962	0.952	0.961
B12	0.472	0.564	0.726	0.767	0.800	0.832	0.809	0.850	0.967	0.998	0.966	1.000	0.963	0.954	0.954
B13	0.488	0.593	0.765	0.805	0.858	0.889	0.881	0.909	0.895	0.960	0.962	0.963	1.000	0.997	0.973
B14	0.470	0.578	0.754	0.793	0.852	0.886	0.881	0.907	0.877	0.951	0.952	0.954	0.997	1.000	0.969
B15	0.497	0.593	0.760	0.789	0.843	0.867	0.864	0.893	0.880	0.951	0.961	0.954	0.973	0.969	1.000

range(0.7 to 1.0)

Table 18: P-values Matrix of Spearman's Rho Correlation Matrix for TUR-concurrent Bands

TUR	B1	B2	B3	B4	B5	B6	B7	B8	B9	B10	B11	B12	B13	B14
B2	0.000													
B3	0.000	0.000												
B4	0.000	0.000	0.000											
B5	0.000	0.000	0.000	0.000										
B6	0.000	0.000	0.000	0.000	0.000									
B7	0.000	0.000	0.000	0.000	0.000	0.000								
B8	0.000	0.000	0.000	0.000	0.000	0.000	0.000							
B9	0.003	0.000	0.000	0.000	0.000	0.000	0.000	0.000						
B10	0.004	0.000	0.000	0.000	0.000	0.000	0.000	0.000	0.000					
B11	0.005	0.001	0.000	0.000	0.000	0.000	0.000	0.000	0.000	0.000				
B12	0.005	0.001	0.000	0.000	0.000	0.000	0.000	0.000	0.000	0.000	0.000			
B13	0.003	0.000	0.000	0.000	0.000	0.000	0.000	0.000	0.000	0.000	0.000	0.000		
B14	0.005	0.000	0.000	0.000	0.000	0.000	0.000	0.000	0.000	0.000	0.000	0.000	0.000	
B15	0.003	0.000	0.000	0.000	0.000	0.000	0.000	0.000	0.000	0.000	0.000	0.000	0.000	0.000

The matrix plots and correlation matrices show that the bands which are close to each other are high correlated. For example Band 1 is high correlated with Bands 2, 3 and 4 and less correlated to Bands 12, 13, 14 and 15.

5.3. Models

The correlation between the measured water quality parameters and extracted reflectances from MERIS imagery showed no statistically significant correlations between any of the measured water quality parameters and the individual TOA reflectances of the 15 MERIS bands. However, the ratios of some of the bands showed high correlations with the water parameters. Spearman's Rho used because of the nonlinearity of the water quality parameters as well as the reflectances. The correlation coefficients are shown in Table 19. All correlations are statistically significant at α=0.05. Appendix E shows the correlation matrices between the water quality parameters and the extracted reflectance ratios more fully.

Table 19: Correlation between TOA band ratios and water parameters

	TUR	CHL	TDS
B9/B5	0.64	0.24	-0.56
B9/B6	0.84	0.54	-0.70
B9/B7	0.89	0.81	-0.67
B9/B8	0.83	0.80	-0.61
B11/B7	0.64	0.38	-0.52
B12/B15	0.55	0.60	-0.34

Where B5 = Band 5, B6 = Band 6, B7 = Band 7, B8 = Band 8, B9 = Band 9, B11 = Band 11, B12 = Band 12, and B15 = Band 15

The highlighted cells represent the highest correlated band ratios and water quality parameters. B9/B7 is highly correlated with TUR and CHL. And B9/B6 is highly correlated with TDS. Scatter plot between TUR, CHL, and TDS vs. B9/B7, B9/B7, and B9/B6 respectively are shown in Figure 31, Figure 32, and Figure 33.

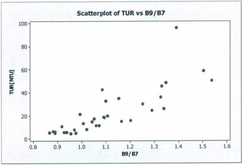

Figure 31: Scatter plot TUR vs. B9/B7

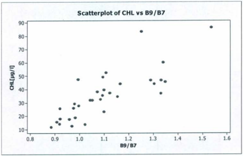

Figure 32: Scatter plot CHL vs. B9/B7

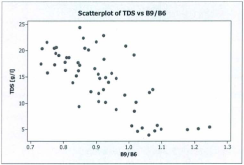

Figure 33: Scatter plot TDS vs. B9/B6

The previous analyses show linearity in the relationship between the measured water quality parameters and the extracted reflectances. As a result, linear regression models were developed between the water quality parameters and the extracted reflectances from MERIS. All water quality and image extracted variables were log-transformed to better fulfill the assumptions of the regression. First, two and three explanatory variables models were tried. At α=0.05, the significant model was the Log (TDS) model vs. Log (B9/B5) and Log (B9/B8). By trying one explanatory variable, both TUR and CHL models vs. B9/B7 were significant at α=0.05. All developed models are presented in Equations 5, 6, and 7. Figure 34 to 38 show the graphical representation of the developed models. Figure 34 shows that the TUR model fits the data points very well, which can be described in the high value of R^2 that equals 0.78. CHL model, Figure 35, also shows good fit with the data points, R^2 equals 0.64. Figure 36 show the graphical representation of the TDS model, the figure reveals good fit between the TDS model and the data points.

Log (TUR) = 1.04 + 4.55 Log (B9/B7)……………….……………………[5]

Log (CHL) = 1.39 + 2.98 Log (B9/B7) …………………………………... [6]

Log (TDS) = 1.01 - 1.34 Log (B9/B5) - 1.86 Log (B9/B8)……..…………[7]

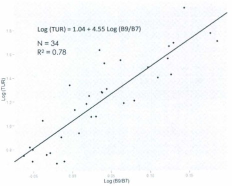

Figure 34: TUR model

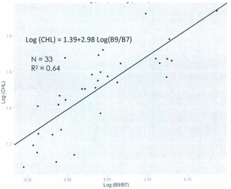

Figure 35: CHL model

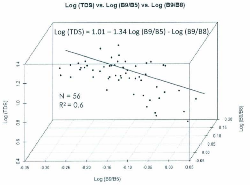

Figure 36: TDS model

Models statistics are shown in Table 20. The statistics reveal that the coefficient of determination (R2) is higher for TUR than CHL and TDS. For the NSE coefficient, TUR also has he higher values then CHL and TDS. The table also shows the number of points as well as the P-values of the developed models, Average and the standard deviation of the residuals.

Figure 37, Figure 38, Figure 39 show the calculated vs. measured TUR, CHL, and TDS plots respectively as well as the 45 degree line.

Table 20: The Models Statistics

Model	R^2	NSE	n	P-value	Average (Residuals)	σ (Residuals)
TUR	76.9	0.76	34	0.00	1.37 [NTU]	12.45 [NTU]
CHL	64.5	0.64	33	0.00	1 [μg/l]	11.24 [μg/l]
TDS	60.0	0.61	56	0.00	0.46 [g/l]	4.2 [g/l]

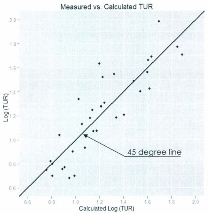

Figure 37: Measured vs. Calculated TUR values

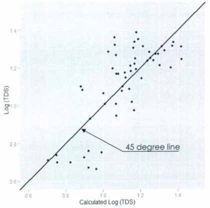

Figure 38: Measured vs. calculated TDS values

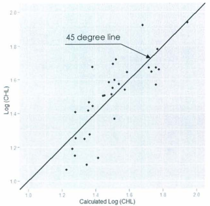

Figure 39: Measured vs. calculated CHL

For the uncertainly of the developed models, the average of the residuals as shown in the previous table are 1.37 [NTU], 1 [μg/l], and 0.46 [g/l] for TUR, CHL, and TDS respectively, and the standard deviation of the residuals are 12.45 [NTU], 11.25 [μg/l], and 4.26 [g/l] for TUR, CHL, and TDS respectively.

By applying the developed equations on all the image pixels, a map of water quality parameters can be obtained. As an example of the developed water quality map,

Figure 40,

Figure 41, and

Figure 42 are the water quality parameters maps which generated by applying the developed equations on the entire water surface of the Lake. Used image in this example was acquired July 29th, 2009. And the maps produced for TUR, CHL, and TDS. As these values are log transformed, the maps are showing the median estimated values only. For the values displayed in the map key, Table 21 shows the 95% confidence intervals for each displayed value.

Table 21: 95 % Confidence intervals for values displayed in the maps key

<table>
<tr><th></th><th></th><th>Value</th><th>Lower Limit</th><th>Upper Limit</th></tr>
<tr><td rowspan="3">TUR</td><td rowspan="3">[NTU]</td><td>8</td><td>6.18</td><td>11.29</td></tr>
<tr><td>25</td><td>17.38</td><td>41.38</td></tr>
<tr><td>35</td><td>21.85</td><td>49.28</td></tr>
<tr><td rowspan="3">CHL</td><td rowspan="3">[μg/l]</td><td>20</td><td>18.29</td><td>23.17</td></tr>
<tr><td>35</td><td>31.77</td><td>53.99</td></tr>
<tr><td>45</td><td>32.48</td><td>58.57</td></tr>
<tr><td rowspan="3">TDS</td><td rowspan="3">[g/l]</td><td>10</td><td>7.99</td><td>11.74</td></tr>
<tr><td>15</td><td>14.00</td><td>17.67</td></tr>
<tr><td>20</td><td>17.67</td><td>23.41</td></tr>
</table>

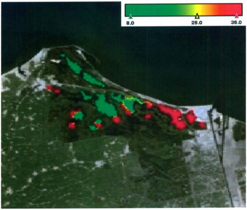

Figure 40: TUR [NTU] map July 29th, 2009.

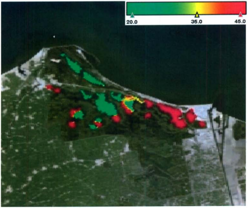

Figure 41: CHL [µg/l] map July 29th, 2009.

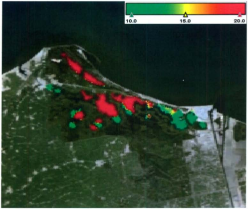

Figure 42: TDS [g/l] map July 29th, 2009.

The complete set of the median water quality parameters maps are attached with this thesis in appendices F, G, and H. Based on the final water quality distribution maps, Lake Manzalah can be divided into three different areas: Areas 1, 2, and 3. Area 1 includes the south-eastern and south-western part of the Lake (see Figure 43) which is characterized by high TUR, high CHL, and low TDS concentrations. The reason for the high concentrations of CHL and TUR is the contact between this part of the lake and the agricultural drains that flow into the lake. Area 2 is the northern part of the lake which is located parallel to the coast of the Mediterranean. Area 2 has low values of TUR and CHL concentrations, but it has high values of TDS concentration as a result of the connection with the salt water in the Mediterranean Sea. Area 3 is the area in between area 1 and 2. As a result, it has medium values of all water parameters under study (TUR, CHL, and TDS). The next chapter is a discussion about the results and the conclusion in addition to the recommendations from this thesis.

Figure 43: Lake Manzalah water quality Areas

6. Discussion and Conclusions

This chapter discusses the results obtained from the study and the issues that were encountered with the data collection, and statistical model development. The limitations of developed models are also discussed. This is followed by conclusion and recommendations for further study.

6.1. Discussion

Band 9 is common in all band ratios that are highly correlated with the in-situ measured water quality parameters. This is likely because Band 9 was originally tailored for sensing the water quality parameters which are optically active in Case 2 waters. Band 9 is located in the chlorophyll-a spectrum's peak (Doerffer *et al.*, 1999). Since no atmospheric correction procedure was implemented for this study, the ratio between MERIS bands can be considered as a relative atmospheric correction (C-Core, 2009).

The proposed method in this thesis is simple and easy to implement. It is not limited to Lake Manzalah only, it can be adapted to any water body that is monitored using the RTWQ network. In addition, it can develop a relationship between some of the non-optically active water parameters such as TDS and the extracted reflectances from the satellite imagery. The explanation of the relationship between TDS and the extracted reflectances can be attributed to the high correlation between the TDS and the TUR which is optically active. TUR is used as a surrogate to develop the TDS model. In the future, the models can be extended to other inactive water quality parameters such as pH and Temperature using a corresponding optical active surrogate.

By collecting more coincident in-situ and satellite measurements, it is expected to improve the developed models. The improvement would include the existing models as well as developing new models for predicting other parameters that are already being measured using the in-situ water quality monitoring stations. The parameters that can be included in the improvement are dissolved oxygen, ammonium, and pH.

The developed models only can capture the variation during the span of data collection time (August 2009 – October 2009). Therefore, the captured variation in the lake's water quality is confined to one season. Collecting more coincident in-situ and satellite data can improve the developed models to include other seasons which might be exist in the lake water quality cycle. The improvements that can be obtained from collecting more coincident data points also include formulating new models for areas within the same lake system that has different water quality characteristics.

For the uncertainty of the developed models, the average of the residuals are 1.37 [NTU], 1 [μg/l], and 0.46 [g/l] for TUR, CHL, and TDS respectively, and the standard deviation of the residuals are 12.45 [NTU], 11.25 [μg/l], and 4.26 [g/l] for TUR, CHL, and TDS respectively. The reason that the average of the residuals not equal to zero is due to the log transformation that applied to the water parameters quality data sets. But the predicted values are median values not means so the bias is acceptable

As the developed models are regression-based models, it is important to note that the use of the developed models is limited to the range of measured data and the case study area. These models are not suitable for case studies other than Lake Manzalah, but the procedure of developing these models can be implemented independent of location. Therefore, the developed models are only suitable for generating Lake Manzalah's median water quality distribution maps for the imagery that was acquired between July 29 and October 25, 2009. Due to their limitations, the developed models need to be enhanced by collecting more satellite and in-situ data. The collection of this data is needed to update and validate the developed models.

6.2. Conclusions

In this research, the RTWQ monitoring stations integrated with the satellite extracted water quality data. The final output is a water quality distribution maps. The conclusions which can be drawn from this thesis are:

The integration between RTWQ monitoring and satellite systems using the communication technologies generates a new water quality monitoring system using the advantages of both systems. The new system final output is a water quality map that has a moderate spatial resolution (300m) as well as a high temporal resolution (3 days).

The proposed procedure does not depend on bio-optical irradiative transfer models, which are unique for each site. The proposed procedure instead depends on a simple linear relationship between the in-situ RTWQ monitoring measurements and extracted MERIS imagery reflectances.

From the water quality point of view, Lake Manzalah is divided into three different areas; each with its own water quality characteristics. Area 1 is the southeastern and southwestern parts, area 2 is the northern part of the Lake and area 3 is the area in between area 1 and area 2.

The water quality characteristics throughout the lake are influenced by the proximity to the Mediterranean Sea from the North and the flows into the lake of the agricultural drains from the Southeast and Southwest.

6.3. Recommendations

Collect more coincident points to enhance and update the developed models to cover all seasons and to try other methods of relating the in situ data with satellite data such as artificial neural networks, or principal component regression.

Develop individual models for different areas of the lake. However this will need additional data from each area.

Analyze the bands reflectances using the PCA as the correlations between the extracted reflectances are high.

Extend the number of water quality variables to include variables such as Dissolved oxygen and pH.

Examine the proposed approach to other lakes in both Egypt and Canada that have existing RTWQ monitoring systems. This will ensure that the proposed approach is universally applicable.

7. References

Antoine, D., André, J.-M. and Morel, A. (1995) Oceanic primary production. 2. Estimation at global scale from satellite (Coastal Zone Color Scanner) chlorophyll. Global Biogeochem. Cycles, 10, 57–69.

Arar, Elizabeth J. and Collins, Gary B., In Vitro Determination of Chlorophyll-a and Pheophytin-a in Marine and Freshwater Phytoplankton by Fluorescence, National Exposure Research Laboratory Office of Research and Development, U.S. Environmental Protection Agency. 1997. Available online at http://www.epa.gov/microbes/m445_0.pdf [Accessed: Jan 13, 2011].

Avery, Thomas Eugene, and Graydon Lennis Berlin (1992). Fundamentals of Remote sensing and Airphoto Interpretation, 5th edition.

American Public Health Association (AWWA). 1995, Standard Methods for the Examination of Water and Wastewater. 19th Edition, Method 2130 Turbidity, pp. 2-8 to 2-9

Bailey, S.W. and Werdell, P.J., A multi-sensor approach for the on-orbit validation of ocean color satellite data products(2006), Remote Sensing of Environment 102 (2006), pp. 12–23

Barakat AO (2003) Assessment of Persistent Toxic Substances in the Environment of Egypt. Environment International 9: 181–195

Barale, V., & Schlittenhardt, P. M. (1993). Ocean colour: theory and applications in a decade of CZCS experience, ECSC, EEC, EAEC, Brussels and Luxembourg, 367 pp.

Bartram, J., Balance, R., 1996. Water Quality Monitoring: A Practical Guide to the Design and Implementation of Freshwater Quality Studies and Monitoring Programmes. Chapman & Hall, London.

Bastos, A. Catarina, Magan, Naresh(2006). Potential of an electronic nose for the early detection and differentiation between Streptomyces in potable water.Sensors and Actuators B 116 (2006) 151–155

Bastos, A. Catarina, Magan, Naresh (2006). Potential of an electronic nose for the early detection and differentiation between Streptomyces in potable water Sensors and Actuators B 116 (2006) 151–155

Becker Richard H., Sultan, Mohamed I., Boyer, Gregory L., Michael R. Twiss, Elizabeth Konopko, Mapping cyanobacterial blooms in the Great Lakes using MODIS, Journal of Great Lakes Research, Volume 35, Issue 3, September 2009, Pages 447-453, ISSN 0380-1330, DOI: 10.1016/j.jglr.2009.05.007.

Behrenfeld, M. J. and Falkowski, P. G. (1997) Photosynthetic ratesf derived from satellite-based chlorophyll concentration. Limnol. Oceanogr.,42,1–20.

Bierman, P., Lewis M., Ostendorf B., Tanner J. (2011). A review of methods for analysing spatial and temporal patterns in coastal water quality. Ecological Indicators, Volume 11, Issue 1, January 2011, Pages 103-114

Brockmann, (2011). BEAM online help. *Retrieved from* www.brockmann-consult.de Jan., 2011.

Binding, Caren E., Jerome, John H., Bukata, Robert P., Booty, William G., (2008)Spectral absorption properties of dissolved and particulate matter in Lake Erie, Remote Sensing of Environment, Volume 112, Issue 4, 15 April 2008, Pages 1702-1711

BirdLife International (2009) Important Bird Area factsheet: Lake Manzala, Egypt. Downloaded from the Data Zone at http://www.birdlife.org on 24/6/2010

Bishai, H. M. & S. F. Yuossef, 1977. Some aspects of the hydrography, physico-chemical characteristics and fisheries of lake Manzala. UAR Bull Inst. Oceanogr. Fish 7: 1–30.

Bourgeois W, Burgess JE and Stuetz RM, On-line monitoring of wastewater quality: a review. J Chem Technol Biotechnol 76: 337–348 (2001). DOI:10.1002/jctb.393.

Brignell, J.E. (1996) , Measurement and control feature on intelligent instruments, Measurement and Control 29 (1996) 164.

Bukata, R. P., Bruton, J. E., Jerome, J. H., Jain, S. C. and Zwick, H. H. (1981). Optical water quality model of Lake Ontario. 2. Determination of chlorophyll a and suspended mineral concentrations of natural waters from submersible and low altitude remote sensors. Appl. Optics 20: 1704-1714.

Bukata, R. P., Bruton, J. E., Jerome, J. H., Jain, S. C. and Zwick, H. H. (1981a). Optical water quality model of Lake Ontario. 2. Determination of chlorophyll a and suspended mineral concentrations of natural waters from submersible and low altitude remote sensors. Appl. Optics 20: 1704-1714.

Bukata, R. P., Jerome, J. H., Bruton, J. E., Jain, S. C. and Zwick, H. H. (1981b). Optical water quality model of Lake Ontario. 1. Determination of the optical cross sections of organic and inorganic particulates in Lake Ontario. Appl. Optics 20: 1696-1703.

Bukata, R. P., Jerome, J. H., Kondratyev, K. Y. and Pozdnyakov, D. V. (1991). Satellite monitoring of optically-active components of inland waters: an essential input to regional climate change impact studies. J. Great Lakes Res 17: 470-478.

Campbell, J., 2001. Map Use and Analysis, fourth edition. McGraw Hill, 372p.

Canhoto, O., Magan, N., Electronic nose technology for the detection of microbial and chemical contamination of potable water, Sens. Actuators B 106 (2005) 3–6.

Carder, K. L., Chen, F. R., Lee, Z. P., Hawes, S. K. and Kamykowski, D. (1999). Semianalytic Moderate- Resolution Imaging Spectrometer algorithms for chlorophyll a and absorption with bio-optical domains based on nitrate- depletion temperatures. J. Geophys. Res. 104: 5403-5421.

Carpenter, S. R., N. F. Caraco, D. L. Correll, R. W. Howarth, A. N. Sharpley, and V. H. Smith. (1998). Nonpoint pollution of surface waters with phosphorus and nitrogen. Ecological Applications, 8:559–568.

Cavalli, Rosa M., Laneve G., Fusilli L., Stefano Pignatti, Federico Santini, (2009). Remote sensing water observation for supporting Lake Victoria weed management, Journal of Environmental Management, Volume 90, Issue 7, May 2009, Pages 2199-2211

C-CORE (2007). Satellite Monitoring of Lake Water Quality in Egypt — Validation and Final Project Report (D46 and D50), C CORE Report R 07 042 404 v1.1, December 2007

C-CORE (2009a) Satellite Monitoring of Lake Water Quality in Egypt – Enhanced System Demonstration: System Validation and Assessment Report (D4) and Final Project Report (D5). C-

CORE Report R-09-056-631, December 2009.

C-CORE (2009b). Satellite Monitoring of Lake Water Quality in Egypt – Enhanced System Demonstration Technical Specification Vol. 1: User Requirements, Non-EO System Components, and Configuration Scenarios, C-CORE Report R-08-051-631 v1.0, January 2009.

Chafez, P. (1988). An improved dark-object subtraction technique for atmospheric scattering correction of multispectral data, Remote Sensing of Environment Volume 24, Issue 3, April 1988, Pages 459-479

Chambers, P.A., M. Guy, E.S. Roberts, M.N. Charlton, R. Kent, C. Gagnon, G. Grove and N. Foster, 2001. Nutrients and their impact on the Canadian environment, Agriculture and Agri-Food Canada, Environment Canada, Fisheries and Oceans Canada, Health Canada and Natural Resource Canada. 241 p.

Chapman, D. (Ed.), 1996. Water Quality Assessments. A Guide to the Use of Biota, Sediments and Water in Environmental Monitoring. Chapman & Hall, London.

Charef, Azedine, Ghauch, Antoine, Baussand, Patrick and Martin-Bouyer, Michel. Water quality monitoring using a smart sensing system (2000), Measurement, Volume 28, Issue 3, October 2000, Pages 219-224

Chavula, Geoffrey ; Brezonik, Patrick ; Thenkabail, Prasad ; Johnson, Thomas ; Bauer, Marvin (2009a). Estimating chlorophyll concentration in Lake Malawi from MODIS satellite imagery. Physics and Chemistry of the Earth, Parts A/B/C, Volume 34, Issue 13-16, 2009, Pages 755-760

Chavula, G., Brezonik, P., Thenkabail, P., Thomas Johnson, Marvin Bauer, (2009b) Estimating chlorophyll concentration in Lake Malawi from MODIS satellite imagery, Physics and Chemistry of the Earth, Parts A/B/C, Volume 34, Issues 13-16, 9th WaterNet/WARFSA/GWP-SA Symposium: Water and Sustainable Development for Improved Livelihoods, 2009, Pages 755-760, ISSN 1474-7065, DOI: 10.1016/j.pce.2009.07.015.

Chen, Xiaolin and Yu, Zhifeng (2009), Remote Sensing of Water Environment, Geospatial Technology for Earth Observation, Pages 431-471, Springer US, SN 978-1-4419-0050-0.

Christensen, V.G., Rasmussen, P.P., and Ziegler A.C. (2001). Real-time water-quality monitoring and regression analysis to estimate nutrient and bacteria concentrations in Kansas streams: in Melching, C.S., and Alp, Emre, eds., Conference proceedings, 5th International Conference, Diffuse/nonpoint pollution and watershed management, Milwaukee, Wisconsin, June 10-15, 2001: International Water Association, CD-ROM, session 9, p. 1-9.

Cipollini, P., Barale, V., Davidov, A. and Melin, F. (1999). Updated MOS bio-optical algorithms in the Northwestern Black Sea. 3rd International Workshop on MOS-IRS and Ocean Colour, Wissenschaft und Technik Verlag, Berlin, 93-100.

Colwell (1983), Editor, Manual of Remote Sensing Vol. I, American Society of Photogrammetry, Falls Church, Va.-USA (1983)

Colwell, Robert N., ed.(1983) Manual of Remote Sensing. Washington, DC.: American society of photogrammetery. Vol I

Dall'Olmo, G., Gitelson, Anatoly A., Rundquist, Donald C., Leavitt, B., Barrow ,T., Holz, John C. (2005). Assessing the potential of SeaWiFS and MODIS for estimating chlorophyll concentration in turbid productive waters using red and near-infrared bands. Remote Sensing of Environment 96 (2005) 176 – 187.

Dekker, A. G., Malthus, T. J. and Seyhan, E. (1991). Quantitative modeling of inland water quality for high-resolution MSS systems. IEEE Trans. Geosci. Remote Sens. 29: 89-95.

Dekker, A.G., Hoogenboom, H.J., Goddijn, L.M. and Malthus, T.J. (1997), The relation between inherent optical properties and reflectance spectra in turbid inland waters, Remote Sensing Reviews 15, pp. 59–74.

Dell'Acqua, F. (2005). Testing the effect of atmospheric correction on urban hyperspectral data through classifier performance comparison: A case study. 5th International Symposium Remote Sensing of Urban Areas (URS 2005), Netherlands.

Dewettinck, T., Hege, K. Van. and Verstraete, W. (2001). The Electronic Nose as A Rapid sensor for Volatile Compounds in Treated Domestic Wastewater. Wat. Res. Vol. 35, No. 10, pp. 2475–2483, 2001

Dewidar, Kh. and Khedr, A. (2001). Water quality assessment with simulations Landsat-5 TM at Manzalah Lagoon, Egypt. Hydrobiologia 457: 49-58, 2001.

Doerffer, R. and Fischer, J. (1994). Concentrations of chlorophyll, suspended matter, and gelbstoff in case II waters derived from satellite coastal zone color scanner data with inverse modeling methods. J. Geophys. Res. 99: 7457-7466.

Doerffer, R.and Schiller H. (2007). the MERIS Case II water algorithm. International Journal of Remote Sensing, 28, 517-535.

Doerffer, R., Schiller, H., May (2008). MERIS regional coastal and lake case 2 water project atmospheric correction ATBD. Tech. rep., GKSS Research Center 21502 Geesthacht.

Doerffer, R., Rensen K. Sé, Aiken, J. (1999). MERIS potential for coastal zone applications. int. j. remote sensing, 1999, vol. 20, no. 9, 1809 – 1818.

DRI, (2010). GIS data base of Drainage research institute (DRI), National Water Research Center (NWRC), Ministry of Water Resources and Irrigation (MWRI).

Dowidar, N.M. and W.R. Hamza. (1983). Primary Productivity and biomass of Lake Manzalah, Egypt, RAPP. P. –V. REUN. CIESM, Vol. 28, No. 6, pp. 189-192.

Downing. J. (2005), Turbidity monitoring, in Environmental Instrumentation and Analysis Handbook, R.D. Down, J.H. Lehr, Ed. New Jersey: John Wiley & Sons, Inc., 2005, pp. 511-546.

Ebaid , Hala M.I., Ismail, Sherine S. (2010).Lake Nasser evaporation reduction study.Journal of Advanced Research, Volume 1, Issue 4, October 2010, Pages 315-322.

Environmental Study on Manzala Lake, Environment and Climate Research Institute (ECRI), National Water Research Center (NWRC) , Egypt, 2003.

Environment Canada. Retrieved January, 2011. www.ec.gc.ca

El-Baz, Amro A., Kamal M., Ewida, T., Shouman M. Abbas, El-Halwagi, Mahmoud M., (2005). Material flow analysis and integration of watersheds and drainage systems: I. Simulation and application to ammonium management in Bahr El-Baqar drainage system, Clean Techn Environ Policy (2005) 7: 51–61 DOI 10.1007/s10098-004-0258-7

El Raey, M., O. Firhy, S. Nasr & Kh. Dewidar, 1999. Vulnerability assessment of sea level rise over Port Said governorate, Egypt. Env. Monit. Ass. 56: 113–128.

El-Wakeel, SK. and S.D. Wahby, (1970). Hydrography and chemistry of Lake Manzalah, Egypt, Arch. Hydrobiol, Vol. 67, No. 2, pp. 173-200.

EPA (2001),Parameters of water quality interpretation and standards, *Published by the Environmental Protection Agency, Ireland.*

EPA (2005), Technologies and Techniques for Early Warning Systems to Monitor and Evaluate Drinking Water Quality: A State-of-the-Art Review. U.S. Environmental Protection Agency, Office of Water, Office of Science and Technology, Health and Ecological Criteria Division, August 25, 2005.

EPA, U.S. Environmental Protection Agency, Drinking Water Contaminants,. [Online]. Available: http://water.epa.gov [Accessed: Jan 13, 2011].

ESA, (2010). Retrieved from http://www.esa.int

Fischer, J. (1985). On the information content of multispectral radiance measurements over an ocean. Int. J. Remote Sensing 6: 773-786.

Floricioiu D., Riedl C., Rott E., and Rott H. (2003). Envisat MERIS Capabilities for Monitoring the Water Quality of Perialpine Lakes. 0-7803-7929-2/03 2003, IEEE.

Fomferra, N. and Brockmann, C., Beam—The ENVISAT MERIS and AATSR toolbox. In: ESA/ESRIN, Editor, Proceedings of the MERIS-(A)ATSR workshop. Frascati, Italy (2005, September) URL http://www.brockmann-consult.de/beam/.

Frihy, O., Kh. Dewidar, S. Nasr & M. El Raey, (1998). Change detection of the northern Nile delta of Egypt: shoreline changes, Spit evolution, margin changes of Manzala lagoon and its islands. Int. J. Remote Sensing 19: 1901–1912.

Fu, G., Schieber, B.D., Settle, K.J., Darzi, M., McClain, C.R., & Arrigo, K.R. (1996). SeaDAS: A processing package for ocean color satellite imagery, Proceedings of the Twelfth International Conference on Interactive Information and Processing Systems for Meteorology, Oceanography, and Hydrology (pp. 451–456). Boston, Massachusetts: American Meteorological Society.

Gao, B.-C., Montes, M.J., Li, R.-R., Dierssen, H.M. and Davis, C.O., An atmospheric correction algorithm for remote sensing of bright coastal waters using MODIS land and ocean channels in the solar spectral region, IEEE Transactions on Geoscience and Remote Sensing **45** (2007), pp. 1835–1843.

Gardner, J.W. and Bartlett , P.N. (eds.) (1992) Sensors and Sensory Systems for an Electronic Nose. Kluwer, Dordrecht.

Gardner J. W., Craven M., Dow C. and Hines E. L. (1998) The prediction of bacteria type and culture growth phase by an electronic nose with a multi-layer perceptron network. Meas. Sci. Technol. 9, 120–127.

Gauglitz, Guenter (2005). Direct optical sensors: principles and selected applications. Anal Bioanal Chem (2005) 381: 141–155

Guanter, L., Ruiz-Verdu, A., Odermatt, D., Giardino, C., Stefan Simis, Victor Estelles, Thomas

Heege, Jose Antonio Dominguez-Gomez, Jose Moreno, (2009). Atmospheric correction of ENVISAT/MERIS data over inland waters: Validation for European lakes, Remote Sensing of Environment, Volume 114, Issue 3, 15 March 2010, Pages 467-480, ISSN 0034-4257, DOI: 10.1016/j.rse.2009.10.004.

Giardino, C., V.E. Brando, A.G. Dekker, N. Strmbeck and G. Candiani, (2007). Assessment of water quality in Lake Garda (Italy) using Hyperion, Remote Sensing of Environment, 109(2): 183-195.

Gibson T. D., Prosser O., Hulbert J. N., Marshall R. W., Corcoran P., Lowery P., Ruck-Keene E. A. and Heron S. (1997) Detection and simultaneous identification of microorganisms from headspace samples using electronic noses. Sensors Actuators B 44, 413–422.

Gitelson, A. (1992). The peak near 700nm on radiance spectra of algae and water: relationships of its magnitude and position with chlorophyll concentration. Int. J. Remote Sensing 13: 3367-3373.

Glasgow, Howard B., Burkholder, JoAnn M., Reed, Robert E., Lewitus, Alan J. and Kleinman, Joseph E (2004). Real-time remote monitoring of water quality: a review of current applications, and advancements in sensor, telemetry, and computing technologies. Journal of Experimental Marine Biology and Ecology, Volume 300, Issues 1-2, 31 March 2004, Pages 409-448

Gons, Herman J., Rijkeboer, Machteld, Ruddick, Kevin G. A chlorophyll-retrieval algorithm for satellite imagery (Medium Resolution Imaging Spectrometer) of inland and coastal waters (2002), Journal of Plankton Research volume24, number9, pages 947–951, 2002

Gons , Herman J., Martin T. Auer, Steven W. Effler (2008). MERIS satellite chlorophyll mapping of oligotrophic and eutrophic waters in the Laurentian Great Lakes. Remote Sensing of Environment

112 (2008) 4098–4106

Gons , Herman J., Martin T. Auer, Steven W. Effler, (2008). MERIS satellite chlorophyll mapping of oligotrophic and eutrophic waters in the Laurentian Great Lakes, Remote Sensing of Environment, Volume 112, Issue 11, 15 November 2008, Pages 4098-4106

Gordon, H. R. and Morel, A. (1983). Remote Assessment of Ocean Color for Interpretation of Satellite Visible Imagery. A Review, Lecture Notes on Coastal and Estuarine Studies, R. T. Barber, N. K. Mooers, M. J. Bowman and B. Zeitzschel (eds.), Springer Verlag, New York, 114 p.

Gordon, H.R., Atmospheric correction of ocean color imagery in the Earth Observating System era (1997), Journal of Geophysical Research 102 (1997), pp. 17081–17105.

Grattan, K.T.V. (1997). Principles of optical fibre sensing for water industry applications. Measurement Vol. 20, No. 2, pp. 109-119, 1997

Gray,J. (2005). Conductivity analyzers and their application in Environmental Instrumentation and Analysis Handbook, R.D. Down, Ed, J.H. Lehr, Ed. Hoboken, NJ: John Wiley & Sons, Inc., 2005, pp. 491-510.

Greenberg, A. E., L. S. Clesceri, and A. D. Eaton (ed.). (1995). Standard methods for the examination of water and wastewater, 19th ed. American Public Health Association, Washington, D.C.

Guanter, L. at al., (2009). Atmospheric correction of ENVISAT/MERIS data over inland waters: Validation for European lakes. Remote sensing of Environment (2009), doi:10.1016/j.rse.2009.10.004

Guanter, L., Ruiz-Verdú, A., Odermatt, D., Giardino C., Simis S., Estellés V., Heege T., Domínguez-Gómez, J. A., Moreno J., (2010). Atmospheric correction of ENVISAT/MERIS data over inland waters: Validation for European lakes, Remote Sensing of Environment, Volume 114, Issue 3, 15 March 2010, Pages 467-480

Hana, 2010. Retrieved from www.hannainst.com October, 2010.

Hellweger, F.L. ; Schlosser, P. ; Lall, U. ; Weissel, J.K.(2004). Use of satellite imagery for water quality studies in New York Harbor. Estuarine, Coastal and Shelf Science, Volume 61, Issue 3, Pages 437-448

Herdendorf, C. E. (1982). Large Lakes of the World. Journal of Great Lakes Research,Volume 8, Issue 3, 1982, Pages 379-412

Hobbs P. J., Misselbrook T. M. and Pain B. F. (1995) Assessment of odours from livestock wastes by a photoionization detector, an electronic nose, olfactometry and gas chromatography-mass spectrometry. J. Agric. Engng Res. 60, 137–144.

Hoge, F. E. and Swift, R. N. (1986). Chlorophyll pigment concentration using spectral curvature algorithms: an evaluation of present and proposed satellite ocean color sensor bands. Appl. Optics 25: 3677-3682.

Holmberg M., Gustafsson F., Ho¨ rnsten E. G., Winquist F.,Nilsson L. E., Ljung L. and Lundstro¨m I. (1998) Bacteria classification based on feature extraction from sensor data. Biotechnol. Tech. 12(4), 319–324.

Hooker, S. B., McClain, C. R. (2000), The calibration and validation of SeaWiFS data Progress In

Oceanography, Volume 45, Issues 3-4, April 2000, Pages 427-465

Horsburgh, Jeffery S., Jones, Amber Spackman, Stevens David K., Tarboton, David G., Mesner, Nancy O. (2010). A sensor network for high frequency estimation of water quality constituent fluxes using surrogates. Environmental Modelling & Software 25 (2010) 1031–1044

Hydrolab, SERIES 5 Water Quality Instruments. (2005). In *Campbell Scientific*. Retrieved from http://www.campbellsci.ca/Catalogue/Series_5_Br.pdf

Hydrolab, SERIES 5 Water Quality Instruments. (2005). In *Campbell Scientific*. Retrieved from http://www.campbellsci.ca/Catalogue/Series_5_Specs.pdf

Hydrolab DS5X, DS5, and MS5 Water Quality Multiprobes. (February 2006). In *Campbell Scientific*. Retrieved from http://www.campbellsci.ca/Catalogue/Series_5_Man.pdf

Ibrahim M. D., Puestow T., Khan A. A., and Lye L. M. (2010) Satellite Water Quality Monitoring Validation: Case Study of Lake Manzalah, Egypt. CSCE 2010 General Conference, Winnipeg, Manitoba. June 9-12, 2010.

IOCCG (2000). Remote Sensing of Ocean Colour in Coastal, and Other Optically-Complex, Waters. Sathyendranath, S. (ed.), Reports of the International Ocean-Colour Coordinating Group, No. 3, IOCCG, Dartmouth, Canada.

Jacob, F., Petitcolin, F., Schmugge, Thomas, É. V., French, A., Ogawa, K., (2004). Comparison of land surface emissivity and radiometric temperature derived from MODIS and ASTER sensors Remote Sensing of Environment, Volume 90, Issue 2, 30 March 2004, Pages 137-152

Jer´onimo, Paula C.A., Alberto N. Ara´ujo, M. Conceic¸ ˜ao B.S.M. Montenegro Optical sensors and biosensors based on sol–gel films (2007). Talanta 72 (2007) 13–27

Kang-Ren Jin, Zhen-Gang Ji, and R. Thomas James (2007). Three-dimensional Water Quality and SAV Modeling of a Large Shallow Lake. J. Great Lakes Res. 33:28–45.

Karamouz, M., Baghvand A., Nokhandan A. K., and Kerachian R., (2006). Design of River a Water Quality Monitoring Network: An Entropy Based Approach. ASCE Conf. Proc. 200, 86 (2006), DOI:10.1061/40856(200)86

Kersey, Alan D. A Review of Recent Developments in Fiber Optic Sensor Technology. optical fiber technology 2, 291–317 (1996)

Khalil M. T. (1990). The physical and chemical environment of Lake Manzala, Egypt. Hydrobiologia 196: 193-199, 1990.

Khan A A, Paterson R and Khan H. Modification and Application of the Canadian Council of Ministers of the Environment Water Quality Index (CCME WQI) for the Communication of Drinking Water Quality Data in Newfoundland and Labrador. Water Qual. Res. J. Canada , Vol. 39, (2004), pp 285–293.

Khedr, Abdel-Hamid A. (1997). Aquatic macrophyte distribution in Lake Manzala, Egypt. International Journal of Salt Lake Research 5: 221-239, 1997.

Kloiber S. M., Brezonik, P. L., Olmanson, L. G., Bauer M. E. (2002). A procedure for regional lake water clarity assessment using Landsat multispectral data. Remote Sensing of Environment, Volume 82, Issue 1, September 2002, Pages 38-47

Krantz-Rülcker, C., Stenberg, Maria., Winquist, Fredrik., Lundström, Ingemar (2001). Electronic tongues for environmental monitoring based on sensor arrays and pattern recognition: a review. Analytica Chimica Acta 426 (2001) 217–226

Krawczyk, H., Neumann, A., Walzel, T. and Zimmermann, G. (1993). Investigation of interpretation possibilities of spectral high dimensional measurements by means of principal component analysis - a concept for physical interpretation of those measurements. Proc. SPIE 1938: 401-411.

Krawczyk, H., Neumann, A. and Hetscher, M. (1999). Mathematical and physical background of principal component inversion. In: Proceedings 3rd International Workshop on MOS-IRS and Ocean Colour, Wissenschaft und Technik Verlag, Berlin, 83-92.

Kuchinke, C.P., Gordon, H.R. and Franz, B.A., Spectral optimization for constituent retrieval in case 2 waters I: Implementation and performance, Remote Sensing of Environment **113** (2009), pp. 571–587

Kwiatkowski, R.E. (1985). Importance of Temporal Variability to the Design of Large Lake Water Quality Networkse. Journal of Great Lakes Research, Volume 11, Issue 4, 1985, Pages 462-477.

Lavender, S.J., Pinkerton, M.H., Moore, G., Aiken, J. and Blondeau-Patissier, D., Modification to the atmospheric correction of SeaWiFS ocean colour images over turbid waters, Continental Shelf Research **25** (2005), pp. 539–555

Lee, Z. P., Carder, K. L., Peacock, T. G., Davis, C. O. and Mueller, J. L. (1996). Method to derive ocean absorption coefficients from remote-sensing reflectance. Appl. Optics 35: 453-462.

Lee, Z., Carder, K. L., Mobley, C. D., Steward, R. G. and Patch, J. S. (1999). Hyperspectral remote sensing for shallow waters: 2. Deriving bottom depths and water properties by optimization. Appl.

Optics 38: 3831-3843.

Lettenmaier, Dennis P. (1978), Design considerations for ambient stream quality monitoring. American water resources association, vol 14, n0. 4, p 884-902.

Liu, X.L., Wang, W.J., Ren, H.R., Li, W., Zhang, C.Y., Han, D.J., Liang, Yang, K., R. (2009). Quality monitoring of flowing water using colorimetric method based on a semiconductor optical wavelength sensor. Measurement, Volume 42, Issue 1, January 2009, Pages 51-56

Longhurst, A., Sathyendranath, S., Platt, T. and Caverhill, C. (1995) An estimate of global primary production in the ocean from satellite radiometer data. J. Plankton Res., 17, 1245–1271.

MacCraith, B. D., Grattan, K. T. V., Connolly, D., Briggs, R., Boyle, W. J. O. and Avis, M. (1994), Results of a cross-comparison study: optical monitoring of total organic carbon (TOC) of a limited range of samples. *Sensors and Actuators,* 1994, 22B, 149-153.

Matthews, Mark W., Stewart Bernard, Kevin Winter, (2010). Remote sensing of cyanobacteria-dominant algal blooms and water quality parameters in Zeekoevlei, a small hypertrophic lake, using MERIS, Remote Sensing of Environment, Volume 114, Issue 9, 15 September 2010, Pages 2070-2087

Mimendia, A., Gutie´ rrez, J.M., Leija, L., Herna´ndez, Favari, P.R., Mun˜oz, L., Valle, R., M. del. (2010). A review of the use of the potentiometric electronic tongue in the monitoring of environmental systems. Environmental Modelling & Software 25 (2010) 1023–1030

Misselbrook T. M., Hobbs P. J. and Persaud K. C. (1997) Use of an electronic nose to measure odour concentration following application of cattle slurry to grassland. J. Agri. Engng Res. 66, 213–

220.

Montasir, A. H. (1937). Ecology of Lake Manzala, Egyptian Univ. Bull. Soc. Sci. 12: 1-50.

Moore, G.F., Aiken, J. and Lavender, S.J., The atmospheric correction of water colour and the quantitative retrieval of suspended particulate matter in case II waters: Application to MERIS, International Journal of Remote Sensing **20** (1999), pp. 1713–1733.

Morel, A. and Bélanger, S., Improved detection of turbid waters from ocean color sensors information, Remote Sensing of Environment **102** (2006), pp. 237–249.

Morel, A. and Prieur, L. (1977). Analysis of variations in ocean color. Limnol. Oceanogr. 22:709-722.

Morel, A. (1998). Minimum requirements for an operational ocean-colour sensor for the open ocean. IOCCG Report Number 1, IOCCG Project Office, Dartmouth, Nova Scotia, 46 pp.

Mueller, J. L. (1973). Influence of phytoplankton on ocean color spectra, Ph.D., School of Oceanography, Oregon State University, Corvallis, Oregon.

Mueller, J. L. (1976). Ocean color measured off the Oregon Coast: characteristic vectors. Appl.Optics 15: 394-402.

Nash, J. E., Sutcliffe, J. V., (1970). River flow forecasting through conceptual models part I - a discussion of principles. Journal of Hydrology 10 (1970) 282-290.

Nelder, J. A. and Mead, R. (1965). A simplex method for function minimization. Comput. J. 7: 308-313.

Neumann A., Doerffer R., Krawczyk H., Dowell M. D., Arnone R., Davis C. O., Kishino M., Tanaka A., Hu C., Bukata R. P., Gordon H. R., Campbell J., Sathyendranath S. (2000). Algorithms for Case 2 Waters. Reports of the International Ocean-Colour Coordinating Group, No. 3, IOCCG, Dartmouth, Canada.

National Oceanic and Atmospheric Administration, NOAA, (2010). Retrieved from http://www.noaa.gov/

Odermatt D., Heege T., Nieke J., Kneubühler M. and Itten K. (2008). Water Quality Monitoring for Lake Constance with a Physically Based Algorithm for MERIS Data. Sensors 2008, 8, 4582-4599.

Odermatt D., Claudia Giardino, Thomas Heege (2010). Chlorophyll retrieval with MERIS Case-2-Regional in perialpine lakes. Remote Sensing of Environment 114 (2010) 607–617

Patel, P. D., (2002). (Bio) sensors for measurement of analytes implicated in food safety: a review. Trends in analytical chemistry, vol. 2, No. 2, Pg. 96-116.

Paulson, R.W., (1975). Use of earth satellite technology or telemetry of hydrometerological station data, Padova, Italy. In: International Seminar on Modern Development in Hydrology, pp. 1–75.

Petersen, W., Wehde, H., Krasemann H., Colijn, F., Schroeder, F. (2008). FerryBox and MERIS e Assessment of coastal and shelf seaecosystems by combining in situ and remotely sensed data. Estuarine, Coastal and Shelf Science 77 (2008) 296e307

Pettinger, L.R., 1971. Field data collection—an essential element in remote sensing applications. In: Proceedings of the International Workshop on Earth Resources Survey Systems, Washington, DC, pp. 49–64.

Phillips, S. L., Mack, D. A., and MacLeod, W. D. (1974). Instrumentation for Water quality Monitoring. Analytical Chemistry 1974 46 (3), 345A-356A

Prieur, L. and Sathyendranath, S. (1981). An optical classification of coastal and oceanic waters based on the specific spectral absorption curves of phytoplankton pigments, dissolved organic matter, and other particulate materials. Limnol. Oceanogr. 26: 671-689.

Purrington, Heidi M. (2010). A Multi-Sensor Chip for Monitoring the Quality of Drinking Water. M. Sc. thesis, Department of, Electrical and Microelectronic Engineering, Kate gleason College of Engineering, Rochester Institute of Technology

Qiu, Y.; Zhang, H.; Tong, X.; Chen, L.; Zhao, J., (2006). Water Quality Monitoring of Water Resources Conservation Area in City of Shanghai Based on Remote Sensing, Geoscience and Remote Sensing Symposium, 2006. IGARSS 2006. IEEE International Conference on , vol., no., pp.3434-3437, July 31 2006-Aug. 4 2006 doi: 10.1109/IGARSS.2006.881

Ramdani, M., Flower, Roger J., Elkhiati N., Kraïem, Mohammed M., Fathi, Adel A., Birks, Hilary H. and Patrick, Simon T. (2001). North African wetland lakes: characterization of nine sites included in the CASSARINA Project. Aquatic Ecology 35: 281–302, 2001.

Rast, M., Bézy, J. L., & Bruzzi, S. (1999). The ESA Medium Resolution Imaging Spectrometer MERIS—A review of the instrument and its mission. International Journal of Remote Sensing, 20, 1681−1702.

Roesler, C. S. and Perry, M. J. (1995). In situ phytoplankton absorption, fluorescence emission, and particulate backscattering spectra determined from reflectance. J. Geophys. Res. 100: 13,279-

13,294.

Ruiz, A. -Verdú, Koponen, S., T. Heege, Doerffer, R., Brockmann, Kallio, C., K., Pyhälahti, T., Peña-Martínez, R., Ángel Polvorinos, J. Heblinski, P. Ylöstalo, L. Conde, D. Odermatt, V. Estellés and J. Pulliainen, Development of MERIS lake water algorithms: Validation results from Europe. In: ESA/ESRIN, Editor, Proceedings of the 2nd MERIS/(A)ATSR user workshop. Frascati, Italy (2008, September).

Said, M.A. and Abdel-Maoti, M.A.R.. 1995. Water budget of Lake Manzala , Egypt, Mahasagar, Vol., 28, Issues 1-2, pp. 75-81.

Sathyendranath, S. and Morel, A. (1983). Light emerging from the sea — interpretation and uses in remote sensing. In: Remote Sensing Applications in Marine Science and Technology, A. P. Cracknell (ed.), D. Reidel Publishing Company, Dordrecht, 323-357.

Sathyendranath, S. and Platt, T. (1989). Remote sensing of ocean chlorophyll: Consequence of non-uniform pigment profile. Appl. Optics 28: 490-495.

Sathyendranath, S., Hoge, F. E., Platt, T. and Swift, R. N. (1994). Detection of phytoplankton pigments from ocean colour: Improved algorithms. Appl. Optics 33: 1081-1089.

Sathyendranath, S., Platt, T., Cota, G., Stuart, V. and Borstad, G. (1997a). Some Canadian experiments on modelling and interpreting ocean-colour data. In: 1st International Workshop on MOS-IRS and Ocean Colour, Berlin, April 28-30, 1997, Institute of Space Sensor Technology, DLR (ed.), Wissenschaft und Technik Verlag, Berlin.

Schalles, J. F., Gitelson, A. A., Yacobi, Y. Z. and Kroenke, A. E. (1998). Estimation of chlorophyll a from time series measurements of high spectral resolution reflectance in an eutrophic lake. J. Phycol. 34: 383-390.

Schroeder, Th., Behnert, I., Schaale, M., Fischer, J. and Doerffer, R.(2007) 'Atmospheric correction algorithm for MERIS above case-2 waters', International Journal of Remote Sensing, 28: 7, 1469 — 1486

Sharp, W. E. (1971), A Topologically Optimum Water-Sampling Plan for Rivers and Streams, Water Resour. Res., 7(6), 1641–1646, doi:10.1029/WR007i006p01641.

Shutler, J.D., Land, P.E., Smyth, T.J., Groom, S.B., (2007). Extending the MODIS 1 km ocean colour atmospheric correction to the MODIS 500 m bands and 500 m chlorophyll-a estimation towards coastal and estuarine monitoring, Remote Sensing of Environment, Volume 107, Issue 4, 30 April 2007, Pages 521-532, ISSN 0034-4257, DOI: 10.1016/j.rse.2006.10.004.

Siegel, FR (1995) Environmental Geochemistry in Development Planning: An Example from the Nile delta, Egypt. J. Geochemical Exploration 55(1–3): 265–273

Smith, V. H. 1990. Introduction to Applied Phycology, SPB Academic Publishing.

Smith, V. H. (2002). Eutrophication of freshwater and coastal marine ecosystems a global problem. Environmental Science and Pollution Research ,Volume 10, Number 2, 126-139, DOI: 10.1065/espr2002.12.142

Song, Conghe , Woodcock, Curtis E. , Seto , Karen C. , Pax Lenney, Mary and Scott A. Macomber, (2001). Classification and Change Detection Using Landsat TM Data: When and How to Correct Atmospheric Effects?, Remote Sensing of Environment

Volume 75, Issue 2, February 2001, Pages 230-244

Strobl, Robert O., and Robillard, Paul D., (2006), Network design for water quality monitoring of surface freshwaters: A review, Journal of Environmental Management, Volume 87, Issue 4, June 2008, Pages 639-648

Swenson, Sean., John Wahr , (2009). Monitoring the water balance of Lake Victoria, East Africa, from space, Journal of Hydrology, Volume 370, Issues 1-4, 30 May 2009, Pages 163-176

Tanner, A.H. and White, N.M., Virtual instrumentation: a solution to the problem of design complexity in intelligent instruments. *Measurement and Control* **29** (1996), pp. 165–171.

Teillet, P.M., Dudelzak, A.E., Pultz, T.J., McNairn, H. and Chichagov, A., (2001). A framework for in-situ sensor measurement assimilation in remote sensing. In: Proceedings of the 23rd Canadian Symposium on Remote Sensing, Québec City, Québec, 21–24 August, pp. 111–118.

Teillet, P.M., Dudelzak, A.E., Pultz, T.J., McNairn, H. and Chichagov, A., (2001). A framework for in-situ sensor measurement assimilation in remote sensing. In: Proceedings of the 23rd Canadian Symposium on Remote Sensing, Québec City, Québec, 21–24 August, pp. 111–118.

Turner, J.F. and Woodham, W.M., (1980). Evaluation of remote hydrologic data-acquisition systems. USGS Water Resources Investigations 79-102, West-Central Florida, USGS, Reston, VA.

Tyler, A. N. , Svab, E. , Preston, T., Pre´ sing, M., and Kova´ cs, W. A. (2006). Remote sensing of the water quality of shallow lakes: A mixture modeling approach to quantifying phytoplankton in water characterized by high-suspended sediment. International Journal of Remote Sensing Vol. 27, No. 8, 20 April 2006, 1521–1537

Tyler, A. N., Svab, E., Preston, T., Pre´ sing, M., and Kova´ cs, W. A. (2006), Remote sensing of the water quality of shallow lakes: A mixture modeling approach to quantifying phytoplankton in water characterized by high-suspended sediment.International Journal of Remote Sensing, Vol. 27, No. 8, 20 April 2006, 1521–1537

UNDP, (1997). Project Document– Lake Manzala Engineered Wetland, United Nations Development Program, Project Number: EGY/93/G31, March 1997.

USGS, (2010). Retrieved from http://www.usgs.gov/ January 2011.

Vernon, T., Stack ,Jr. (1972). Water quality surveillance Analytical Chemistry 1972 44 (8), 32A-44a

Wang ,Y., Xia, H., Fu J., Sheng G. (2004). Water quality change in reservoirs of Shenzhen, China: detection using LANDSATyTM data Science of the Total Environment 328 (2004) 195–206

Wetering, B. G. M. v. d., Groot, S. Water quality monitoring in the state-managed waters of The Netherlands, (1986). Water Research, Volume 20, Issue 8, August 1986, Pages 1045-1050,1986

WHO 1980 Environmental Management for Vector Control. Fourth report of the WHOExpert Committee on Vector Biology and Control, Technical Report Series No. 649,World Health Organization, Geneva, 67 pp.

WHO 1982 Manual for Environmental Management for Mosquito Control, with SpecialEmphasis on Malaria Vectors. WHO Offset Publication No. 66, World HealthOrganization, Geneva, 281 pp.

Wilson, Jon S. (2005). Sensor Technology Handbook.. Elsevier. Online version available at: http://www.knovel.com/web/portal/browse/display?_EXT_KNOVEL_DISPLAY_bookid=1659&Ve

rticalID=0

Xi, H., Zhan, Y., Chen J., Water components retrieval in the pearl river estuary from MERIS data, 2008, 978-1-4244-2808-3/08/$25.00 ©2008 IEEE

Yamaguchi, Y., Kahle, A., Tsu, H., Kawakami, T., & Pniel, M. (1998). Overview of Advanced Space-borne Thermal Emission and Reflection Radiometer (ASTER). IEEE Transactions on Geoscience and Remote Sensing, 36, 1282– 1289.

Zahran, M. A., Abu Ziada, M. E., El-Demerdash, M. A., and Khedr, A. A. (1989). A note on the vegetation on islands in Lake Manzala, Egypt, Vegetatio 85: 83-88, 1989.

Zalat, Abdelfattah and Vildary, Simone Servant (2005) .Distribution of diatom assemblages and their relationship to environmental variables in the surface sediments of three northern Egyptian lakes. Journal of Paleolimnology (2005) 34:159–174

Appendix A

RTWQ Data Series Station 1

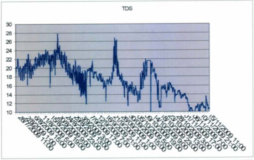
TDS
30
28
26
24
22
20
18
16
14
12
10

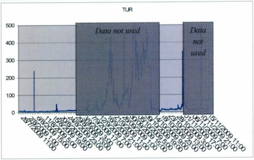
TUR
500
400
300
200
100
0
Data not used
Data not used

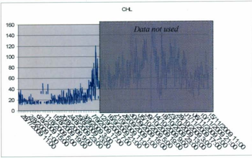
CHL
160
140
120
100
80
60
40
20
0
Data not used

Appendix B

RTWQ Data Series Station 2 and 2a

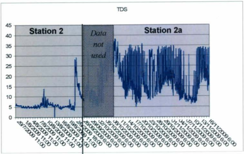
TDS
Station 2
Data not used
Station 2a

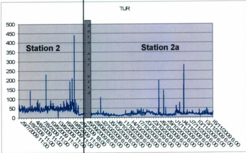
TUR
Station 2
Station 2a

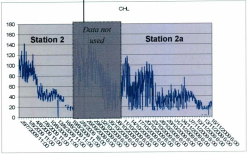
CHL
Station 2
Data not used
Station 2a

Appendix C

RTWQ Data Series Station 3

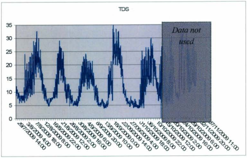
TDS
Data not used

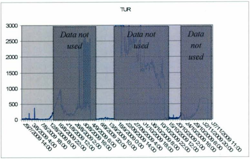
TUR
Data not used
Data not used
Data not used

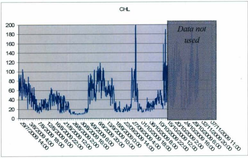
CHL
Data not used

Appendix D

Matrix plots, Correlation Matrices and p-value matrices of the concurrent reflectances with water quality parameters (TUR, CHL, and TDS)

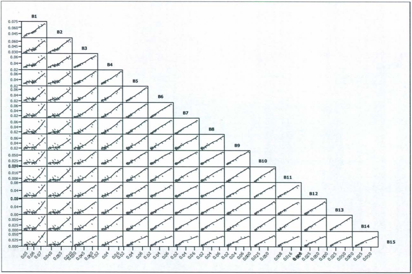

Figure 44: Matrix plot of TUR-concurrent reflectances

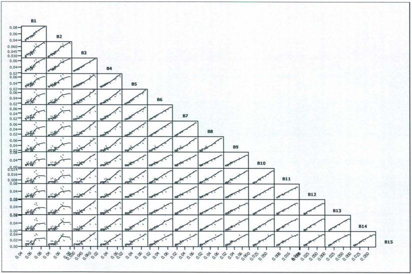

Figure 45: Matrix plot of CHL-concurrent reflectances

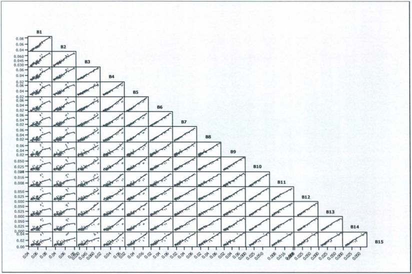

Figure 46: Matrix plot of TDS-concurrent Reflectances

Table 22: Correlation Matrix for TUR-concurrent (Spearman Rho)

	B1	B2	B3	B4	B5	B6	B7	B8	B9	B10	B11	B12	B13	B14	B15
B1	1.000	0.983	0.891	0.859	0.745	0.711	0.669	0.677	0.497	0.486	0.473	0.472	0.488	0.470	0.497
B2	0.983	1.000	0.950	0.923	0.825	0.792	0.752	0.759	0.572	0.579	0.559	0.564	0.593	0.578	0.593
B3	0.891	0.950	1.000	0.990	0.938	0.919	0.893	0.901	0.701	0.739	0.724	0.726	0.765	0.754	0.760
B4	0.859	0.923	0.990	1.000	0.965	0.952	0.928	0.936	0.747	0.778	0.763	0.767	0.805	0.793	0.789
B5	0.745	0.825	0.938	0.965	1.000	0.991	0.977	0.980	0.761	0.806	0.808	0.800	0.858	0.852	0.843
B6	0.711	0.792	0.919	0.952	0.991	1.000	0.984	0.991	0.781	0.837	0.840	0.832	0.889	0.886	0.867
B7	0.669	0.752	0.893	0.928	0.977	0.984	1.000	0.994	0.731	0.814	0.835	0.809	0.881	0.881	0.864
B8	0.677	0.759	0.901	0.936	0.980	0.991	0.994	1.000	0.782	0.854	0.872	0.850	0.909	0.907	0.893
B9	0.497	0.572	0.701	0.747	0.761	0.781	0.731	0.782	1.000	0.964	0.913	0.967	0.895	0.877	0.880
B10	0.486	0.579	0.739	0.778	0.806	0.837	0.814	0.854	0.964	1.000	0.967	0.998	0.960	0.951	0.951
B11	0.473	0.559	0.724	0.763	0.808	0.840	0.835	0.872	0.913	0.967	1.000	0.966	0.962	0.952	0.961
B12	0.472	0.564	0.726	0.767	0.800	0.832	0.809	0.850	0.967	0.998	0.966	1.000	0.963	0.954	0.954
B13	0.488	0.593	0.765	0.805	0.858	0.889	0.881	0.909	0.895	0.960	0.962	0.963	1.000	0.997	0.973
B14	0.470	0.578	0.754	0.793	0.852	0.886	0.881	0.907	0.877	0.951	0.952	0.954	0.997	1.000	0.969
B15	0.497	0.593	0.760	0.789	0.843	0.867	0.864	0.893	0.880	0.951	0.961	0.954	0.973	0.969	1.000

range(0.7 to 1.0)

Table 23: P-values Matrix of Spearman's Rho Correlation Matrix for TUR-concurrent Bands

TUR	B1	B2	B3	B4	B5	B6	B7	B8	B9	B10	B11	B12	B13	B14
B2	0.000													
B3	0.000	0.000												
B4	0.000	0.000	0.000											
B5	0.000	0.000	0.000	0.000										
B6	0.000	0.000	0.000	0.000	0.000									
B7	0.000	0.000	0.000	0.000	0.000	0.000								
B8	0.000	0.000	0.000	0.000	0.000	0.000	0.000							
B9	0.003	0.000	0.000	0.000	0.000	0.000	0.000	0.000						
B10	0.004	0.000	0.000	0.000	0.000	0.000	0.000	0.000	0.000					
B11	0.005	0.001	0.000	0.000	0.000	0.000	0.000	0.000	0.000	0.000				
B12	0.005	0.001	0.000	0.000	0.000	0.000	0.000	0.000	0.000	0.000	0.000			
B13	0.003	0.000	0.000	0.000	0.000	0.000	0.000	0.000	0.000	0.000	0.000	0.000		
B14	0.005	0.000	0.000	0.000	0.000	0.000	0.000	0.000	0.000	0.000	0.000	0.000	0.000	
B15	0.003	0.000	0.000	0.000	0.000	0.000	0.000	0.000	0.000	0.000	0.000	0.000	0.000	0.000

Table 24: Correlation Matrix for TUR-concurrent (Kendall's Tau)

	B1	B2	B3	B4	B5	B6	B7	B8	B9	B10	B11	B12	B13	B14	B15
B1	1.000	0.907	0.733	0.690	0.572	0.529	0.480	0.480	0.355	0.344	0.319	0.337	0.340	0.330	0.351
B2	0.907	1.000	0.825	0.783	0.658	0.615	0.558	0.572	0.419	0.422	0.398	0.415	0.433	0.422	0.437
B3	0.733	0.825	1.000	0.943	0.804	0.768	0.733	0.740	0.529	0.561	0.551	0.554	0.594	0.576	0.576
B4	0.690	0.783	0.943	1.000	0.861	0.825	0.775	0.790	0.572	0.604	0.586	0.597	0.629	0.604	0.604
B5	0.572	0.658	0.804	0.861	1.000	0.943	0.886	0.893	0.604	0.651	0.654	0.643	0.704	0.686	0.679
B6	0.529	0.615	0.768	0.825	0.943	1.000	0.914	0.943	0.633	0.679	0.683	0.672	0.740	0.736	0.708
B7	0.480	0.558	0.733	0.775	0.886	0.914	1.000	0.957	0.597	0.658	0.690	0.658	0.747	0.743	0.715
B8	0.480	0.572	0.740	0.790	0.893	0.943	0.957	1.000	0.633	0.693	0.725	0.693	0.775	0.772	0.743
B9	0.355	0.419	0.529	0.572	0.604	0.633	0.597	0.633	1.000	0.861	0.772	0.861	0.758	0.733	0.725
B10	0.344	0.422	0.561	0.604	0.651	0.679	0.658	0.693	0.861	1.000	0.868	0.979	0.861	0.836	0.836
B11	0.319	0.398	0.551	0.586	0.654	0.683	0.690	0.725	0.772	0.868	1.000	0.868	0.865	0.840	0.847
B12	0.337	0.415	0.554	0.597	0.643	0.672	0.658	0.693	0.861	0.979	0.868	1.000	0.868	0.843	0.843
B13	0.340	0.433	0.594	0.629	0.704	0.740	0.747	0.775	0.758	0.861	0.865	0.868	1.000	0.975	0.889
B14	0.330	0.422	0.576	0.604	0.686	0.736	0.743	0.772	0.733	0.836	0.840	0.843	0.975	1.000	0.879
B15	0.351	0.437	0.576	0.604	0.679	0.708	0.715	0.743	0.725	0.836	0.847	0.843	0.889	0.879	1.000

range(0.7 to 1.0)

Table 25: Correlation Matrix for CHL-concurrent (Spearman Rho)

	B1	B2	B3	B4	B5	B6	B7	B8	B9	B10	B11	B12	B13	B14	B15
B1	1.000	0.956	0.870	0.840	0.759	0.704	0.660	0.664	0.567	0.577	0.508	0.558	0.553	0.533	0.547
B2	0.956	1.000	0.963	0.944	0.884	0.842	0.800	0.807	0.721	0.729	0.647	0.715	0.704	0.686	0.693
B3	0.870	0.963	1.000	0.995	0.966	0.941	0.911	0.915	0.833	0.847	0.777	0.837	0.828	0.814	0.822
B4	0.840	0.944	0.995	1.000	0.981	0.961	0.936	0.942	0.862	0.878	0.818	0.868	0.861	0.847	0.854
B5	0.759	0.884	0.966	0.981	1.000	0.991	0.977	0.978	0.899	0.913	0.869	0.906	0.906	0.897	0.892
B6	0.704	0.842	0.941	0.961	0.991	1.000	0.991	0.994	0.916	0.932	0.895	0.926	0.928	0.921	0.916
B7	0.660	0.800	0.911	0.936	0.977	0.991	1.000	0.998	0.902	0.927	0.909	0.925	0.936	0.932	0.930
B8	0.664	0.807	0.915	0.942	0.978	0.994	0.998	1.000	0.913	0.938	0.915	0.935	0.942	0.937	0.934
B9	0.567	0.721	0.833	0.862	0.899	0.916	0.902	0.913	1.000	0.979	0.951	0.977	0.950	0.941	0.929
B10	0.577	0.729	0.847	0.878	0.913	0.932	0.927	0.938	0.979	1.000	0.975	0.997	0.979	0.971	0.962
B11	0.508	0.647	0.777	0.818	0.869	0.895	0.909	0.915	0.951	0.975	1.000	0.978	0.977	0.973	0.965
B12	0.558	0.715	0.837	0.868	0.906	0.926	0.925	0.935	0.977	0.997	0.978	1.000	0.984	0.977	0.970
B13	0.553	0.704	0.828	0.861	0.906	0.928	0.936	0.942	0.950	0.979	0.977	0.984	1.000	0.998	0.983
B14	0.533	0.686	0.814	0.847	0.897	0.921	0.932	0.937	0.941	0.971	0.973	0.977	0.998	1.000	0.983
B15	0.547	0.693	0.822	0.854	0.892	0.916	0.930	0.934	0.929	0.962	0.965	0.970	0.983	0.983	1.000

range(0.85 to 1.0)

Table 26: P-values Matrix of Spearman's Rho Correlation Matrix for CHL-concurrent Bands

CHL	B1	B2	B3	B4	B5	B6	B7	B8	B9	B10	B11	B12	B13	B14
B2	0.000													
B3	0.000	0.000												
B4	0.000	0.000	0.000											
B5	0.000	0.000	0.000	0.000										
B6	0.000	0.000	0.000	0.000	0.000									
B7	0.000	0.000	0.000	0.000	0.000	0.000								
B8	0.000	0.000	0.000	0.000	0.000	0.000	0.000							
B9	0.001	0.000	0.000	0.000	0.000	0.000	0.000	0.000						
B10	0.000	0.000	0.000	0.000	0.000	0.000	0.000	0.000	0.000					
B11	0.003	0.000	0.000	0.000	0.000	0.000	0.000	0.000	0.000	0.000				
B12	0.001	0.000	0.000	0.000	0.000	0.000	0.000	0.000	0.000	0.000	0.000			
B13	0.001	0.000	0.000	0.000	0.000	0.000	0.000	0.000	0.000	0.000	0.000	0.000		
B14	0.001	0.000	0.000	0.000	0.000	0.000	0.000	0.000	0.000	0.000	0.000	0.000	0.000	
B15	0.001	0.000	0.000	0.000	0.000	0.000	0.000	0.000	0.000	0.000	0.000	0.000	0.000	0.000

Table 27: Correlation Matrix for CHL-concurrent (Kendall's Tau)

	B1	B2	B3	B4	B5	B6	B7	B8	B9	B10	B11	B12	B13	B14	B15
B1	1.000	0.867	0.727	0.697	0.602	0.557	0.515	0.515	0.420	0.420	0.364	0.409	0.402	0.386	0.409
B2	0.867	1.000	0.860	0.830	0.727	0.682	0.633	0.648	0.530	0.538	0.473	0.527	0.527	0.511	0.527
B3	0.727	0.860	1.000	0.970	0.860	0.822	0.773	0.788	0.655	0.678	0.614	0.667	0.667	0.652	0.659
B4	0.697	0.830	0.970	1.000	0.890	0.852	0.803	0.818	0.678	0.708	0.644	0.697	0.697	0.682	0.689
B5	0.602	0.727	0.860	0.890	1.000	0.939	0.890	0.898	0.742	0.765	0.716	0.761	0.769	0.754	0.746
B6	0.557	0.682	0.822	0.852	0.939	1.000	0.943	0.958	0.780	0.795	0.754	0.792	0.807	0.799	0.784
B7	0.515	0.633	0.773	0.803	0.890	0.943	1.000	0.977	0.777	0.792	0.765	0.795	0.826	0.818	0.811
B8	0.515	0.648	0.788	0.818	0.898	0.958	0.977	1.000	0.792	0.814	0.780	0.818	0.833	0.826	0.818
B9	0.420	0.530	0.655	0.678	0.742	0.780	0.777	0.792	1.000	0.902	0.830	0.898	0.822	0.807	0.799
B10	0.420	0.538	0.678	0.708	0.765	0.795	0.792	0.814	0.902	1.000	0.890	0.973	0.883	0.867	0.852
B11	0.364	0.473	0.614	0.644	0.716	0.754	0.765	0.780	0.830	0.890	1.000	0.894	0.894	0.879	0.856
B12	0.409	0.527	0.667	0.697	0.761	0.792	0.795	0.818	0.898	0.973	0.894	1.000	0.894	0.879	0.864
B13	0.402	0.527	0.667	0.697	0.769	0.807	0.826	0.833	0.822	0.883	0.894	0.894	1.000	0.985	0.909
B14	0.386	0.511	0.652	0.682	0.754	0.799	0.818	0.826	0.807	0.867	0.879	0.879	0.985	1.000	0.909
B15	0.409	0.527	0.659	0.689	0.746	0.784	0.811	0.818	0.799	0.852	0.856	0.864	0.909	0.909	1.000

range(0.7 to 1.0)

Table 28: Correlation Matrix for TDS-concurrent (Spearman Rho)

	B1	B2	B3	B4	B5	B6	B7	B8	B9	B10	B11	B12	B13	B14	B15
B1	1.000	0.969	0.893	0.858	0.776	0.714	0.678	0.681	0.608	0.591	0.555	0.582	0.564	0.544	0.541
B2	0.969	1.000	0.966	0.944	0.879	0.826	0.792	0.795	0.723	0.713	0.675	0.705	0.692	0.674	0.667
B3	0.893	0.966	1.000	0.994	0.956	0.921	0.901	0.905	0.820	0.828	0.800	0.821	0.820	0.808	0.799
B4	0.858	0.944	0.994	1.000	0.979	0.952	0.933	0.938	0.852	0.863	0.838	0.857	0.857	0.847	0.835
B5	0.776	0.879	0.956	0.979	1.000	0.988	0.974	0.975	0.873	0.888	0.873	0.884	0.897	0.889	0.869
B6	0.714	0.826	0.921	0.952	0.988	1.000	0.990	0.992	0.889	0.909	0.898	0.908	0.925	0.919	0.896
B7	0.678	0.792	0.901	0.933	0.974	0.990	1.000	0.997	0.862	0.899	0.898	0.899	0.929	0.927	0.906
B8	0.681	0.795	0.905	0.938	0.975	0.992	0.997	1.000	0.886	0.921	0.919	0.921	0.943	0.941	0.923
B9	0.608	0.723	0.820	0.852	0.873	0.889	0.862	0.886	1.000	0.976	0.948	0.976	0.930	0.916	0.915
B10	0.591	0.713	0.828	0.863	0.888	0.909	0.899	0.921	0.976	1.000	0.982	0.999	0.979	0.970	0.969
B11	0.555	0.675	0.800	0.838	0.873	0.898	0.898	0.919	0.948	0.982	1.000	0.982	0.980	0.974	0.978
B12	0.582	0.705	0.821	0.857	0.884	0.908	0.899	0.921	0.976	0.999	0.982	1.000	0.980	0.971	0.970
B13	0.564	0.692	0.820	0.857	0.897	0.925	0.929	0.943	0.930	0.979	0.980	0.980	1.000	0.998	0.984
B14	0.544	0.674	0.808	0.847	0.889	0.919	0.927	0.941	0.916	0.970	0.974	0.971	0.998	1.000	0.984
B15	0.541	0.667	0.799	0.835	0.869	0.896	0.906	0.923	0.915	0.969	0.978	0.970	0.984	0.984	1.000

range (0.7-1.0)

Table 29: P-values Matrix of Spearman's Rho Correlation Matrix for TDS-concurrent Bands

TDS	B1	B2	B3	B4	B5	B6	B7	B8	B9	B10	B11	B12	B13	B14
B2	0.000													
B3	0.000	0.000												
B4	0.000	0.000	0.000											
B5	0.000	0.000	0.000	0.000										
B6	0.000	0.000	0.000	0.000	0.000									
B7	0.000	0.000	0.000	0.000	0.000	0.000								
B8	0.000	0.000	0.000	0.000	0.000	0.000	0.000							
B9	0.000	0.000	0.000	0.000	0.000	0.000	0.000	0.000						
B10	0.000	0.000	0.000	0.000	0.000	0.000	0.000	0.000	0.000					
B11	0.000	0.000	0.000	0.000	0.000	0.000	0.000	0.000	0.000	0.000				
B12	0.000	0.000	0.000	0.000	0.000	0.000	0.000	0.000	0.000	0.000	0.000			
B13	0.000	0.000	0.000	0.000	0.000	0.000	0.000	0.000	0.000	0.000	0.000	0.000		
B14	0.000	0.000	0.000	0.000	0.000	0.000	0.000	0.000	0.000	0.000	0.000	0.000	0.000	
B15	0.000	0.000	0.000	0.000	0.000	0.000	0.000	0.000	0.000	0.000	0.000	0.000	0.000	0.000

Table 30: Correlation Matrix for TDS-concurrent (Kendall's Tau)

	B1	B2	B3	B4	B5	B6	B7	B8	B9	B10	B11	B12	B13	B14	B15
B1	1.000	0.871	0.735	0.687	0.594	0.536	0.495	0.497	0.434	0.423	0.390	0.41558	0.397	0.383	0.382
B2	0.871	1.000	0.864	0.816	0.714	0.660	0.616	0.626	0.536	0.534	0.500	0.52597	0.518	0.506	0.497
B3	0.735	0.864	1.000	0.947	0.832	0.783	0.752	0.760	0.639	0.655	0.623	0.64675	0.647	0.635	0.618
B4	0.687	0.816	0.947	1.000	0.883	0.834	0.797	0.808	0.677	0.695	0.661	0.68701	0.687	0.673	0.656
B5	0.594	0.714	0.832	0.883	1.000	0.927	0.873	0.878	0.713	0.729	0.710	0.72338	0.736	0.727	0.703
B6	0.536	0.660	0.783	0.834	0.927	1.000	0.930	0.945	0.744	0.757	0.747	0.75455	0.781	0.777	0.736
B7	0.495	0.616	0.752	0.797	0.873	0.930	1.000	0.966	0.716	0.749	0.752	0.74935	0.799	0.797	0.755
B8	0.497	0.626	0.760	0.808	0.878	0.945	0.966	1.000	0.742	0.781	0.781	0.78052	0.819	0.818	0.775
B9	0.434	0.536	0.639	0.677	0.713	0.744	0.716	0.742	1.000	0.878	0.813	0.87792	0.784	0.765	0.761
B10	0.423	0.534	0.655	0.695	0.729	0.757	0.749	0.781	0.878	1.000	0.901	0.98182	0.886	0.866	0.857
B11	0.390	0.500	0.623	0.661	0.710	0.747	0.752	0.781	0.813	0.901	1.000	0.8987	0.896	0.879	0.878
B12	0.416	0.526	0.647	0.687	0.723	0.755	0.749	0.781	0.878	0.982	0.899	1.000	0.888	0.869	0.862
B13	0.397	0.518	0.647	0.687	0.736	0.781	0.799	0.819	0.784	0.886	0.896	0.88831	1.000	0.978	0.904
B14	0.383	0.506	0.635	0.673	0.727	0.777	0.797	0.818	0.765	0.866	0.879	0.86883	0.978	1.000	0.905
B15	0.382	0.497	0.618	0.656	0.703	0.736	0.755	0.775	0.761	0.857	0.878	0.86234	0.904	0.905	1.000

range(0.7-1.0)

Appendix E

Correlation Matrix between water quality parameters (TUR, CHL, and TDS) and extracted MERIS reflectances

	TUR		TUR		TUR		TUR		TUR		TUR		TUR		TUR
B1.B1	-	B3.B1	-0.10	B5.B1	-0.04	B7.B1	-0.20	B9.B1	0.42	B11.B1	0.24	B13.B1	0.10	B15.B1	0.06
B1.B2	0.03	B3.B2	-0.12	B5.B2	-0.01	B7.B2	-0.17	B9.B2	0.46	B11.B2	0.27	B13.B2	0.10	B15.B2	0.09
B1.B3	0.10	B3.B3	-	B5.B3	0.02	B7.B3	-0.21	B9.B3	0.54	B11.B3	0.33	B13.B3	0.14	B15.B3	0.10
B1.B4	0.05	B3.B4	-0.10	B5.B4	-0.01	B7.B4	-0.22	B9.B4	0.58	B11.B4	0.33	B13.B4	0.13	B15.B4	0.09
B1.B5	0.04	B3.B5	-0.02	B5.B5	-	B7.B5	-0.26	B9.B5	0.64	B11.B5	0.34	B13.B5	0.15	B15.B5	0.14
B1.B6	0.07	B3.B6	-0.01	B5.B6	0.10	B7.B6	-0.36	B9.B6	0.84	B11.B6	0.45	B13.B6	0.18	B15.B6	0.16
B1.B7	0.20	B3.B7	0.21	B5.B7	0.26	B7.B7		B9.B7	0.89	B11.B7	0.64	B13.B7	0.24	B15.B7	0.28
B1.B8	0.10	B3.B8	0.07	B5.B8	0.10	B7.B8	-0.54	B9.B8	0.84	B11.B8	0.61	B13.B8	0.22	B15.B8	0.24
B1.B9	-0.42	B3.B9	-0.54	B5.B9	-0.64	B7.B9	-0.89	B9.B9	-	B11.B9	-0.32	B13.B9	-0.18	B15.B9	-0.30
B1.B10	-0.23	B3.B10	-0.29	B5.B10	-0.30	B7.B10	-0.58	B9.B10	0.11	B11.B10	-0.08	B13.B10	-0.30	B15.B10	-0.46
B1.B11	-0.24	B3.B11	-0.33	B5.B11	-0.34	B7.B11	-0.64	B9.B11	0.32	B11.B11	-	B13.B11	-0.17	B15.B11	-0.27
B1.B12	-0.24	B3.B12	-0.29	B5.B12	-0.32	B7.B12	-0.57	B9.B12	0.04	B11.B12	-0.16	B13.B12	-0.43	B15.B12	-0.55
B1.B13	-0.10	B3.B13	-0.14	B5.B13	-0.15	B7.B13	-0.24	B9.B13	0.18	B11.B13	0.17	B13.B13	-	B15.B13	-0.27
B1.B14	-0.08	B3.B14	-0.11	B5.B14	-0.13	B7.B14	-0.19	B9.B14	0.21	B11.B14	0.20	B13.B14	0.38	B15.B14	-0.08
B1.B15	-0.06	B3.B15	-0.10	B5.B15	-0.14	B7.B15	-0.28	B10.B1	0.23	B11.B15	0.27	B13.B15	0.27	B15.B15	-
B2.B1	-0.03	B4.B1	-0.05	B6.B1	-0.07	B8.B1	-0.10	B10.B2	0.24	B12.B1	0.24	B14.B1	0.08		
B2.B2	-	B4.B2	-0.06	B6.B2	-0.07	B8.B2	-0.09	B10.B3	0.29	B12.B2	0.26	B14.B2	0.10		
B2.B3	0.12	B4.B3	0.10	B6.B3	0.01	B8.B3	-0.07	B10.B4	0.29	B12.B3	0.29	B14.B3	0.11		
B2.B4	0.06	B4.B4	-	B6.B4	-0.02	B8.B4	-0.12	B10.B5	0.30	B12.B4	0.30	B14.B4	0.09		
B2.B5	0.01	B4.B5	0.01	B6.B5	-0.10	B8.B5	-0.10	B10.B6	0.38	B12.B5	0.32	B14.B5	0.13		
B2.B6	0.07	B4.B6	0.02	B6.B6	-	B8.B6	-0.10	B10.B7	0.58	B12.B6	0.39	B14.B6	0.16		
B2.B7	0.17	B4.B7	0.22	B6.B7	0.36	B8.B7	0.54	B10.B8	0.58	B12.B7	0.57	B14.B7	0.19		
B2.B8	0.09	B4.B8	0.12	B6.B8	0.10	B8.B8		B10.B9	-0.11	B12.B8	0.55	B14.B8	0.18		
B2.B9	-0.46	B4.B9	-0.58	B6.B9	-0.84	B8.B9	-0.84	B10.B10	-	B12.B9	-0.04	B14.B9	-0.21		
B2.B10	-0.24	B4.B10	-0.29	B6.B10	-0.38	B8.B10	-0.58	B10.B11	0.08	B12.B10	0.43	B14.B10	-0.31		
B2.B11	-0.27	B4.B11	-0.33	B6.B11	-0.45	B8.B11	-0.61	B10.B12	-0.43	B12.B11	0.16	B14.B11	-0.20		
B2.B12	-0.26	B4.B12	-0.30	B6.B12	-0.39	B8.B12	-0.55	B10.B13	0.30	B12.B12	-	B14.B12	-0.42		
B2.B13	-0.10	B4.B13	-0.13	B6.B13	-0.18	B8.B13	-0.22	B10.B14	0.31	B12.B13	0.43	B14.B13	-0.38		
B2.B14	-0.10	B4.B14	-0.09	B6.B14	-0.16	B8.B14	-0.18	B10.B15	0.46	B12.B14	0.42	B14.B14	-		
B2.B15	-0.09	B4.B15	-0.09	B6.B15	-0.16	B8.B15	-0.24	B10.B1.B1	0.18	B12.B15	0.55	B14.B15	0.08		

Highest correlation coefficients

	CHL		CHL		CHL		CHL		CHL		CHL		CHL		CHL
B1.B1		B3.B1	-0.32	B5.B1	-0.31	B7.B1	-0.39	B9.B1	-0.06	B11.B1	-0.17	B13.B1	-0.23	B15.B1	-0.27
B1.B2	0.28	B3.B2	-0.35	B5.B2	-0.27	B7.B2	-0.42	B9.B2	0.01	B11.B2	-0.14	B13.B2	-0.23	B15.B2	-0.28
B1.B3	0.32	B3.B3		B5.B3	-0.18	B7.B3	-0.44	B9.B3	0.12	B11.B3	-0.04	B13.B3	-0.23	B15.B3	-0.26
B1.B4	0.32	B3.B4	0.27	B5.B4	-0.14	B7.B4	-0.44	B9.B4	0.15	B11.B4	-0.02	B13.B4	-0.22	B15.B4	-0.26
B1.B5	0.31	B3.B5	0.18	B5.B5		B7.B5	-0.43	B9.B5	0.24	B11.B5	-0.02	B13.B5	-0.21	B15.B5	-0.25
B1.B6	0.32	B3.B6	0.27	B5.B6	0.37	B7.B6	-0.53	B9.B6	0.55	B11.B6	0.11	B13.B6	-0.20	B15.B6	-0.19
B1.B7	0.39	B3.B7	0.44	B5.B7	0.43	B7.B7		B9.B7	0.81	B11.B7	0.38	B13.B7	-0.12	B15.B7	-0.08
B1.B8	0.35	B3.B8	0.34	B5.B8	0.35	B7.B8	-0.22	B9.B8	0.80	B11.B8	0.42	B13.B8	-0.18	B15.B8	-0.12
B1.B9	0.06	B3.B9	-0.12	B5.B9	-0.24	B7.B9	-0.81	B9.B9		B11.B9	-0.51	B13.B9	-0.44	B15.B9	-0.53
B1.B10	0.16	B3.B10	0.12	B5.B10	0.10	B7.B10	-0.26	B9.B10	0.38	B11.B10	0.13	B13.B10	-0.49	B15.B10	-0.54
B1.B11	0.17	B3.B11	0.04	B5.B11	0.02	B7.B11	-0.38	B9.B11	0.51	B11.B11		B13.B11	-0.34	B15.B11	-0.44
B1.B12	0.15	B3.B12	0.11	B5.B12	0.10	B7.B12	-0.24	B9.B12	0.36	B11.B12	0.14	B13.B12	-0.55	B15.B12	-0.60
B1.B13	0.23	B3.B13	0.23	B5.B13	0.21	B7.B13	0.12	B9.B13	0.44	B11.B13	0.34	B13.B13		B15.B13	-0.23
B1.B14	0.23	B3.B14	0.24	B5.B14	0.22	B7.B14	0.20	B9.B14	0.44	B11.B14	0.37	B13.B14	0.46	B15.B14	-0.05
B1.B15	0.27	B3.B15	0.26	B5.B15	0.25	B7.B15	0.08	B10.B1	-0.16	B11.B15	0.44	B13.B15	0.23	B15.B15	
B2.B1	-0.28	B4.B1	-0.32	B6.B1	-0.32	B8.B1	-0.35	B10.B2	-0.15	B12.B1	-0.15	B14.B1	-0.23		
B2.B2		B4.B2	-0.31	B6.B2	-0.35	B8.B2	-0.35	B10.B3	-0.12	B12.B2	-0.14	B14.B2	-0.23		
B2.B3	0.35	B4.B3	-0.27	B6.B3	-0.27	B8.B3	-0.34	B10.B4	-0.10	B12.B3	-0.11	B14.B3	-0.24		
B2.B4	0.31	B4.B4		B6.B4	-0.29	B8.B4	-0.35	B10.B5	-0.10	B12.B4	-0.11	B14.B4	-0.24		
B2.B5	0.27	B4.B5	0.14	B6.B5	-0.37	B8.B5	-0.35	B10.B6	-0.04	B12.B5	-0.10	B14.B5	-0.22		
B2.B6	0.35	B4.B6	0.29	B6.B6		B8.B6	-0.33	B10.B7	0.26	B12.B6	-0.04	B14.B6	-0.22		
B2.B7	0.42	B4.B7	0.44	B6.B7	0.53	B8.B7	0.22	B10.B8	0.26	B12.B7	0.24	B14.B7	-0.20		
B2.B8	0.35	B4.B8	0.35	B6.B8	0.33	B8.B8		B10.B9	-0.38	B12.B8	0.21	B14.B8	-0.22		
B2.B9	-0.01	B4.B9	-0.15	B6.B9	-0.55	B8.B9	-0.80	B10.B10		B12.B9	-0.36	B14.B9	-0.44		
B2.B10	0.15	B4.B10	0.10	B6.B10	0.04	B8.B10	-0.26	B10.B11	-0.13	B12.B10	0.00	B14.B10	-0.48		
B2.B11	0.14	B4.B11	0.02	B6.B11	-0.11	B8.B11	-0.42	B10.B12	0.00	B12.B11	-0.14	B14.B11	-0.37		
B2.B12	0.14	B4.B12	0.11	B6.B12	0.04	B8.B12	-0.21	B10.B13	0.49	B12.B12		B14.B12	-0.53		
B2.B13	0.23	B4.B13	0.22	B6.B13	0.20	B8.B13	0.18	B10.B14	0.48	B12.B13	0.55	B14.B13	-0.46		
B2.B14	0.23	B4.B14	0.24	B6.B14	0.22	B8.B14	0.22	B10.B15	0.54	B12.B14	0.53	B14.B14			
B2.B15	0.28	B4.B15	0.26	B6.B15	0.19	B8.B15	0.12	B10.B1.B1	-0.20	B12.B15	0.60	B14.B15	0.05		

Highest correlation coefficients

	TDS		TDS		TDS		TDS		TDS		TDS		TDS		TDS
B1.B2	0.08	B3.B1	-0.06	B5.B1	-0.05	B7.B1	-0.02	B9.B1	-0.39	B11.B1	-0.28	B13.B1	-0.18	B15.B1	-0.14
B1.B3	0.06	B3.B2	-0.05	B5.B2	-0.06	B7.B2	-0.03	B9.B2	-0.43	B11.B2	-0.30	B13.B2	-0.18	B15.B2	-0.15
B1.B4	0.08	B3.B4	0.12	B5.B3	-0.03	B7.B3	0.00	B9.B3	-0.50	B11.B3	-0.34	B13.B3	-0.20	B15.B3	-0.16
B1.B5	0.05	B3.B5	0.03	B5.B4	0.01	B7.B4	0.01	B9.B4	-0.55	B11.B4	-0.36	B13.B4	-0.19	B15.B4	-0.15
B1.B6	0.06	B3.B6	0.09	B5.B6	0.06	B7.B5	-0.01	B9.B5	-0.60	B11.B5	-0.37	B13.B5	-0.21	B15.B5	-0.19
B1.B7	0.02	B3.B7	0.00	B5.B7	0.01	B7.B6	0.08	B9.B6	-0.70	B11.B6	-0.45	B13.B6	-0.23	B15.B6	-0.20
B1.B8	0.06	B3.B8	0.06	B5.B8	0.08	B7.B8	0.40	B9.B7	-0.67	B11.B7	-0.52	B13.B7	-0.27	B15.B7	-0.27
B1.B9	0.39	B3.B9	0.50	B5.B9	0.60	B7.B9	0.67	B9.B8	-0.62	B11.B8	-0.49	B13.B8	-0.25	B15.B8	-0.24
B1.B10	0.27	B3.B10	0.31	B5.B10	0.34	B7.B10	0.54	B9.B10	0.02	B11.B9	0.16	B13.B9	0.07	B15.B9	0.15
B1.B11	0.28	B3.B11	0.34	B5.B11	0.37	B7.B11	0.52	B9.B11	-0.16	B11.B10	0.14	B13.B10	0.16	B15.B10	0.26
B1.B12	0.28	B3.B12	0.32	B5.B12	0.35	B7.B12	0.55	B9.B12	0.05	B11.B12	0.19	B13.B11	0.03	B15.B11	0.12
B1.B13	0.18	B3.B13	0.20	B5.B13	0.21	B7.B13	0.27	B9.B13	-0.07	B11.B13	-0.03	B13.B12	0.26	B15.B12	0.34
B1.B14	0.16	B3.B14	0.17	B5.B14	0.17	B7.B14	0.21	B9.B14	-0.09	B11.B14	-0.06	B13.B14	-0.25	B15.B13	0.18
B1.B15	0.14	B3.B15	0.16	B5.B15	0.19	B7.B15	0.27	B10.B1	-0.27	B11.B15	-0.12	B13.B15	-0.18	B15.B14	0.07
B2.B1	-0.08	B4.B1	-0.08	B6.B1	-0.06	B8.B1	-0.06	B10.B2	-0.28	B12.B1	-0.28	B14.B1	-0.16		
B2.B3	0.05	B4.B2	-0.07	B6.B2	-0.05	B8.B2	-0.07	B10.B3	-0.31	B12.B2	-0.29	B14.B2	-0.16		
B2.B4	0.07	B4.B3	-0.12	B6.B3	-0.09	B8.B3	-0.06	B10.B4	-0.33	B12.B3	-0.32	B14.B3	-0.17		
B2.B5	0.06	B4.B5	-0.01	B6.B4	-0.06	B8.B4	-0.07	B10.B5	-0.34	B12.B4	-0.33	B14.B4	-0.16		
B2.B6	0.05	B4.B6	0.06	B6.B5	-0.06	B8.B5	-0.08	B10.B6	-0.40	B12.B5	-0.35	B14.B5	-0.17		
B2.B7	0.03	B4.B7	-0.01	B6.B7	-0.08	B8.B6	-0.10	B10.B7	-0.54	B12.B6	-0.40	B14.B6	-0.18		
B2.B8	0.07	B4.B8	0.07	B6.B8	0.10	B8.B7	-0.40	B10.B8	-0.54	B12.B7	-0.55	B14.B7	-0.21		
B2.B9	0.43	B4.B9	0.55	B6.B9	0.70	B8.B9	0.62	B10.B9	-0.02	B12.B8	-0.54	B14.B8	-0.19		
B2.B10	0.28	B4.B10	0.33	B6.B10	0.40	B8.B10	0.54	B10.B11	-0.14	B12.B9	-0.05	B14.B9	0.09		
B2.B11	0.30	B4.B11	0.36	B6.B11	0.45	B8.B11	0.49	B10.B12	0.43	B12.B10	-0.43	B14.B10	0.18		
B2.B12	0.29	B4.B12	0.33	B6.B12	0.40	B8.B12	0.54	B10.B13	-0.16	B12.B11	-0.19	B14.B11	0.06		
B2.B13	0.18	B4.B13	0.19	B6.B13	0.23	B8.B13	0.25	B10.B14	-0.18	B12.B13	-0.26	B14.B12	0.25		
B2.B14	0.16	B4.B14	0.16	B6.B14	0.18	B8.B14	0.19	B10.B15	-0.26	B12.B14	-0.25	B14.B13	0.25		
B2.B15	0.15	B4.B15	0.15	B6.B15	0.20	B8.B15	0.24	B10.B1.B1	-0.22	B12.B15	-0.34	B14.B15	-0.07		

Highest correlation coefficients

Appendix F

TUR Water Quality Maps

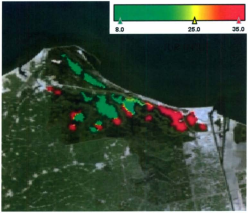

Figure 47 TUR Distribution Map July 29, 2009

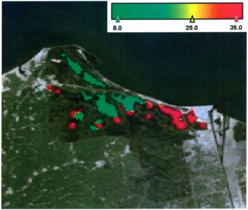

Figure 48 TUR Distribution Map August 1, 2009

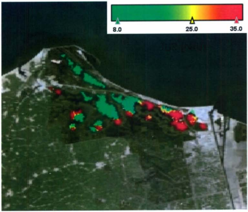

Figure 49 TUR Distribution Map August 7, 2009

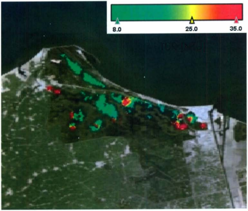

Figure 50 TUR Distribution Map August 10, 2009

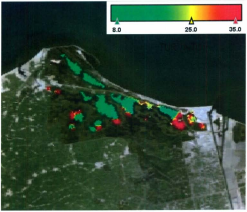

Figure 51 TUR Distribution Map August 13, 2009

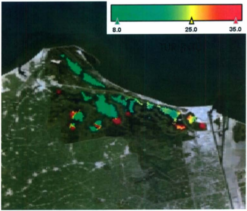

Figure 52 TUR Distribution Map August 16, 2009

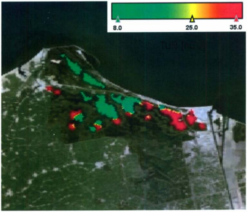

Figure 53 TUR Distribution Map August 19, 2009

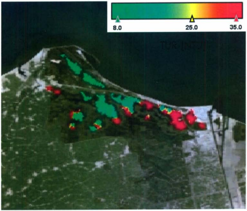

Figure 54 TUR Distribution Map August 20, 2009

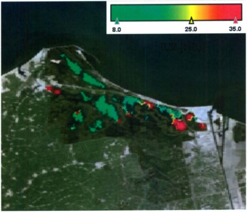

Figure 55 TUR Distribution Map August 23, 2009

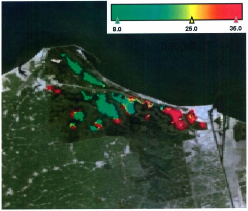

Figure 56 TUR Distribution Map August 26, 2009

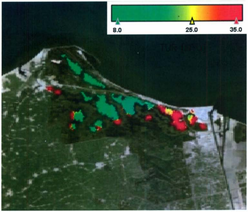

Figure 57 TUR Distribution Map August 29, 2009

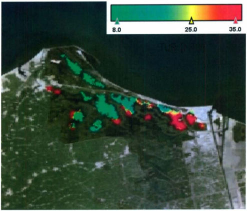

Figure 58 TUR Distribution Map September 1, 2009

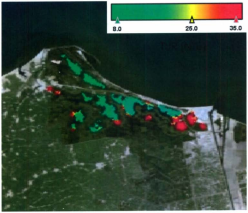

Figure 59 TUR Distribution Map September 4, 2009

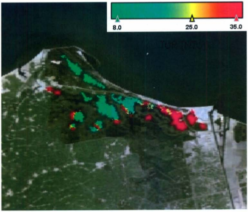

Figure 60 TUR Distribution Map September 5, 2009

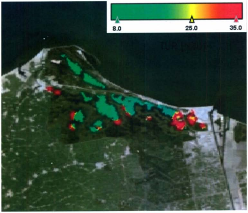

Figure 61 TUR Distribution Map September 8, 2009

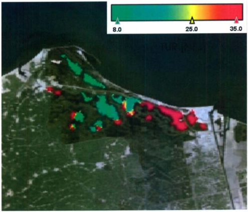

Figure 62 TUR Distribution Map September 11, 2009

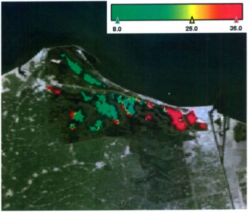

Figure 63 TUR Distribution Map September 14, 2009

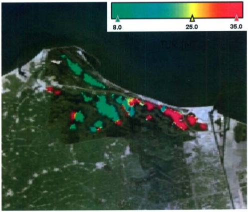

Figure 64 TUR Distribution Map September 17, 2009

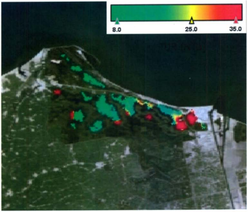

Figure 65 TUR Distribution Map September 20, 2009

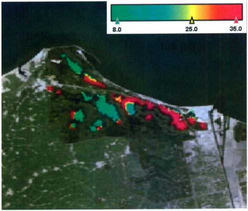

Figure 66 TUR Distribution Map October 6, 2009

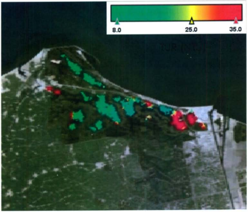

Figure 67 TUR Distribution Map October 9, 2009

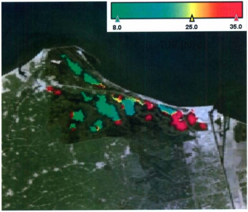

Figure 68 TUR Distribution Map October 10, 2009

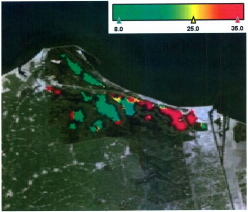

Figure 69 TUR Distribution Map October 13, 2009

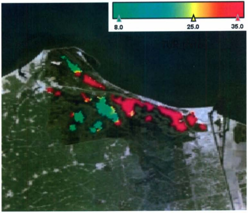

Figure 70 TUR Distribution Map October 22, 2009

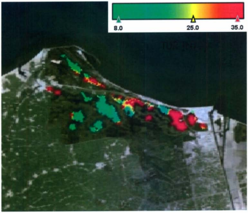

Figure 71 TUR Distribution Map October 25, 2009

Appendix G

CHL Water Quality Maps

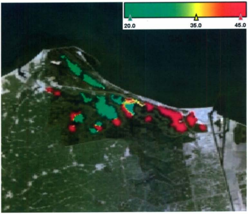

Figure 72 CHL Distribution Map July 29, 2009.

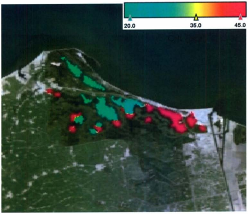

Figure 73 CHL Distribution Map August 1, 2009.

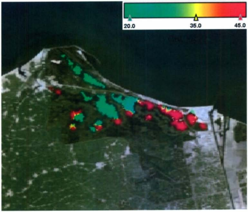

Figure 74 CHL Distribution Map August 7, 2009.

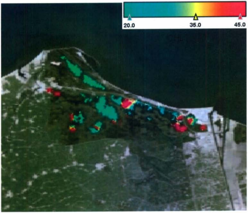

Figure 75 CHL Distribution Map August 10, 2009.

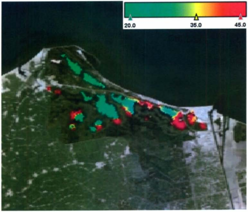

Figure 76 CHL Distribution Map August 13, 2009.

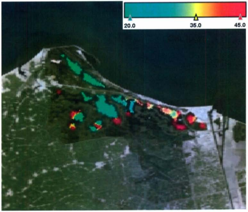

Figure 77 CHL Distribution Map August 16, 2009.

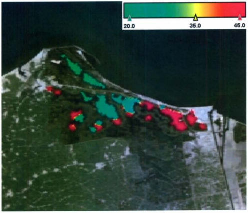

Figure 78 CHL Distribution Map August 19, 2009.

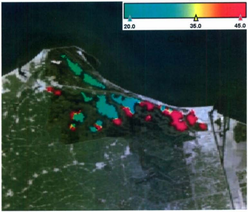

Figure 79 CHL Distribution Map August 20, 2009.

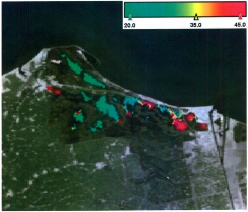

Figure 80 CHL Distribution Map August 23, 2009.

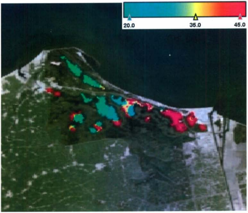

Figure 81 CHL Distribution Map August 26, 2009

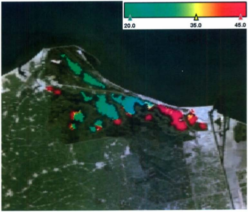

Figure 82 CHL Distribution Map August 29, 2009.

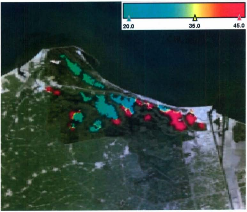

Figure 83 CHL Distribution Map September 1, 2009.

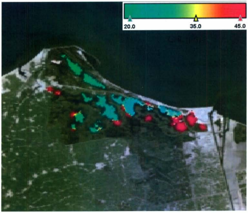

Figure 84 CHL Distribution Map September 4, 2009.

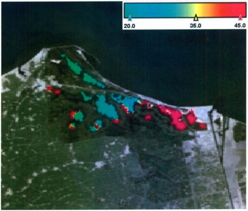

Figure 85 CHL Distribution Map September 5, 2009.

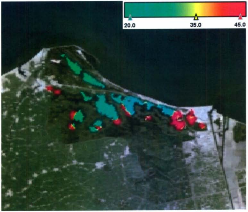

Figure 86 CHL Distribution Map September 8, 2009.

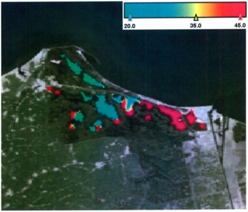

Figure 87 CHL Distribution Map September 11, 2009.

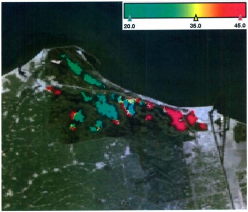

Figure 88 CHL Distribution Map September 14, 2009.

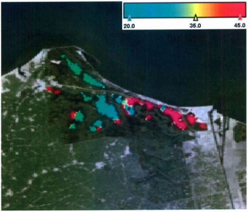

Figure 89 CHL Distribution Map September 17, 2009.

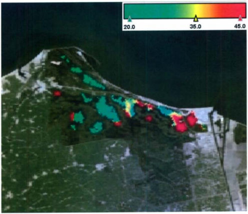

Figure 90 CHL Distribution Map September 20, 2009.

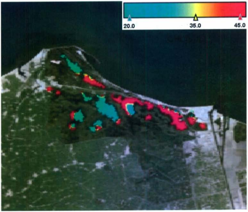

Figure 91 CHL Distribution Map October 6, 2009.

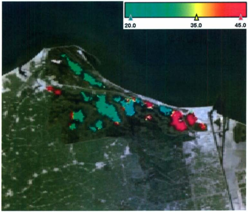

Figure 92 CHL Distribution Map October 9, 2009

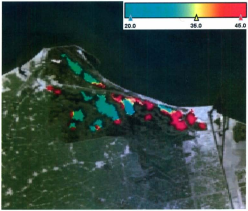

Figure 93 CHL Distribution Map October 10, 2009

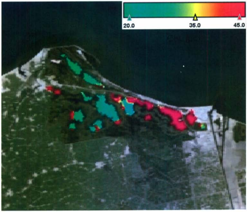

Figure 94 CHL Distribution Map October 13, 2009

Figure 95 CHL Distribution Map October 22, 2009

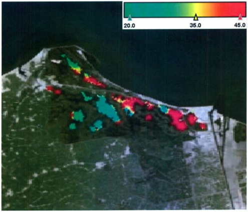

Figure 96 CHL Distribution Map October 25, 2009

Appendix H

TDS Water Quality Maps

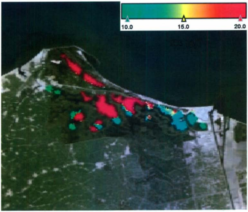

Figure 97 TDS Distribution Map July 29, 2009.

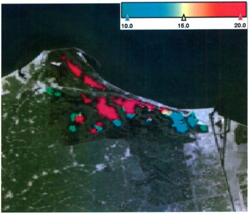

Figure 98 TDS Distribution Map August 1, 2009.

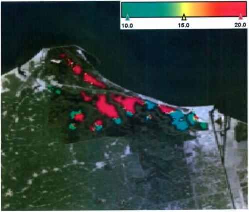

Figure 99 TDS Distribution Map August 7, 2009.

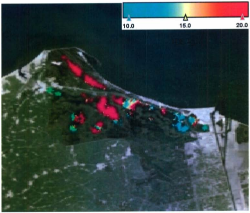

Figure 100 TDS Distribution Map August 10, 2009.

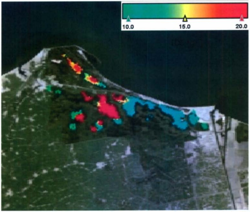

Figure 101 TDS Distribution Map August 13, 2009.

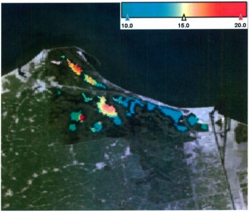

Figure 102 TDS Distribution Map August 16, 2009.

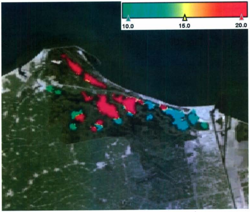

Figure 103 TDS Distribution Map August 19, 2009.

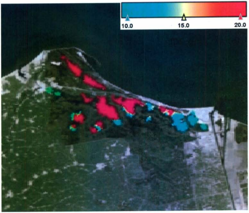

Figure 104 TDS Distribution Map August 20, 2009.

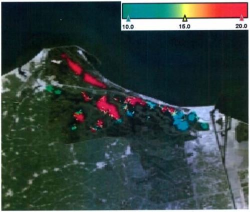

Figure 105 TDS Distribution Map August 23, 2009.

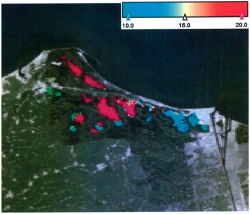

Figure 106 TDS Distribution Map August 26, 2009.

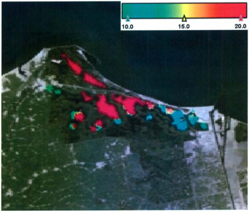

Figure 107 TDS Distribution Map August 29, 2009.

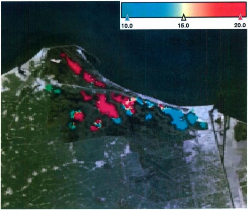

Figure 108 TDS Distribution Map September 1, 2009.

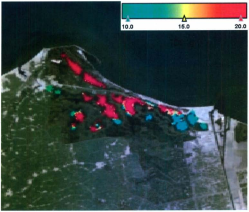

Figure 109 TDS Distribution Map September 4, 2009.

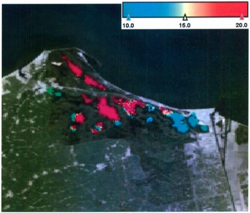

Figure 110 TDS Distribution Map September 5, 2009.

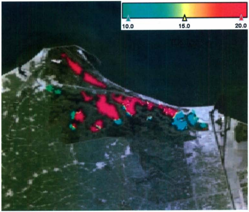

Figure 111 TDS Distribution Map September 8, 2009.

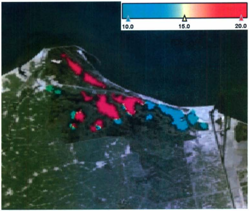

Figure 112 TDS Distribution Map September 11, 2009.

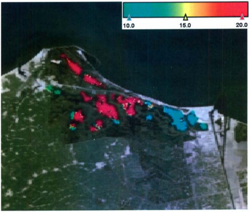

Figure 113 TDS Distribution Map September 14, 2009.

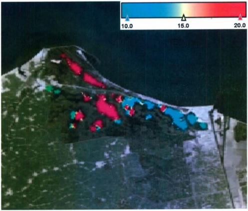

Figure 114 TDS Distribution Map September 17, 2009.

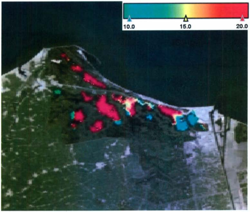

Figure 115 TDS Distribution Map September 20, 2009.

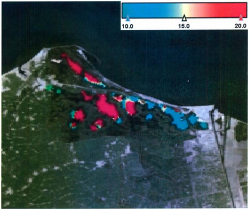

Figure 116 TDS Distribution Map October 6, 2009.

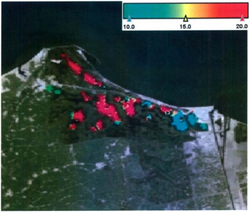

Figure 117 TDS Distribution Map October 9, 2009.

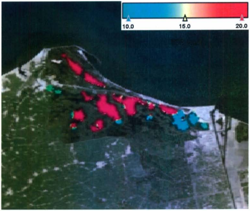

Figure 118 TDS Distribution Map October 10, 2009.

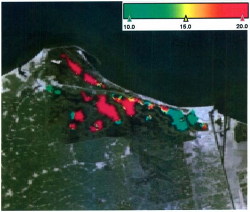

Figure 119 TDS Distribution Map October 13, 2009.

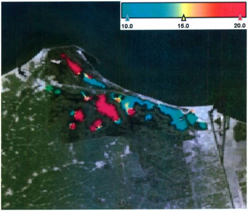

Figure 120 TDS Distribution Map October 22, 2009.

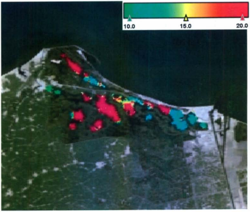

Figure 121 TDS Distribution Map October 25, 2009.